High frequency gravitational waves from photon sphere of supermassive black holes

齊藤，海秀

(Degree)
博士（理学）

(Date of Degree)
2023-03-25

(Date of Publication)
2024-03-01

(Resource Type)
doctoral thesis

(Report Number)
甲第8584号

(URL)
https://hdl.handle.net/20.500.14094/0100482332

Doctoral Dissertation

High frequency gravitational waves from photon sphere of supermassive black holes

(超巨大ブラックホール光子球からの高周波重力波)

January 2023

Graduate School of Science, Kobe University

Kaishu Saito

(齊藤 海秀)

Doctoral Dissertation

High frequency gravitational waves from photon sphere of supermassive black holes

(超巨大ブラックホール光子球からの高周波重力波)

January 2023

Graduate School of Science, Kobe University

Kaishu Saito

(齊藤 海秀)

Abstract

In 2015, LIGO had opened up gravitational wave astronomy. Since LIGO has the sensitivity in the frequency range 10-10^3Hz, the main sources of gravitational waves(GWs) are binary systems of stellar mass black holes or neutron stars. Clearly, it is worth trying to extend observable frequency ranges. Indeed, to probe beyond the standard model, we need to observe GWs with frequencies higher than 1kHz. Thus, detection of high-frequency GWs may provide the opportunity of testing new physics. To promote the future developments of high-frequency GW detectors, the existence of guaranteed sources are essential. From this perspective, we propose a guaranteed source, namely a photon sphere of a supermassive black hole which steadily emits high-frequency GWs through the photon-graviton mixing(conversion). Assuming the hot accretion flow model, we find that the typical frequency of the GWs is 10^{19}-10^{20}Hz. Since the frequency of the GWs is not sensitive to the mass of the supermassive black hole, each signal cannot be resolved and forms stochastic GWs background with 10^{19}-10^{20}Hz. We find that its density parameter becomes $\Omega_{\rm GW} \sim 10^{-15}$ at the maximum. We also discuss the possible application of our graviton creation mechanism to other low-mass particle creation near the photon sphere of supermassive black holes.

Contents

Notations

Indices, Metric signature, and Epsilon tensor

We use Greek indices $\alpha, \beta, ...$ for spacetime components $0, 1, 2, 3$. Roman indices $i, j, k...$ denote only three spatial components $1, 2, 3$.
We use metric signature $(-, +, +, +)$.
$\hat{\epsilon}^{\mu\nu\rho\sigma}$ with $\hat{\epsilon}^{0123} = +1$ denote the flat epsilon tensor in the four-dimensional Minkowski spacetime. When we consider a curved spacetime, it is generalized as follows:

$$\epsilon_{\mu\nu\rho\sigma} := \sqrt{-g}\hat{\epsilon}_{\mu\nu\rho\sigma}, \quad \epsilon^{\mu\nu\rho\sigma} := \frac{1}{\sqrt{-g}}\hat{\epsilon}^{\mu\nu\rho\sigma}.$$

Covariant derivative, Christoffel symbols, and Riemann curvature tensor

In a curved spacetime with the metric tensor $g_{\mu\nu}$, the covariant derivative D of a vector V is defined by

$$D_\mu V^\nu = \partial_\mu V^\nu + \Gamma^\nu_{\rho\mu} V^\rho, \quad D_\mu V_\nu = \partial_\mu V_\nu - \Gamma^\rho_{\nu\mu} V_\rho,$$

where Γ denotes the Christoffel symbols. By demanding $D_\mu g_{\nu\rho} = 0$ and $\Gamma^\nu_{\rho\mu} = \Gamma^\nu_{\mu\rho}$, the Christoffel symbols can be written in terms of the metric as

$$\Gamma^\rho_{\mu\nu} = \frac{1}{2} g^{\rho\sigma} \left(\partial_\mu g_{\sigma\nu} + \partial_\nu g_{\sigma\mu} - \partial_\sigma g_{\mu\nu} \right).$$

We define the Riemann curvature as follows:

$$\left[D_\mu, D_\nu \right] V^\rho = R^\rho{}_{\sigma\mu\nu} V^\sigma,$$
$$\left[D_\mu, D_\nu \right] V_\rho = R^\sigma{}_{\rho\nu\mu} V_\sigma,$$

where $[\ ,\ ]$ is the commutator. From this definition, the Riemann tensor is explicitly written as

$$R^\mu{}_{\nu\rho\sigma} = \partial_\rho \Gamma^\mu_{\nu\sigma} - \partial_\sigma \Gamma^\mu_{\nu\rho} + \Gamma^\mu_{\alpha\rho} \Gamma^\alpha_{\nu\sigma} - \Gamma^\mu_{\alpha\sigma} \Gamma^\alpha_{\nu\rho}.$$

The Ricci tensor is defined by $R_{\mu\nu} = R^{\alpha}{}_{\mu\alpha\nu}$. Its trace $R = g^{\mu\nu}R_{\mu\nu}$ is referred to as the Ricci scalar.

Einstein-Hilbert action

The gravitational action is given by the Einstein-Hilbert action

$$S_{\rm EH} = \frac{c^3}{16\pi G}\int d^4x\sqrt{-g}R$$

plus action of matter $S_{\rm M}$. Here $d^4x = c\,dt\,d^3x$. Since the infinitesimal variation of each part with respect to metric are

$$\delta S_{\rm EH} = \frac{c^3}{16\pi G}\int d^4x\sqrt{-g}\left[R^{\mu\nu} - \frac{1}{2}Rg^{\mu\nu}\right](-\delta g_{\mu\nu}),$$
$$\delta S_{\rm M} = \frac{1}{2c}\int d^4x\sqrt{-g}T^{\mu\nu}\delta g_{\mu\nu},$$

the Einstein equations are given by

$$R_{\mu\nu} - \frac{1}{2}g_{\mu\nu}R = \frac{8\pi G}{c^4}T_{\mu\nu}.$$

Ionized gas

In the context of compact stars and accretion disks, matter is often treated as an ionized gas. Here we shall summarize the quantities that describe an ionized gas. Since the matter is completely ionized, the total particle number of the system $N_{\rm tot}$ is given by the number of ions $N_{\rm i}$ plus the number of electrons $N_{\rm e}$. We often use the mean molecular weight μ which is the mass of baryons per one particle(including electrons) measured in units of the proton mass $m_{\rm p}$. For example, in the case of the ionized hydrogen gas, we have two particles a hydrogen ion and an electron, and the mass of the hydrogen ion is $m_{\rm p}$, so $\mu = 1/2$. For the ionized helium-4 gas, we have three particles a helium-4 ion and two electrons, and the mass of the helium-4 ion is $\sim 4m_{\rm p}$, so $\mu = 4/3$.

If an ionized gas can be treated as an ideal gas, its equation of state is given by

$$PV = N_{\rm tot}k_{\rm B}T,$$

where $N_{\rm tot} = N_{\rm i} + N_{\rm e}$. Since ion's contribution dominates the mass density, the mass density of an ionized gas is given by

$$\rho = N_{\rm tot}\,\mu\,m_{\rm p}/V.$$

Then, one can rewrite the equation of state as

$$P = \frac{k_{\rm B}T}{\mu m_{\rm p}}\rho.$$

In the context of accretion disks, the equation of state is often written with the sound speed $c_{\rm s}$ as

$$P = c_{\rm s}^2\rho,$$

where $c_{\rm s}$ is defined by

$$c_{\rm s} := \sqrt{\frac{dP}{d\rho}} = \sqrt{\frac{k_{\rm B}T}{\mu m_{\rm p}}}.$$

Chapter 1

Introduction

Current status of gravitational-wave observations

Binary systems composed of the stellar-mass black hole(BH) [1] and the neutron star radiate gravitational-waves(GWs) with a frequency of about $f_{\rm GW} \sim 10^{1\text{-}3}$Hz. Aiming at this frequency range, ground-based laser interferometers such as LIGO were designed. When the first GWs from a binary stellar-mass BH were detected [1] in 2015, it became possible to extract the physical information of compact stars from GWs. That was the dawn of the GW astronomy.

Toward multiwavelength GW astronomy

As the research of astronomy has been extended from optical to other multiwavelength, GWs with a frequency other than the frequency range of the LIGO have attracted much interest. In a low-frequency range, stochastic GWs from supermassive black hole(SMBH) binaries are reported [2–6]. On the other hand, in a high-frequency range, there are interesting predictions of GWs from the beyond standard model and primordial black holes(PBHs), etc.. Therefore, GWs not only provide information of compact stars but also give the opportunity of testing various unconfirmed physics. Thus, it is worth realizing multiwavelength GW observation in future.

Why we study high-frequency GWs?

In this thesis, we discuss high-frequency GWs. First of all, let us realize the importance of high-frequency GW research. Let us consider hypothetical light bosons called the axion which are motivated by the strong CP problem in QCD

[1]The black holes which have the mass of order a few times $10M_\odot$ are called the stellar-mass black holes, where $M_\odot$ is the mass of the sun.

[7–11] and string theories [12]. The axion extracts the rotation energy from the BH through the superradiant instability and forms a bound state around the BH. This bound state is called the axion cloud. The axion cloud decays by radiating GW with a frequency around $f_{\rm GW} \sim 10^4 {\rm Hz}\,(m_\phi/10^{-10}{\rm eV})$ [13–15], where m_ϕ is the mass of the axion. Moreover, in a GHz range, there may exist GWs from thermal plasma in the primordial universe [16–19]. In a more high-frequency range, stochastic GWs from evaporating PBHs are expected. For the PBHs which had evaporated before the Big Bang Nucleosynthesis (BBN), the maximal frequency reaches 10^{17}Hz [20–22]. Thus, high-frequency GWs are related to various high-energy physics, and they carry important information to test a new theory.

High-frequency GWs above 10^{14}Hz $\sim$ collaboration with axion experiments $\sim$

In the previous paragraph, we introduced high-frequency GWs over a broad frequency range. Although GWs in such frequency range has not yet been detected, there are several proposals for the high-frequency GW detector [23]. In this thesis, we focus on high-frequency GWs above 10^{14}Hz. As for the GWs above 10^{14}Hz, we can use existing axion detectors. In fact, since the axion detection is currently an active research area both for theorists and experimentalists, further updates of the detector are promising.

Now, let's explain the aforementioned duality between axion detection and high-frequency GW detection. In axion detection, we utilize interaction between axion and photon. Under the existence of a background magnetic field, perturbative description of axion photon interaction is given by (1.1), and axion and photon are mixed by effective coupling of order $g_{\phi\gamma}\bar{B}$, where $g_{\phi\gamma}$ is the axion photon coupling constant, $\bar{B}$ is the strength of a background magnetic field. ϕ and A are perturbations of axion and photon from the background respectively[2]. Preparing a background magnetic field in the laboratory, we can detect optical and X-ray signals arising from the axion photon mixing by CCD camera. This is the idea of axion experiments such as the CERN Axion Solar Telescope(CAST) [24].

$$-\frac{1}{4}g_{\phi\gamma}\phi F_{\mu\nu}\tilde{F}^{\mu\nu} \sim g_{\phi\gamma}\bar{B}\phi\partial_t A \tag{1.1}$$

Meanwhile, in a background magnetic field, the minimal coupling between gravity and electromagnetic field can perturbatively be written as

$$-\frac{1}{4}g^{\mu\rho}g^{\nu\sigma}F_{\mu\nu}F_{\rho\sigma} \sim \frac{\bar{B}}{M_{\rm pl}}h\partial A, \tag{1.2}$$

[2]Here, background configuration of axion is set to zero.

where h is the perturbation from a background metric, $M_{\rm pl}$ is the Planck mass. This would be very similar to an aforementioned axion photon interaction in a background magnetic field (also observe that, in the case of photon and graviton system, effective coupling constant is $\bar{B}/M_{\rm pl}$). Then we found that, in a background magnetic field, mixing between graviton and photon occurs [25–27], and it is possible to detect the GWs above 10^{14}Hz from space by converting it to visible light or X-ray as we do so in axion experiments. Fig.1.1 shows constraint for the amplitude of stochastic GWs above 10^{14}Hz obtained by reinterpreting results of axion experiments up to now. One of the currently projected axion experiment can exclude down to $h \sim 10^{-32}$ for $f_{\rm GW} \sim 10^{15}$Hz.

To summarize, for the GWs above 10^{14}Hz, one can utilize the existing data of axion experiments to constrain the GW amplitude.

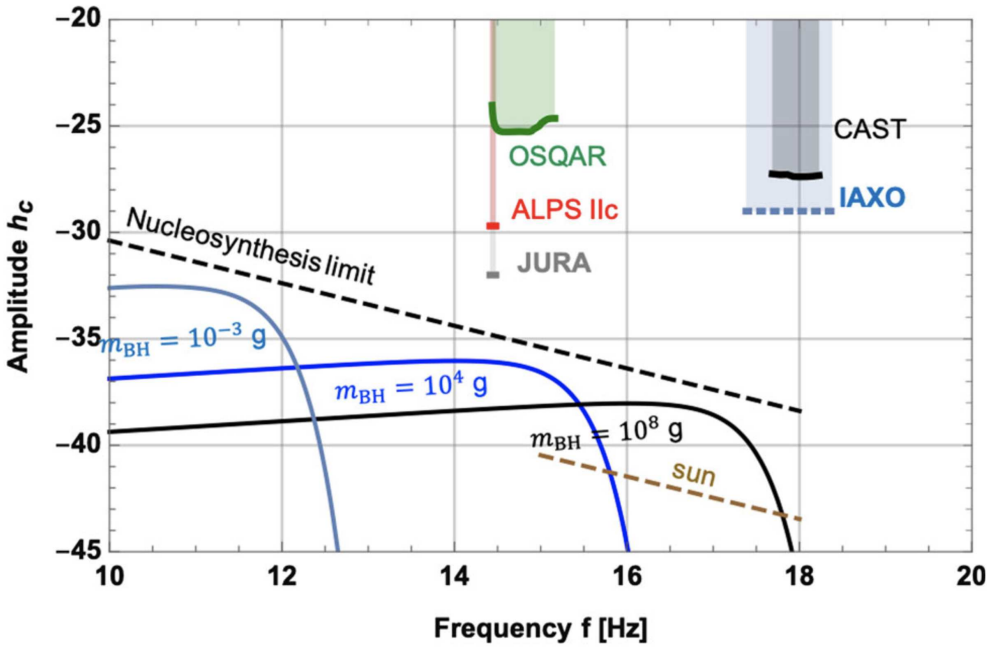

Figure 1.1: The strain of GWs vs. frequency, from [28]. The curves below the nucleosynthesis limit show the stochastic GWs background originating from evaporating primordial black holes with mass $m_{\rm BH}$. The dashed yellowish-brown line shows GWs from the solar core [29]. The plasma in the solar core has a high density of about $n_{\rm e} \sim 10^{25}{\rm cm}^{-3}$ and a high temperature of about $T \sim 10^{7}$K. Therefore, even if the GWs originating from each plasma collision are faint, the total amount of radiation becomes substantial.

High-frequency GWs above 10^{14}Hz $\sim$ necessity of guaranteed sources and a goal of our research $\sim$

For the further progress of detecting GWs above 10^{14}Hz, we shall clarify the issue that should be addressed from theoretical physics and establish a goal of our research. Firstly, let us see Fig.1.1. There is the GW spectrum from the sun ranged over from 10^{15}Hz to 10^{18}Hz [29]. This is the GW from thermal motion of dense plasma in the solar core. From the microscopic point of view, this can be understood as the integration of faint GWs radiated from Rutherford scattering of thermal electrons by proton. Incidentally, the maximum frequency of this GW is determined by the typical temperature of the solar core as $f_{\rm GW} \sim 10^7$K $\sim 10^{18}$Hz. We call the GW sources whose existence is well confirmed such as the solar core guaranteed sources. Needless to say, the existence of guaranteed sources is essential for proposing and performing experiments. However, to the best of my knowledge, except for the sun, there are no guaranteed sources of GWs above 10^{14}Hz. Note that, as one can observe from Fig.1.1, the GW amplitude from the solar core is not so large. In consideration of the above situation, it is natural to seek guaranteed sources for high-frequency GWs above 10^{14}Hz.

In our research, *we are aiming to propose a new guaranteed source of high-frequency GW above* 10^{14}*Hz*. Consequently, we proposed a new guaranteed source with frequency $f_{\rm GW} \sim 10^{19\text{-}20}$Hz in the paper [30]. In this thesis, we give a detailed review about this new guaranteed source of high-frequency GWs. In the rest of this introduction, we briefly summarize our results.

Step I $\sim$ mechanism of GW radiation $\sim$

Our proposed source radiates GWs in a very different way from the well-known compact star binary. First of all, remember the conversion from graviton to photon by the magnetic field of axion detectors. According to (1.2), if there is a magnetic field, the inverse process, conversion from photon to graviton can also occurs. Since the frequency of a particle does not change between before and after the conversion, a produced GW is necessarily high-frequency. Based on the fact that magnetic fields are ubiquitous in astrophysical phenomena, we examine the possibility of GW radiation through the photon graviton conversion from known astrophysical systems. To guess the candidate phenomena in which the graviton production through the conversion is efficient, it is sufficient to look on the formula of conversion probability. In Chapter 4, we derive the conversion probability in a uniform magnetic field and plasma (note that the assumption of plasma medium is natural for astrophysical systems). If the incident photon has a specific frequency called the resonance frequency, the conversion becomes efficient, and the

conversion probability is given by

$$P_{\gamma g}\left(\bar{B}, z\right) = \sin^2\left(\frac{\bar{B}}{M_{\rm pl}} z\right) \sim \left(\frac{\bar{B}}{M_{\rm pl}} z\right)^2, \tag{1.3}$$

where $\bar{B}$ is the strength of a background magnetic field, z is the mean-free-path of a photon in a magnetic field. According to (1.3), systems that possess a strong magnetic field and long mean-free-path of a photon become strong candidates for the GW source through the photon graviton conversion.

Step II ∼ Application of the photon graviton conversion to the photon sphere of a supermassive black hole ∼

As an environment where such conditions are satisfied, we consider the photon sphere of a supermassive black hole(SMBH). The photon sphere is the unstable circular orbit of the photon propagating around a BH. For the Schwarzschild BH (i.e. non-rotating BH), it is located at $r = 3M$, where r is the radial component of the Schwarzschild coordinates, M is the mass of the BH. In the vicinity of the photon sphere, there is a relatively strong magnetic field generated by the accretion disk. The Event Horizon Telescope(EHT) experiment reported its strength as in (1.4) and (1.5) [31, 32]. According to this, the magnetic field near the photon sphere is 10^7 times stronger than that of interstellar space.

$$n_{\rm e} \sim 1.0 \times 10^6 {\rm cm}^{-3}, \quad \bar{B} \sim 29{\rm G} \qquad \text{for SgA*}, \tag{1.4}$$

$$n_{\rm e} \sim 10^4 {\rm cm}^{-3}, \quad \bar{B} \sim 10{\rm G} \qquad \text{for M87*}. \tag{1.5}$$

On the other hand, to make the photon graviton conversion efficient, a long mean-free-path of a photon(equivalently, z in (1.3)) is also required. Since the EHT experiments also provide the estimation of plasma density as in (1.4) and (1.5), we can calculate the ratio of the mean-free-path of a photon to the Schwarzschild radius as

$$\frac{l_{\rm T}}{r_{\rm S}} \sim 0.509 \times 10^6 \left(\frac{n_{\rm e}}{10^4 {\rm cm}^{-3}}\right)^{-1} \left(\frac{M}{10^9 M_\odot}\right)^{-1}, \tag{1.6}$$

where $r_{\rm S}$ is the Schwarzschild radius. $l_{\rm T}$ denotes the mean-free-path of a photon due to the Thomson scattering. Therefore, in the vicinity of the photon sphere, we find that the absorption of photons by the plasma is almost negligible, and the propagation length of a photon becomes at least of order the Schwarzschild radius. Since, for SMBHs, the Schwarzschild is $r_{\rm S} \sim 10^{14}{\rm cm}(M/10^9 M_\odot)$, we conclude that long mean-free-path of a photon is ensured in the vicinity of the photon sphere.

There is one other reason why we consider SMBHs as candidates for GW sources through the photon graviton conversion. That is the enormous photon luminosity from the accretion disk. The accretion is the viscous fluid of plasma which is ubiquitous around the BHs. The gravitational potential energy of the gas is released as the thermal energy through viscosity, and consequently the disk intensely shines. Its maximal luminosity reaches the so-called Eddington luminosity given by $L_{\rm Edd} \sim 1.26 \times 10^{47} {\rm ergsec}^{-1} \left(\frac{M}{10^9 M_\odot}\right)$. An enormous number of photons from the accretion disk are also supplied to the photon sphere, and this fact makes the number of gravitons produced through the conversion effectively large. We summarize the GW emission mechanism from our proposed source as in a cartoon figure(see Fig.1.2). In the vicinity of the photon sphere, photons can propagate at least the Schwarzschild radius in a strong magnetic field of order 10G. Therefore, the region around the photon sphere becomes an efficient zone of the photon graviton conversion. Once an enormous amount of photons from the accretion disk flows into this region, a part of it is converted to high-frequency GWs and emitted to infinity.

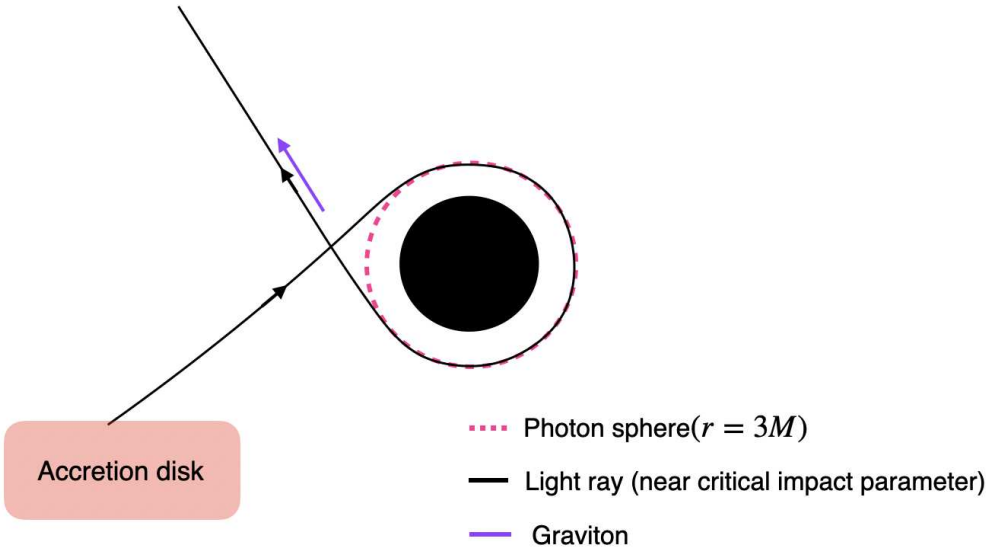

Figure 1.2: Schematic illustration of the emission mechanism. The black circle represents a central SMBH.

Step III $\sim$ High-frequency GWs from photon sphere of supermassive black holes, frequency, GW luminosity $\sim$

Now, let us explain how the frequency and the luminosity of our proposed GWs are determined.

As we mentioned, the conversion becomes efficient only when an incident photon has a special frequency called the resonance frequency. Only in that case, the conversion probability is given by (1.3). The resonance frequency - although we do not show its explicit formula here - is determined by the strength of a background magnetic field $\bar{B}$ and the plasma density $n_{\rm e}$. Let us refer to the resonance frequency as $f_{\rm r}(\bar{B}, n_{\rm e})$. If one can estimate the value of resonance frequency near the photon sphere $f_{\rm r}(\bar{B}, n_{\rm e})\,|_{r=3M}$, we find that photons with a frequency of around $f_{\rm r}(\bar{B}, n_{\rm e})\,|_{r=3M}$ are converted into gravitons. Since the frequency of particles does not change by the conversion, we conclude that the frequency of resulting GW is given by $f_{\rm GW} \sim f_{\rm r}(\bar{B}, n_{\rm e})\,|_{r=3M}$.

The background magnetic field near the photon sphere is generated by the accretion disk. Therefore, to estimate the resonance frequency $f_{\rm r}(\bar{B}, n_{\rm e})\,|_{r=3M}$, we need to solve the dynamics of the accretion disk. As we show in Chapter 3, depending on which cooling process is dominant, there are several static accretion solutions. The two representative solutions are the standard disk [33–35] and the ADAF [36–38]. In the standard disk model, the disk is cooled by the black body radiation from its surface. This implies that the standard disk is optically thick by definition. On the other hand, in the ADAF model, gas carries thermal energy and freely fall toward the black hole. This energy flow causes local cooling, and the black body radiation is subdominant this time. This implies that ADAF is optically thin by definition. According to the multiwavelength observation of active galactic nuclei(AGNs), in the real system, coexistence of the different types of accretion flow is suggested. Although the relative position of these accretion flow is an open problem, it is known that the two-zoon model, where inner ADAF is truncated at a certain radius and connected to the outer standard disk, well reproduces observed spectra. This model is sometimes referred to the inner ADAF paradigm. Incidentally, inner ADAF has a tendency to cause outflow [3] , so the inner ADAF paradigm is also consistent with the observed jet at the center of AGNs. We estimate the resonance frequency near the photon sphere $f_{\rm r}(\bar{B}, n_{\rm e})\,|_{r=3M}$, under an assumption of the inner ADAF paradigm. Then, we found that the frequency of the GW is insensitive to the mass of the central BH, and it roughly becomes $f_{\rm GW} \sim f_{\rm r}(\bar{B}, n_{\rm e})\,|_{r=3M} \sim 10^{19\text{-}20}$Hz.

[3] As we discuss in Chapter 3, the EoM of ADAF implies that it has positive Bernoulli parameter. Therefore, particles that have an outward velocity with respect to a BH can reach infinity. This fact also confirms the observed tenuous plasma density in the vicinity of the photon sphere as in (1.4) and (1.5).

From the discussion so far, it turns out that hard X-rays emitted from the accretion disk flow into the vicinity of the photon sphere, and are converted to GWs. However, needless to say, it is not the case that all photons emitted from the accretion disk flow into the vicinity of the photon sphere, so we can not estimate the GW luminosity as a simple product between the conversion probability and the luminosity of accretion disk. In addition to this, the orbiting time around the photon sphere differs between light rays flowing around the photon sphere, so those conversion probabilities also dose. To quantitatively handle the above issues, we parametrize light rays by the impact parameter to BH and calculate the energy of graviton produced per unit time for each impact parameter. Integrating these with respect to impact parameters, we obtain the total luminosity of the GWs. For simplicity, we assume the luminosity of the accretion disk as the Eddington luminosity for the X-ray band, then the result is roughly

$$\frac{dE_{\rm GW}}{dt} \sim 10^{27}{\rm ergsec}^{-1}\left(\frac{M}{10^9 M_\odot}\right)^3. \tag{1.7}$$

The GW luminosity obtained above is extremely smaller than that of binaries. Then, we are forced to find the GW source in our neighborhood, but the most nearest SMBH SgrA* is extremely dark compared to the Eddington luminosity. Therefore it is not realistic to detect GWs through the photon graviton conversion from a single SMBH. However, recalling that the frequency of the GW is insensitive to the mass of the BH, it is rather natural to detect it as the stochastic GWs background. We suppose that all SMBHs in our universe radiates the GWs with $10^{19\text{-}20}$Hz, and estimate the maximal energy density of the stochastic GWs background. The result is $\Omega_{\rm GW} \lesssim 10^{-15}$, where $\Omega_{\rm GW}$ is the energy density of stochastic background in units of the critical energy density of the universe. This upper bound is equivalent to $h \lesssim 10^{-45}$ in terms of the amplitude of GW.

Let us summarize the discussion so far. In our work, we proposed a new stochastic GWs from the photon sphere of the SMBHs. The SMBHs and their photon sphere certainly exist, and the photon graviton conversion is also a phenomenon within the scope of general relativity and electromagnetism, so we can call this source the guaranteed source. Unfortunately, its amplitude is extremely small, and it is not realistic to detect it in near future. So, we should continue to explore guaranteed sources for the GWs above 10^{14}Hz. The quantitative estimate carried out in our study will be the benchmark when applying the photon graviton conversion to another system.

At the end of this introduction, we gather the contents of this thesis. The structure of this thesis is as follows:

- **Chap.2(Review Part): Test Particle Motion around a BH**
  In this chapter, we discuss the trajectory of a freely moving test particle around the Schwarzschild black hole for both massive and massless cases. Section 2.1 summarizes the basics in preparation for the sections that follow. The definition of the action of a freely moving particle in an arbitrary spacetime, the definitions of the Schwarzschild coordinates, and the local observer's coordinates in the Schwarzschild spacetime were given. Section 2.2 describes the geodesics of a massive particle. Its effective potential as the function of the radial coordinate and the angular momentum is essential to understand the qualitative nature of the accretion disk as discussed in Chapter 3. Section2.3 describes the geodesics of a massless particle. In this section, we introduce the unstable circular orbit of massless particles called the photon sphere. As we already mentioned, in order to estimate the conversion probability near the photon sphere of a BH, the propagation length(in other words the orbiting time around the photon sphere) is essential. In Section2.4, we give the formula of orbiting time around the photon sphere of a BH.

- **Chap.3(Review Part): Accretion Onto Black Holes**
  In order to estimate the graviton production rate around the photon sphere, the magnetic field strength and plasma density around it are essential. These are determined by the accretion disk theory. In this chapter, we review the accretion disks from both observational and theoretical points of view. Firstly, in Section3.1 we will observe the spectrum of the active galactic nuclei(AGNs) and summarize the features that accretion disk theory should reproduce. Section 3.2 provides a review of the oldest accretion disk model, that is the standard disk theory. It describes the radiatively efficient and cold accretion. A brief description of how accretion is caused by the viscosity is available in Subsection 3.2.1. In Section 3.3, we discuss the optically thin, hot accretion theory so-called ADAF. The ADAF account for the observed X-ray emission from AGNs. These two contrasting accretion disk theories discussed in Section 3.2 and Section 3.3 are expected to coexist in real AGNs. In Section 3.4, we introduce the hypothetical model that most simply describes their coexistence and see that it reproduces the observed spectra.

- **Chap.4(Review Part): Photon Graviton Conversion**
  The aim of this Chapter is to derive the formula of conversion probability from photon to graviton. In Section 4.1, we define the effective action of the electromagnetic field in a curved spacetime and derive the Einstein equation

and Maxwell equation. The action we define here is the so-called Euler-Heisenberg action in the flat spacetime case, which is the effective theory of the electromagnetic field that incorporates quantum effect due to electron one-loops. We also discuss the cutoff scale of the effective theory. In Section 4.2, we linearize the EoM obtained in Section 4.1. This leads to the coupled EoM for photon and graviton, which are essential for describing the photon graviton conversion. Note that in this section we consider the flat spacetime and an arbitrary background electromagnetic field. In Section 4.3, we write down the EoM for plane waves propagating in a transverse magnetic field. We decompose linear EoM into each polarization. Since we are interested in high-energy photons whose wavelength is much shorter than the typical scale of variation of BHs, further simplification of EoM is possible by imposing the eikonal approximation. Section 4.4 implements this approximation. In Section 4.5, we explore the photon graviton conversion in the case of a uniform magnetic field with the EoM obtained in Section 4.4. The formulae, which are essential to calculate the frequency and the luminosity of GWs from the photon sphere, are available in this section.

- **Chap.5(Main chapter): High-frequency GWs from the Photon Sphere of SMBHs**
  The results of this chapter are based on our work [30]. In this Chapter, using the technique developed in previous chapters, we estimate the frequency and luminosity of the GWs from the photon sphere of SMBHs. In Section 5.1, assuming the simple accretion geometry discussed in Section 3.4, we derive the typical frequency of the GWs. In Section 5.3, we derive the luminosity of the GWs from the photon sphere of a single SMBH with the aid of formulae derived in Section 5.2. Finally, in Section 5.4 we estimate the energy density parameter of the stochastic GWs background formed by the SMBHs in the universe.

- **Chap.6: Application to Axion Search**
  The interaction between photon and graviton has the same form as that of photon and axion. Due to this duality, in the photon sphere of SMBHs, the photon axion conversion also becomes efficient. The conversion causes the dimming of the photon sphere in a certain frequency range by the number of photons that are converted into axions. In this chapter, we propose the above idea as a new method for searching the axions. As a trial, the dimming rate of the photon sphere of M87* is estimated using the technique developed in Chapter 5.

- **Chap.7: Conclusion**
  We draw our conclusion.

- **Appendices**
  For a better understanding of the main part, we have included the following appendices:
  Appendices A.2 and A.3 provide the hydrodynamic and thermodynamic formulae required to understand Chapter 3.
  Appendices A.1 and A.4 provide the formulae used in Chapter 4.
  Appendix A.5 is the derivation of the formula used in Chapter 5.
  Appendix A.6 is the review of the axion photon conversion discussed in Chapter 6.
  Appendix A.7 provides the unit conversion from natural units.

Chapter 2

Test Particle Motion around a Black Hole

In this chapter, we explore the trajectory of a freely moving test particle around a BH for both massive and massless cases. We restrict our discussion to the non-rotating BH(i.e. the Schwarzschild BH). Note that the geometrized units where $G = c = 1$ are used throughout this chapter.

The following is a list of elements necessary to understand the chapters that follow:

- **The effective potential for massive particle**: This plays a key role to understand the dynamics of the accretion disk, readers should look over its angular momentum dependence Fig.2.1.

- **The photon sphere and orbiting time around it**: In Chapter 5, we examine the photon graviton conversion around the photon sphere of a BH. To estimate the resulting GW luminosity, we need the formula of orbiting time around the photon sphere (2.37).

The rest of this chapter is based on the following reference: Section2.1, 2.2 and 2.3 are based on the textbook [39, 40]. Section2.4 is based on [41].

2.1 Geodesics in the Schwarzschild Spacetime

We shall start with the Lagrangian of a freely moving particle in arbitrary curved spacetime as an adjustment of our notation. It is given by

$$L = \frac{1}{2} g_{\mu\nu}(x) \dot{x}^\mu \dot{x}^\nu, \qquad \dot{x}^\mu := \frac{dx^\mu}{d\lambda}, \tag{2.1}$$

where λ is the affine parameter. [1] From this Lagrangian, we obtain the geodesic equation

$$\ddot{x}^\mu + \Gamma^\mu_{\nu\rho}\dot{x}^\nu\dot{x}^\rho = 0. \tag{2.2}$$

At this moment, we did not specify whether the particle considered here is massive or massless. It is specified by choice of four-momentum normalization. The four-momentum of a particle is defined by

$$p_\mu := \frac{\partial L}{\partial \dot{x}^\mu} = g_{\mu\nu}\dot{x}^\nu. \tag{2.3}$$

In the rest of this chapter, we consider the Schwarzschild spacetime

$$ds^2 = -f(r)dt^2 + f(r)^{-1}dr^2 + r^2\left(d\theta^2 + \sin^2\theta d\phi^2\right), \qquad f(r) := 1 - \frac{2M}{r}, \tag{2.4}$$

where coordinate (t, r, θ, ϕ) is called the Schwarzschild coordinates. In the Schwarzschild spacetime, the Lagrangian of freely moving particle (2.1) becomes

$$2L = -f(r)\dot{t}^2 + f(r)^{-1}\dot{r}^2 + r^2\dot{\theta}^2 + r^2\sin^2\theta\dot{\phi}^2. \tag{2.5}$$

Observe that if we choose the coordinates such that the initial particle position and velocity belongs in the $\theta = \pi/2$ plane, subsequent motion is also in the $\theta = \pi/2$ plane. This is easily observed from the EoM of θ. Therefore we can neglect the dynamics along the θ direction. Then the two conserved quantities associated with two cyclic coordinates of the Lagrangian(t and ϕ) are given by

$$p_\phi = r^2\dot{\phi} := l, \tag{2.6}$$
$$p_t = -f(r)\dot{t} := -E. \tag{2.7}$$

These are the angular momentum and energy of a particle respectively. Here we give a short comment on the physical meaning of the energy E defined above. To observe that, we introduce the static observer's frame at (t, r, θ, ϕ) by

$$\begin{aligned}
\vec{e}_{\hat{t}} &= f(r)^{-1/2}\vec{e}_t, \\
\vec{e}_{\hat{r}} &= f(r)^{1/2}\vec{e}_r, \\
\vec{e}_{\hat{\theta}} &= r^{-1}\vec{e}_\theta, \\
\vec{e}_{\hat{\phi}} &= (r\sin\theta)^{-1}\vec{e}_\phi,
\end{aligned} \tag{2.8}$$

[1] Affine parameter is the parametrization of geodesic which makes Lagrangian constant. As easily checked from (2.1), if the geodesic equation is satisfied, we obtain $\frac{dL}{d\lambda} = 0$.

where $\{\vec{e}_t, \vec{e}_r, \vec{e}_\theta, \vec{e}_\phi\}$ is basis correspond to the Schwarzschild coordinates and subscript with hat represents coordinates of the static observer. Then the local energy of the particle can be calculated as

$$E_{\text{local}} := -p_{\hat{t}} = -g\left(\vec{p}, e_{\hat{t}}\right) = -f(r)^{-1/2} p^\mu g\left(\vec{e}_\mu, e_t\right) = \frac{E}{\sqrt{1-\frac{2M}{r}}}, \tag{2.9}$$

where $g(*,*)$ is the inner product of two vectors. Therefore, to obtain locally measured energy, we should translate the conserved energy E into E_{local} by using (2.9), and the energy E can be interpreted as a particle's energy measured at infinity.

2.2 Trajectory of Massive Particle

Now let us examine the trajectory of a massive particle around the Schwarzschild BH. The EoM for t and ϕ are given by the conservation law (2.6) and (2.7) regardless of whether the particle is massive or massless. Therefore, all that remains is EoM for r. To derive this, it is easier to use the normalization of the four-momentum than to derive it directly from the Lagrangian. The four-momentum of the massive particle satisfies $p_\mu p^\mu = -m^2$, where m is the mass of a particle. By using the conservation law, one can eliminate $\dot{t}$ and $\dot{\phi}$ from the normalization of the four-momentum, and obtain

$$\left(\frac{dr}{d\lambda}\right)^2 = E^2 - \frac{l^2}{r^2} f(r) - m^2 f(r). \tag{2.10}$$

Alternatively, it is useful to parametrize trajectory by the proper time $\tau = m\lambda$ as [2]

$$\left(\frac{dr}{d\tau}\right)^2 = \tilde{E}^2 - V_{\text{eff}}(r), \tag{2.11}$$

$$V_{\text{eff}}(r) := f(r)\left(1 + \frac{\tilde{l}^2}{r^2}\right), \tag{2.12}$$

$$\frac{dV_{\text{eff}}}{dr} = \frac{2M}{r^4}\left(r^2 - \frac{\tilde{l}^2}{M} r + 3\tilde{l}^2\right), \tag{2.13}$$

where we defined energy and angular momentum per unit mass as $\tilde{E} := E/m$ and $\tilde{l} := l/m$.

[2] A relation $\tau = m\lambda$ comes from $p_\mu p^\mu = -m^2$ and the definition of the four-momentum (2.3).

Thanks to the clear separation between kinetic energy end potential energy as in (2.11), we can extract information of the radial motion from the effective potential $V_{\text{eff}}(r)$ without directly solving the EoM. Figure 2.1 shows effective potentials for different $\tilde{l}$.

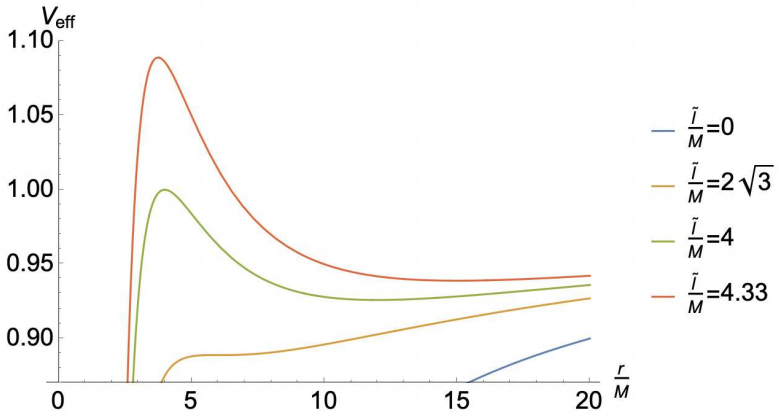

Figure 2.1: Effective potential for a massive particle in the Schwarzschild spacetime. The potential extrema arise when $\tilde{l} \geq 2\sqrt{3}M$.

Observe that, for $\tilde{l} \geq 4M$, an ingoing particle which has energy $\tilde{E} = E/m \sim 1$(i.e. non-relativistic particle at infinity) is reflected by a centrifugal force barrier without falling into the event horizon. This threshold can be derived from the condition that a maximum of the effective potential is equal to 1. Let us express this bound in terms of the impact parameter for a test particle. Firstly, we define the impact parameter as follows: Consider an ingoing particle toward a BH as shown in Fig.2.2. The closest distance between a BH and the dashed line corresponds to the impact parameter, and it can be written as $r \sin\phi = b$. Since initially a particle is placed at $r \to \infty$, this can also be written as $b = r\phi$ with good accuracy. Here the RHS should be written in terms of other conserved quantities E, l because the impact parameter is constant by definition. To observe that, we utilize the EoM for ϕ and t given by

$$r^2 \frac{d\phi}{d\lambda} = l, \quad \frac{dt}{d\lambda} = E, \qquad \text{at r} \to \infty, \tag{2.14}$$

respectively. The quotient of these two EoM becomes

$$\frac{l}{E} = r^2 \frac{d\phi}{dt}, \qquad \text{at r} \to \infty. \tag{2.15}$$

Substituting the definition of the impact parameter $b = r\phi$ for (2.15), we obtain

$$\begin{aligned}\frac{l}{E} &= r^2 \frac{d}{dt}\left(\frac{b}{r}\right) \\ &= -b\frac{dr}{dt} \\ &= -b\frac{dr/d\lambda}{dt/d\lambda} \\ &= \frac{b}{E}\sqrt{E^2 - m^2} \\ \rightarrow b &= \frac{l}{\sqrt{E^2 - m^2}},\end{aligned} \tag{2.16}$$

where we used the EoM for r at $r \to \infty$. Note that this result holds regardless of whether the incident particle is relativistic or not. Therefore, one can state that

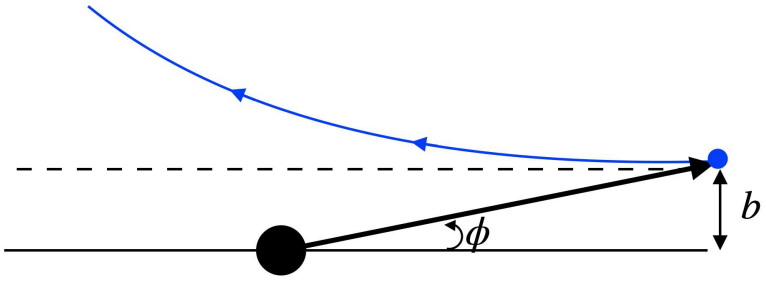

Figure 2.2: Black and blue circle represent a BH and a test particle. The dashed line shows the virtual trajectory if the test particle does not feel gravity. The impact parameter b is defined as the closest distance between the dashed line and the BH.

a massive ingoing particle with impact parameter $b < b_{\rm cap}$ falls into a black hole, where $b_{\rm cap}$ is defined by

$$b_{\rm cap} := \frac{4M}{\sqrt{\tilde{E}^2 - 1}}. \tag{2.17}$$

This defines the capture cross section viewed from infinity by

$$\sigma_{\rm cap} := \pi b_{\rm cap}^2 = \frac{16\pi M^2}{v_\infty^2}, \tag{2.18}$$

where $v_\infty \ll 1$ is velocity of the non-relativistic particle at infinity.

Now let us comment on the stable circular orbit which arises when $\tilde{l} \geq 2\sqrt{3}M$. The radius of this orbit is given by a larger solution of $dV_{\rm eff}/dr = 0$. We denote it

by r_+. Since extrema arise only when $\tilde{l} \geq 2\sqrt{3}M$, we obtain the lower bound for the radius of the stable circular orbit as

$$r_+ \geq 6M. \tag{2.19}$$

The smallest stable circular orbit for a massive particle $r = 6M$ is called the Innermost Stable Circular Orbit(ISCO). To get an intuition of how deep the gravitational potential of ISCO is, let us consider an ingoing massive particle that is nonrelativistic at infinity. Suppose that, by some mechanism, angular momentum and energy of this particle are transported while it falls toward a black hole, and the particle stabilizes at ISCO. Then, because of the energy conservation, the released energy can be estimated as

$$\text{Released energy} = -(\sqrt{V_{\text{eff}}(6M)} - 1) \sim 0.0572. \tag{2.20}$$

Therefore, as much as 5.72% of the rest mass energy would be released. For rotating black holes this efficiency maximally becomes 42.3%. In fact, as we see later, the energy extraction from the gravitational potential is realized by the viscosity of the accretion disk surrounding a BH. In the following chapter, we sometimes assume the energy efficiency of the accretion disk as 0.1 for a rough estimation of the accretion rate $\dot{M}$, etc..

2.3 Trajectory of Massless Particle

Turn now to the trajectory of a massless test particle around the Schwarzschild BH. As we see in the previous section, to derive the EoM for r, it is easier to use the normalization of the four-momentum. Substituting the conservation law (2.6) and (2.7) into $p_\mu p^\mu = 0$, we obtain radial EoM for massless particle as

$$\left(\frac{dr}{d\lambda}\right)^2 = E^2 - \frac{l^2}{r^2} f(r). \tag{2.21}$$

This together with (2.6) and (2.7) gives the complete description of the massless particle's trajectory in the Schwarzschild spacetime. Note that, from the equivalence principle, the trajectory of a massless particle does not depend on its energy E. To make this fact explicit, let us perform reparameterization $\lambda \to \lambda' = E\lambda$, then we obtain

$$\left(\frac{dr}{d\lambda'}\right)^2 = 1 - V_{\text{eff}}^{\text{massless}}(r), \tag{2.22}$$

$$V_{\text{eff}}^{\text{massless}}(r) = \frac{b^2}{r^2} f(r), \tag{2.23}$$

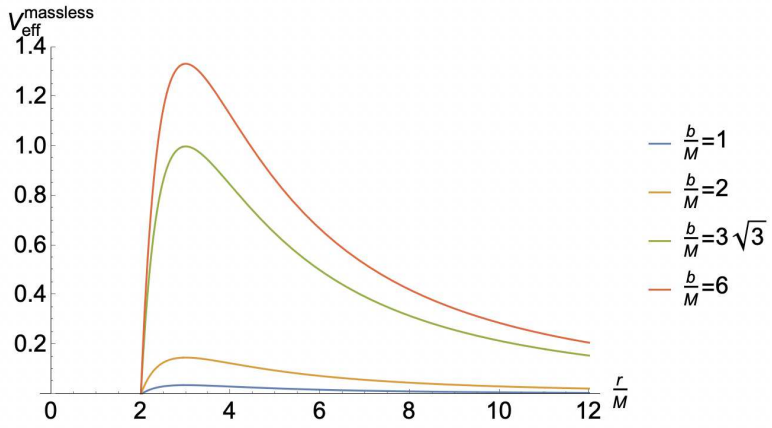

Figure 2.3: Effective potential for a massless particle in the Schwarzschild spacetime.

where we introduce the impact parameter by $b = l/E$. The plot of the effective potential for a massless particle is shown in Figure 2.3.

Observe that there is the critical impact parameter $b_{\text{crit}} := 3\sqrt{3}M$. Below it, an ingoing massless particle falls into the event horizon. Also, observe that a massless particle with the critical impact parameter has an unstable circular orbit at the top of the effective potential. This circular orbit is called a photon sphere, it is located at $r = 3M$.

In the next section, we will estimate the orbiting time in the vicinity of the photon sphere. To this aim, it is more convenient to parametrize the world line by the Schwarzschild time t instead of the affine parameter λ. Then the EoM becomes

$$\frac{dr}{dt} = \pm f(r)\sqrt{1 - \frac{b^2 f(r)}{r^2}}, \tag{2.24}$$

$$\frac{d\phi}{dt} = \frac{bf(r)}{r^2}, \tag{2.25}$$

where the $+(-)$sign corresponds to outward(inward) motion with respect to a black hole. Now we give some remark on (2.24). As we mentioned, (2.24) describe outward and inward radial motion separately. Because of this, it is difficult to treat the trajectory which initially falls toward the event horizon and at some point is reflected by the potential barrier, and then flies away to infinity. The complete description of such an orbit is possible by using the second derivative form of (2.24) given by

$$\frac{d^2r}{dt^2} + \frac{f^{-1}}{r}\left(1 - \frac{5M}{r}\right)\left(\frac{dr}{dt}\right)^2 = \frac{f}{r}\left(1 - \frac{3M}{r}\right). \tag{2.26}$$

This equation can be derived by differentiating (2.24) with respect to t and eliminating the impact parameter b.

Now, as an important example where an analytic approach is possible, we shall discuss the trajectory with the critical impact parameter $b = b_{\rm crit} = 3\sqrt{3}M$. In this case (2.24) becomes

$$\frac{dt}{dr} = \pm\frac{r^{5/2}}{(r-2M)(r-3M)\sqrt{r+6M}}. \tag{2.27}$$

As we expected, this EoM has a solution corresponding to the photon sphere $r(t) = 3M$ which makes both RHS and LHS divergent. More precise information can be obtained by solving (2.27) analytically. The exact solution is given by

$$\begin{aligned} &t(r) = \pm F(r) + \text{const.}, \\ &F(r) := \sqrt{r(r+6M)} + 4M\log\left(\sqrt{\frac{r}{M}} + \sqrt{\frac{r}{M}+6}\right) + 2M\log\left(\frac{2\sqrt{r}+\sqrt{r+6M}}{2\sqrt{r}-\sqrt{r+6M}}\right) \\ &\qquad - 3\sqrt{3}M\log\left|\frac{\sqrt{3r}+\sqrt{r+6M}}{\sqrt{3r}-\sqrt{r+6M}}\right|, \end{aligned} \tag{2.28}$$

where the order of sign corresponds with that of (2.27). Since the last term of $F(r)$ diverges at $r = 3M$, solution (2.28) cannot cross $r = 3M$. Therefore solution $t = +F(r)$ can be divided into two part $t = +F^{\rm out}(r) := +F(r)|_{3M<r<\infty}$ and $t = +F^{\rm in}(r) := +F(r)|_{2M<r<3M}$. The solution $t = +F^{\rm out}(r)$ corresponds to the trajectory which orbits the photon sphere at $t \to -\infty$ and escapes to infinity at $t \to \infty$. On the other hand, $t = +F^{\rm in}$ corresponds to the trajectory which orbits the photon sphere at $t \to -\infty$ and falls into the event horizon at $t \to \infty$. Similarly there are two independent part in $t = -F(r)$ defined by $t = -F^{\rm out}(r)$ and $t = -F^{\rm in}(r)$. These are just the time reversal of $t = +F^{\rm out}$ and $t = +F^{\rm in}$ respectively. Among these four solutions of (2.27), $t = \pm F^{\rm out}$ have special importance to describe the trajectory which flies away to infinity after temporarily orbiting the photon sphere. We will discuss this topic in the next section.

As a preliminary exercise for the next section, let us derive the asymptotic form of $t = F^{(\rm out)}(r) + \text{const.}$ in the vicinity of the photon sphere ($r = 3M$). For $r \to 3M$, (2.28) becomes

$$r - 3M \sim M\exp\left(\frac{t - C - \text{const.}}{3\sqrt{3}M}\right), \tag{2.29}$$

$$C := 3\sqrt{3}M + 4M\log\left(3+\sqrt{3}\right) + 2M\log\left(\frac{2\sqrt{3}+3}{2\sqrt{3}-3}\right) - 3\sqrt{3}M\log 18, \tag{2.30}$$

where const. is the same initial constant in (2.28). The above asymptotic formula is only valid when $t \ll -M$.

2.4 Asymptotic Behavior in the vicinity of the Photon Sphere

In this short section, we focus on the trajectory that initially falls from infinity toward a black hole, then orbits around $r \sim 3M$ over a finite period of time, and finally flies back toward infinity. As we discuss later, in the context of GWs from a supermassive black hole through the photon graviton conversion, this trajectory dominates the total GW luminosity. In order to calculate the conversion rate, the orbiting time around the photon sphere is essential. Motivated by this, below we will derive the formula of orbiting time around the photon sphere.

Firstly let us approximately construct the trajectory explained above by a superposition of two exact solutions as follows: In the infalling phase, the orbit is well approximated by the exact solution with $b = b_{\rm crit}$, that is $t = -F^{\rm out}(r) := G(r)$. For convenience, we use the equivalent form $r - 3M = \tilde{G}(t)$ (this is obtained by solving $t = G(r)$ with respect to r). Similarly escaping phase is well approximated by $t = F^{\rm out}(r) := F(r)$, equivalently $r - 3M = \tilde{F}(t)$. Then intuitively, it is expected that the trajectory we consider here can be constructed by plugging the infalling solution $\tilde{G}(t)$ and the escaping solution $\tilde{F}(t)$ with some orbiting time duration as follows:

$$r - 3M = \tilde{F}(t) + \tilde{G}(t + D), \tag{2.31}$$

where D is a constant time shift that is related to the orbiting time.

In the vicinity of the photon sphere($r = 3M$), this trajectory can be approximated as

$$\delta r := r - 3M \sim M \left[\exp\left(\frac{t - C}{3\sqrt{3}M} \right) + \exp\left(\frac{-(t + D) - C}{3\sqrt{3}M} \right) \right]. \tag{2.32}$$

Note that this asymptotic form solves the linearized version of EoM (2.26)

$$\frac{d^2 \delta r}{dt^2} = \frac{1}{27M^2} \delta r, \tag{2.33}$$

where $\delta r / M \ll 1$.

Then let us determine the constant time shift D. Since, in the orbiting phase $dr/dt \sim 0$, EoM(2.24) is equivalent to $r^2 = b^2 f$ and it can be solved with respect to δr as

$$\delta r \sim \left(\frac{4}{3} \right)^{1/4} M^{1/2} \delta b^{1/2}, \tag{2.34}$$

where $\delta b := b - 3\sqrt{3}M$. By equating (2.34) and the minimum of (2.32), we obtain the time shift D as

$$D = -2C + \frac{3\sqrt{3}M}{2}\log 12 - 3\sqrt{3}M \log\left|\frac{\delta b}{M}\right|. \tag{2.35}$$

Substituting (2.35) for (2.32) gives

$$\delta r \sim M\left[\exp\left(\frac{t'}{3\sqrt{3}M}\right) + \exp\left(-\frac{t' + (-3\sqrt{3}M\log\left|\frac{\delta b}{\sqrt{12}M}\right|)}{3\sqrt{3}M}\right)\right], \tag{2.36}$$

where $t' := t - C$. From this equation, we conclude that the light ray is trapped in $3M < r \ll 4M$ over the time interval

$$T(b) = -3\sqrt{3}M\log\left|\frac{b - b_{\rm crit}}{2\sqrt{3}M}\right|. \tag{2.37}$$

Note that this is the time interval measured by the Schwarzschild time(or the observer at infinity).

Chapter 3

Accretion Onto Black Holes

In the previous chapter, we discussed the motion of a freely moving particle around a BH. Here we move on to the next step, the fluid dynamics around the BH. As we will see later, the viscous fluid around a BH serves as the efficient converter of gravitational energy to radiation energy. This structure is the so-called accretion disk. In our work, the huge luminosity from the accretion disk is supplied to the photon sphere, enhancing the graviton production through the photon graviton conversion.

3.1 Introduction to Accretion Disks

In the early 1960s, star-like bright objects 3C273[1] was discovered with Balmer series emission lines which are shifted from the laboratory experiment value. After that many similar objects were found, and they are named the "Quasars(quasi-stellar-objects)". Here, focusing on typical quasar 3C273, let us start with an overview of the quasar's properties.

The shifted Balmer series implies 3C273 resides in the extra galaxy with redshift $z \sim 0.158$ [42]. The fact that quasar 3C273 is comparably bright to a galactic star even though it is very far away suggests that it has huge luminosity. Its bolometric luminosity is estimated as $L_{\rm bol} \sim 10^{47}{\rm erg\,sec}^{-1}$ [43]. Then how this extremely high luminosity is realized? Today it is well confirmed that the huge luminosity of 3C273 comes from viscous gas surrounding the supermassive black hole with mass $\sim 6.59 \times 10^9 M_\odot$ [43]. Indeed, the Eddington luminosity of supermassive black holes can realize this value as

$$L_{\rm Edd} := \frac{4\pi c G M m_{\rm p}}{\sigma_{\rm T}} \sim 1.26 \times 10^{47}{\rm erg\,sec}^{-1} \left(\frac{M}{10^9 M_\odot}\right). \tag{3.1}$$

[1]Here 3C refers to the 3C catalog. This is the third radio source catalog surveyed by Cambridge University

Now, let us define the Eddington accretion rate for later convenience. It is defined by

$$L_{\rm Edd} = \frac{1}{10}\dot{M}_{\rm Edd}c^2$$
$$\rightarrow \dot{M}_{\rm Edd} \sim 7.05 \times 10^{-7} M_\odot {\rm sec}^{-1} \left(\frac{M}{10^9 M_\odot}\right) = 22.2 M_\odot {\rm yr}^{-1} \left(\frac{M}{10^9 M_\odot}\right). \quad (3.2)$$

where we assumed the energy efficiency of the accretion disk as 10%. Note that there are many conventions, for example, some literature takes efficiency as 1/12 or 1/16(see (2.20) and the sentence below it).

Fig.3.1 is the multi-wavelength spectral energy distribution(SED) of 3C273. As one can see from this, there is optical-UV excess, the so-called blue bump in the spectrum. This behavior is very common in various galactic centers. The aim of the next section is to understand this feature from the optically thick, geometrically thin standard accretion disk theory developed in the 1970s [33–35].

On the other hand, there is also a peak around the X-ray band. This high energy and non-thermal emission cannot be explained by the optically thick standard disk theory. It is expected that these are comes from the inverse Compton scattering of low-energy photons by high-energy electrons or the thermal bremsstrahlung. Another kind of accretion flow so-called advection dominated accretion flow(ADAF) [36–38], is Virialy hot and explains the origin of the high-energy thermal electrons. We will review this flow in Section 3.3.

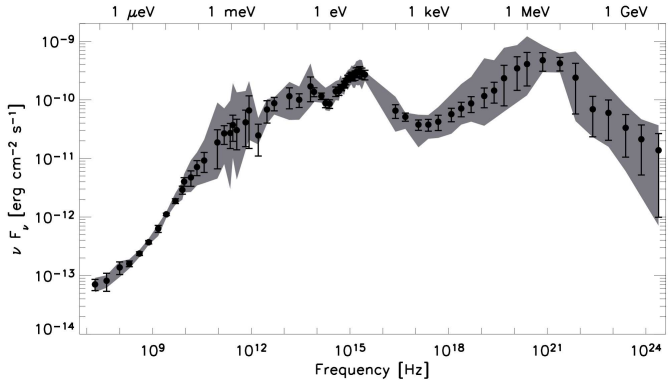

Figure 3.1: The multi-wavelength spectral energy distribution(SED) of 3C273, spanning from 4 to 44 years of observations from [44]. The distance to 3C273 is $d = cz/H_0 \sim 0.146 \times 10^{28} h_0^{-1}$cm. Therefore the typical energy flux $\nu F_\nu = 10^{-10}$ergcm^{-2}sec^{-1} correspond to luminosity $\nu L_\nu \sim 0.3 h_0^{-2} 10^{46}$ergsec^{-1}.

Note that in generally speaking, we cannot explain the observed real spectrum of galactic center by a single type of accretion flow discussed so far. The real

accretion disks are considered to be composed of several distinct types of accretion flows. We will discuss the possible geometry of the accretion disk in Section 3.4.

3.2 Standard Accretion Disk Model

Let us start with the basic and old accretion disk theory. That is the optically thick, geometrically thin, cold accretion disk, so-called standard accretion disk [33–35]. The first problem is how to convert the large gravitational potential energy into observed high radiative energy.

3.2.1 The Role of Viscosity

To realize an observed bright accretion, we need to add the dispersion process from gravitational energy to heat, that is the viscosity. As we see below, viscosity causes angular momentum transport and provides an explanation as to why spread accretion disks are formed. Let us start with an observation of how viscosity work in two parallel fluid with different velocity.

(**Parallel shear flow**)
Consider a parallel flow with two layers of different velocity as in Fig.3.2. We denote lower flow as flow1 and upper flow as flow2. There is friction between the two layers. Since $v_1 > v_2$, lower flow fells friction force to $-x$ direction. This friction force causes momentum to decrease following newton's equation of motion by $\Delta p_1 < 0$, where we take the positive direction of momentum to be $+x$ direction. Then, as expected, we conclude that because of viscosity, there is momentum transport from the fast layer to the slow layer. Eventually, the velocity field of fluid becomes uniform. In summary, we can state that for parallel shear flow, viscosity works so that velocity difference vanishes.

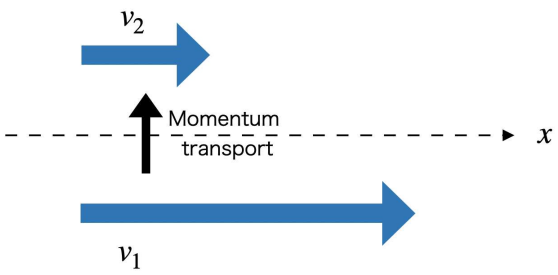

Figure 3.2: The parallel shear flow with two layers. The dashed line represents the boundary on which friction works.

(**Rotating shear flow**)
Remarkably, in the case of rotating shear flow, viscosity works the opposite way compared to a parallel shear flow. It is natural to consider a rotating two-layer flow whose inner layer is faster than the outer layer as in Fig.3.3. For example, in the case of Keplerian rotation realize this setting, because the azimuthal velocity is given by $v_\phi = \sqrt{GM/r}$. As in the case of parallel shear flow, there is friction force on the boundary. The friction force produces torque $\vec{r} \times \vec{F}$ and changes angular momentum $\vec{L}$ for each layer by $\frac{d\vec{L}}{dt} = \vec{r} \times \vec{F}$. Since the torque acting on the inner layer is negative, we conclude that there is angular momentum transport from the quickly rotating inner layer to the slowly rotating outer layer due to the viscosity. The discussion so far is parallel to the previous example, but the difference arises

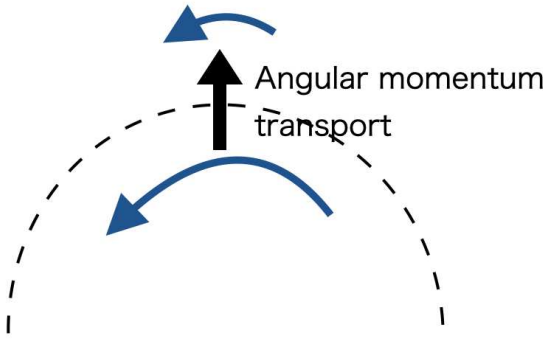

Figure 3.3: The rotating shear flow with two layers. The dashed line represents the boundary on which friction works.

at the point of how the matter moves after the exchange of the angular momentum. In the outer layer, the centrifugal force barrier of the effective potential increase in association with the increase of angular momentum(see Fig.2.1). Therefore matter in the outer layer is driven outward and its azimuthal velocity decreases following Keplerian rotation law. Conversely, the inner layer lost angular momentum, so the centrifugal force barrier decreases. This permits the inner layer to fall toward the central object. Then again from Keplerian rotation law, the inner layer rotating more faster. In summary, we can state that for rotating shear flow, the viscosity works so that the velocity difference grows. Also, observe that the outer layer that obtains angular momentum spread outward because of the centrifugal force barrier. This fact implies that if there are rotating compact objects in a viscous gas medium, the formation of a disk-like structure where gas spreads outward is inevitable.

3.2.2 Basic Equations

In the previous subsection, we see that viscosity causes angular momentum transport outward, and subsequently matter accretes toward a central black hole. Now we will describe this mechanism more quantitatively. Let us start with the equation of continuity for mass.

(**Mass conservation**)
In the following discussion, we shall assume axisymmetric geometry for the accretion disk and introduce the cylindrical coordinates (r, ϕ, z). Let us consider the ring zone at r with a radial thickness Δr. Its cross-sectional view in $z =$ const. plane is shown in Fig. 3.4. The total mass in this fixed ring zone is given by

$$\text{Total mass in the ring at } r = 2\pi r \Delta r \Sigma(t, r), \qquad \Sigma(t, r) := \int_{-\infty}^{\infty} dz \rho, \tag{3.3}$$

where ρ is the mass density per unit volume and $\Sigma(t, r)$ is called the surface density. Here we assume accretion with the radial speed $v_r < 0$, then the mass pass through the cylinder with radius r per unit time is given by $\dot{M}(t, r) = 2\pi r(-v_r)\Sigma(r, t)$. This is called the accretion rate. By using these quantities, mass conservation in a ring at r can be expressed as

$$\begin{aligned} &\frac{\partial}{\partial t}\left(2\pi r \Delta r \Sigma(t, r)\right) = \dot{M}(t, r + \Delta r) - \dot{M}(t, r) \\ \rightarrow\ &\frac{\partial \Sigma}{\partial t} = \frac{1}{2\pi r}\frac{\partial \dot{M}}{\partial r}. \end{aligned} \tag{3.4}$$

Therefore a radial inhomogeneity of the accretion rate results in unsteady mass density.

(**Angular momentum conservation**)
Let us move to describe the angular momentum transport. We again focus on the ring zone at r with a radial thickness Δr. The ring carries the angular momentum amount of $2\pi r \Delta r \Sigma(t, r) r^2 \Omega$. Note that we consider angular velocity Ω independent of t but depend on r. There are two types of contributions that gives the change in angular momentum of the ring. The first one is the torque by friction acting on the surface of the ring. The friction force along ϕ direction per infinitesimal area is given by $df_j \sigma'^{\phi j}$, where σ'^{ij} is shear stress tensor(see Appendix A.2 for definition). The vector df_j is the surface element vector which is normal to the infinitesimal area in question. Then, the total torque acting on the inner surface of the ring(

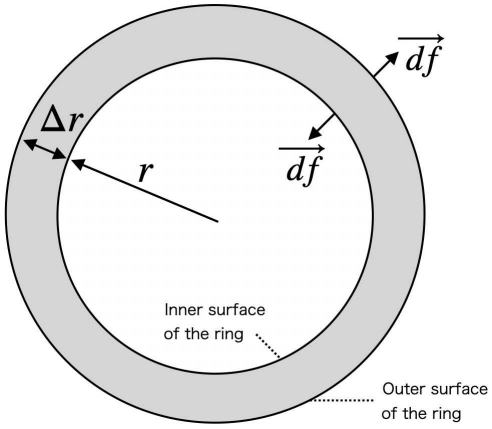

Figure 3.4: View of the accretion disk looking down from z axis. The circle of radius r corresponds to the cylinder with radius r and infinite height.

i.e. cylinder with radius r) becomes [2]

$$\text{Torque acts on the inner surface of the ring} = \int r(-rd\phi\, dz)\sigma'^{\phi r}$$
$$= -2\pi r\nu\Sigma r^2\frac{d\Omega}{dr} := -G(t,r), \quad (3.5)$$

where we defined the torque function $G(t,r)$. The coefficient ν is the kinematic viscosity. By the same calculation, torque act on the outer surface of the ring becomes $G(t, r+\Delta r)$.

The remaining contribution to the angular momentum change of the ring is the inflow and outflow of an angular momentum carried by accreting gas. The angular momentum passing through the cylinder with radius r per unit time can be written as $\dot{M}(t,r)r\Omega r$. Combining the above two contributions, the change in angular momentum of the ring is

$$\frac{\partial}{\partial t}(2\pi r\Delta r\Sigma r^2\Omega) = \dot{M}(t,r+\Delta r)(r+\Delta r)^2\Omega - \dot{M}(t,r)r^2\Omega + G(t,r+\Delta r) - G(t,r)$$
$$\rightarrow \quad \dot{M}\frac{d}{dr}(r^2\Omega) = -\frac{\partial G}{\partial r}, \quad (3.6)$$

where we used the (3.4) to eliminate time derivative of Σ. Therefore if there is torque, mass accrete. So far, we obtained two equations (3.4) and (3.6). These are the quantitative expression of the observation in the previous section.

[2]Note the sign of surface element vector. As you can see from Fig.3.4, df_j on the inner surface is $rd\phi dz(-\vec{e}_r)$. On the other hand, for the outer surface, it is given by $(r+\Delta r)d\phi dz\,\vec{e}_r$, so the signs are reversed.

3.2.3 The Static Solution, Energy Balance, and Spectrum

Here we will derive the radiation spectrum for the static accretion disk. For this aim, firstly let us find a static solution of basic equations (3.4) and (3.6). Under the assumption of static configuration $\partial_t = 0$, the mass conservation law (3.4) becomes

$$\frac{\partial \dot{M}}{\partial r} = 0 \ \rightarrow \ \dot{M} = 2\pi r(-v_r)\Sigma = \text{const.}. \tag{3.7}$$

Then, the conservation law for angular momentum (3.6) can be integrated with respect to r, and one obtain the torque $G(r)$ as

$$G(r) = -\dot{M}\left(r^2\Omega(r) - r_*^2\Omega(r_*)\right), \tag{3.8}$$

where we impose the boundary condition $G(r_*) = 0$ at the star surface $r = r_*$. In the case of accretion onto a non-rotating black hole, we take $r_* = r_{\rm ISCO} = 3r_{\rm S}$, where $r_{\rm S} := 2GM/c^2$ is the Schwarzschild radius. Since the toque $G(r)$ is defined by (3.5), static solution (3.8) can be solved with respect to the combination $\nu\Sigma$ as

$$\nu\Sigma(r) = \frac{-\dot{M}}{2\pi r}\frac{\Omega(r) - (r_*/r)^2\Omega(r_*)}{d\Omega/dr}. \tag{3.9}$$

In the following discussion let us assume Keplerian rotation $\Omega(r) = \sqrt{GM/r^3}$. Then (3.9) becomes

$$\nu\Sigma(r) = \frac{\dot{M}}{3\pi}\left(1 - \sqrt{\frac{r_*}{r}}\right). \tag{3.10}$$

This expression of the static solution is useful to obtain the radiation spectrum.

Now let us move to energy balance in an accretion disk. In a disk, there is viscous friction along ϕ direction and it produces heat energy. For the unit volume element, produced heat energy per unit time is

$$\begin{aligned}\frac{\rho\nu}{2}\left(\partial_i v_k + \partial_k v_i\right)^2 &= \frac{\rho\nu}{2} \times 2\left(\partial_r v^\phi - \frac{v^\phi}{r}\right)^2 \\ &= \frac{9}{4}\nu\rho\Omega^2(r),\end{aligned} \tag{3.11}$$

where in the last line, we assumed Keplerian rotation. Let us consider the energy balance for a straight column region along z direction located at radial coordinates r. The cross-sectional area of this column is a unit area, and the bottom and top

surfaces coincide with the surface of the disk. Then the total energy produced in this column through friction is

$$Q^{+}_{\rm vis} := \int_{-\infty}^{\infty} dz \frac{9}{4}\nu\rho\Omega^2(r) = \frac{9}{4}\nu\Omega^2(r)\Sigma(r). \tag{3.12}$$

On the other hand, the energy release is caused by the radiation of photons from the top and bottom surfaces of the column. *Here we assume the standard accretion disk is optically thick*. Under the optically thick assumption, radiation inside the column goes into equilibrium through absorption and re-radiation by the thermal plasma. Therefore, the observed spectrum from the top and bottom surfaces of the column is the black body, and flux is given by the Stephan Boltzmann law as

$$Q^{-}_{\rm rad} = 2F(r) = 2\sigma_{\rm SB}T^4_{\rm eff}(r), \tag{3.13}$$

where factor 2 counts double contributions of the top and bottom surfaces. $\sigma_{\rm SB} \sim 5.670 \times 10^{-8}{\rm Wm^{-2}K^{-4}}$ is Stephan Boltzmann constant. Equating the heating and cooling process, the energy balance equation for the column region at r is given by

$$Q^{+}_{\rm vis} = Q^{-}_{\rm rad}. \tag{3.14}$$

One might notice here that the energy transport as thermal energy of accreting gas(advection) is missing. In fact, it is an important contribution that leads to the discovery of another accretion solution called the ADAF, which will be discussed in the next section. However, the standard disk model, we are now reviewing, is the model that ignores advection, and we will show in the next section that there exists a geometry(shape) of the disk that justifies this treatment.

The energy balance equation (3.14) can be solved with respect to effective temperature at r as

$$T^4_{\rm eff}(r) = \frac{3}{8\pi\sigma_{\rm SB}}\frac{GM\dot{M}}{r^3}\left(1 - \sqrt{\frac{r_*}{r}}\right). \tag{3.15}$$

From this equation, we find that at a large distance from the central black hole, the effective temperature obeys the simple power law

$$T_{\rm eff}(r) \propto r^{-3/4} \quad \text{for } r \gg r_*. \tag{3.16}$$

This is an important property of the standard accretion disk.

Now let us estimate the specific luminosity of the standard accretion disk. Since we assumed an optically thick disk, radiation from the disk surface is the black body radiation. Its specific intensity is given by the Planck function

$$B_f(T) = \frac{2hf^3/c^2}{\exp(hf/k_{\rm B}T) - 1}, \tag{3.17}$$

where f is the frequency of a photon. Note that the specific energy flux at the surface of a disk is $\pi B_f(T)$. [3] By integrating the specific flux over the entire surface of the disk, the specific luminosity of the disk can be obtained as

$$L_f := \int_0^{2\pi} d\phi \int_{3r_{\rm S}}^{r_{\rm max}} r dr \ \pi B_f(T_{\rm eff}(r)) \tag{3.18}$$

$$\sim 3.1 \times 10^{29}{\rm erg} \left(\frac{\dot{M}}{1M_\odot {\rm yr}^{-1}}\right)^{3/4} \left(\frac{M}{10^8 M_\odot}\right)^{1/2} \times \tilde{f}^3 \int_3^{\tilde{r}_{\rm max}} d\tilde{r} \frac{\tilde{r}}{\exp\left[\tilde{f}\left(\frac{\tilde{r}^3}{1-\sqrt{3/\tilde{r}}}\right)^{1/4}\right]-1}, \tag{3.19}$$

where we introduced the dimensionless radius $\tilde{r} := r/r_{\rm S}$ and frequency

$$\tilde{f} := \frac{f}{k_{\rm B}T_{\rm typ}/h}, \tag{3.20}$$

$$\text{with} \quad T_{\rm typ} := \left(\frac{3}{8\pi\sigma_{\rm SB}}\frac{GM\dot{M}}{r_{\rm S}^3}\right)^{1/4} \sim 5.11 \times 10^5 {\rm K} \left(\frac{\dot{M}}{1M_\odot {\rm yr}^{-1}}\right)^{1/4} \left(\frac{M}{10^8 M_\odot}\right)^{-1/2}. \tag{3.21}$$

Here each quantity is normalized with the quasars in mind. Its typical accretion rate $\dot{M}$ and mass M are given by $1M_\odot {\rm yr}^{-1}$ and $10^8 M_\odot$ respectively. The last integral of (3.19) can be implemented numerically. Here we take the outer edge of accretion disk $\tilde{r}_{\rm max}$ as 10^6. Also, to prevent the exponent in the integrand from divergence at the lower limit of the integral, we change the lower limit from $\tilde{r} = 3$ to $\tilde{r} = 3.001$. Fig.3.5 shows the specific luminosity of the standard accretion disk in the above setting. [4] Since, for typical quasars $k_{\rm B}T_{\rm typ}/h \sim 7.0$eV, specific luminosity has peak between 0.7eV $\sim$ 7eV(i.e. from optical to ultraviolet ray region). This peak is sometimes called the *blue bump*.

We would like to comment here on an important consequence of the standard accretion disk model. Within the framework of the standard accretion disk model, we can conclude that quasars(or AGN) are bright in infrared to ultraviolet and do not emit X-rays. However, real galactic centers have been observed with large luminosities up to hard X-rays. This fact motivated the development of ADAF, a model that can explain high-energy radiation from the accretion disk.

[3] Consider the spherical and isotropic light source such as a star with intensity(brightness) I_f. Then flux at star surface is given by simply πI_f.

[4] Note that specific luminosity has dimension of erg sec^{-1} Hz^{-1} = erg.

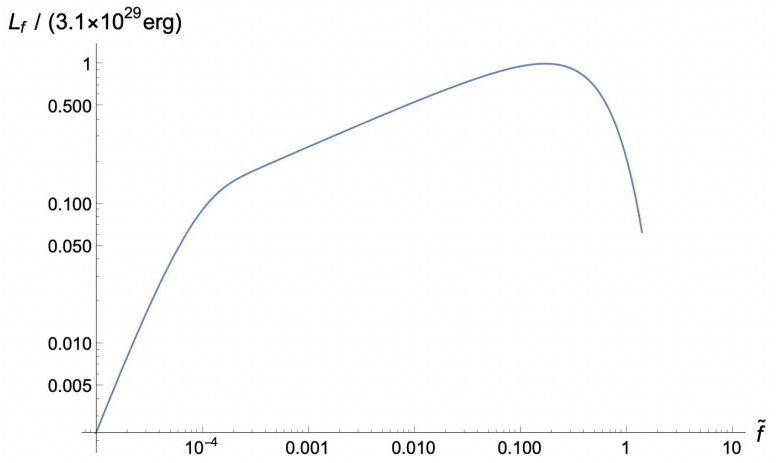

Figure 3.5: Radiation spectrum from typical quasars in the framework of standard accretion disk. We choose parameter as $\dot{M} = 1 M_\odot \mathrm{yr}^{-1}$ and $M = 10^8 M_\odot$ with quasars in mind.

3.2.4 The α Prescription for Viscosity and Geometric Structure of the Disk

In the previous section, we assumed the energy balance between viscosity heating and vertical radiation cooling as (3.14). However, its validity has not been proved. In the following discussion, we will show that there is a geometric shape of the disk which justify the energy balance equation (3.14).

Firstly, as a preparation, let us parametrize the vertical thickness of the disk via hydrostatic equilibrium. Assume the unit volume element at radial coordinate r and $z = H$ as in Fig.3.6. The vertical component of gravity and pressure act on the volume element are balanced and the vertical hydrostatic equilibrium is realized as

$$-\frac{dP}{dz} = -\frac{GM\rho}{r^2}\sin\theta. \tag{3.22}$$

By replacing d/dz with $1/H$ and solving this equation for H, we obtain the vertical half thickness of the disk under hydrostatic equilibrium as

$$H = \frac{1}{\Omega_\mathrm{K}}\sqrt{\frac{P}{\rho}} = \frac{c_\mathrm{s}}{\Omega_\mathrm{K}}, \tag{3.23}$$

with Keplerian rotation $\Omega_\mathrm{K}(r) := \sqrt{GM/r^3}$. In the last equal, we used the equation of state for idealized gas $P = c_\mathrm{s}^2\rho$. Since for idealized gas, $c_\mathrm{s} = \sqrt{k_\mathrm{B}T/\mu m_\mathrm{p}}$,

vertical thickness of the disk proportional to $\sqrt{T}$. This is a very intuitively understandable result, as heating an object causes it to expand. The following different form of (3.23) is also useful.

$$\frac{H}{r} = \frac{c_s}{v_{\rm K}}, \tag{3.24}$$

where $v_{\rm K} := r\Omega_{\rm K}$ is the velocity of Keplerian rotation.

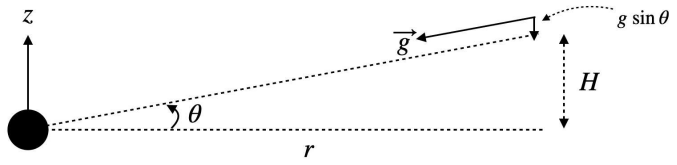

Figure 3.6: Schematic illustration of the disk at constant ϕ.

So far we used the kinematic viscosity ν, however, it is more convenient to use dimensionless viscosity α defined by [5]

$$\nu = \alpha c_{\rm s} H. \tag{3.25}$$

By this parametrization, the dimensionless viscosity α takes value in $0 < \alpha < 1$.

All preparations are now complete. To discuss energy balance, it is clear to identify the timescales of the processes present in the system. There are three time scales associated with the three spatial directions. The first one is the time scale of dynamical disk rotation,

$$t_{\rm dyn} := \Omega^{-1}. \tag{3.26}$$

The second one is the time scale for the vertical direction. Since the typical length and speed for vertical direction are H and $c_{\rm s}$ respectively, it is defined by

$$t_{\rm hyd} := \frac{H}{c_{\rm s}} = \Omega_{\rm K}^{-1}, \tag{3.27}$$

where in the last equal, we used hydrostatic relation for vertical direction (3.23). The last one is the time scale for radial direction, i.e. time scale of accretion. Since the accretion is triggered by the viscosity, it is given by

$$t_{\rm vis} := r^2\nu^{-1} = \alpha^{-1}\left(\frac{r}{H}\right)^2 \Omega_{\rm K}^{-1}, \tag{3.28}$$

[5] This parametrization is sometimes called the α prescription. It is first introduced by Shakura and Sunyaev [33].

where we used the α prescription for kinematic viscosity (3.25). Now let us compare three time scales $t_{\rm dyn}, t_{\rm hyd}$ and $t_{\rm vis}$ introduced above. In the standard disk model, we assume Keplerian rotation $\Omega = \Omega_{\rm K}$, the hierarchy of time scales is determined by the vertical thickness of disk H/r.

- **Geometrically thin case**: $H \ll r$
  In this case, $t_{\rm vis} \gg t_{\rm hyd} \sim t_{\rm dyn}$ is realized. This is the solution, in which heat transport by gas accretion can be negligible compared to the vertical radiative transfer of energy. Therefore, when $H \ll r$, the energy balance equation for standard disk $Q^+_{\rm vis} = Q^-_{\rm rad}$(see (3.14)) is justified. *We conclude that the standard disk should be geometrically thin.*

- **Geometrically thick case**: $H \gtrsim r$
  In this case, $t_{\rm hyd} \sim t_{\rm vis} \gtrsim \alpha t_{\rm vis}$ is realized. Therefore, heat transport by accreting gas is essential for a thick disk, and the energy equation for standard disk (3.14) cannot be applied. It should be corrected by introducing the advection term, i.e. heat transfer as the entropy of accreting gas. The advection process is dominant in the flow, called the ADAF. The ADAF has very different features compared to the standard disk, for example, it is optically thin and very hot.

At the end of this section, we give a short comment on the relationship between vertical thickness and temperature. The following relation is satisfied.

$$\left(\frac{H}{r}\right)^2 = \left(\frac{c_{\rm s}}{v_{\rm K}}\right)^2 = \frac{T}{T_{\rm vir}}, \tag{3.29}$$

with the Virial temperature

$$T_{\rm vir} := \frac{GM\mu m_{\rm p}}{r k_{\rm B}} \;=\; 0.27 \times 10^{13} \left(\frac{r_{\rm S}}{r}\right) {\rm K}, \tag{3.30}$$

where we used a sound speed for an ideal gas, μ is the mean molecular weight of gas(for simplicity, we used the value corresponding to the ionized hydrogen's case $\mu = 1/2$). The Virial temperature is the temperature realized when all released gravitational energy is converted to the thermal energy of gas without being radiated. For standard disk, (3.29) implies $T \ll T_{\rm vir}$. Therefore the standard disk is well-cooled by radiation.

3.3 Advection Dominated Accretion Flow(ADAF)

In the previous section, we review the standard disk model characterized by the energy equation $Q^+_{\rm vis} = Q^-_{\rm rad}$, where $Q^+_{\rm vis}$ is the viscous heating and $Q^-_{\rm rad}$ is the radiative cooling. It is known that the energy balance equation determines the properties of accretion flows and there are several types of accretion flows different from the standard disk depending on which cooling processes are dominant. In this section, we review the radiatively inefficient solution called the advection dominated accretion flow(ADAF) which is first discovered by Ichimaru [36] and rediscovered by Narayan et al via numerical simulation [37]. After that, Narayan and Yi derived the self-similar solution [38]. Since this self-similar solution provides a nice quantitative understanding of the ADAF, in the rest of this section, we give a review of ADAF based on [38]. Firstly, we postulate the following five assumptions for the dynamics of flow:

- The accretion flow has cylindrical geometry with height H. We handle vertically averaged equations. The surface density is $\Sigma = 2H\rho$,
- The flow is steady and axisymmetric, i.e. $\partial_t = \partial_\phi = 0$,
- A hydrostatic equilibrium holds for vertical direction of the flow $\rightarrow H = c_{\rm s}/\Omega_{\rm K}$,
- The Kinematic viscosity ν is parametrized by α prescription $\nu = \alpha c_{\rm s} H$,
- The gas pressure dominate the total pressure $P = c_{\rm s}^2\rho$,
- Almost all viscosity heating is converted to the thermal energy of plasma without being radiated,

where the first to fourth from the top is the same assumptions as we impose in the previous section. The other two assumptions are characteristics of (unmagnetized)ADAF. Note that in the following discussion, we do not assume the Keplerian rotation in advance as we do so in the previous section.

Under the above assumptions, the basic equations, mass conservation, angular momentum conservation, radial EoM, and energy equation, are given by

$$\frac{d}{dr}\left(-4\pi r v_{\rm r} H\rho\right) = 0, \tag{3.31}$$

$$\frac{d}{dr}(r^2\Omega) = \frac{d}{dr}\left(\frac{\alpha r^2 c_{\rm r}^2}{\Omega_{\rm K} v_{\rm r}}\frac{d\Omega}{dr}\right), \tag{3.32}$$

$$v_{\rm r}\frac{dv_{\rm r}}{dr} = r(\Omega^2 - \Omega_{\rm K}^2) - \frac{1}{\rho}\frac{dc_{\rm s}^2\rho}{dr}, \tag{3.33}$$

$$Q^+_{\rm vis} - Q^-_{\rm rad} = \Sigma v_{\rm r} T\frac{ds_{\rm gas}}{dr}, \tag{3.34}$$

respectively. Here $v_{\rm r}$ is the radial velocity, $\Omega_{\rm K} = \sqrt{GM/r^3}$ is angular velocity of the Keplerian rotation, $s_{\rm gas}$ is the entropy of gas per unit mass. The energy equation (3.34), describes the energy balance in the column with height H and unit cross-sectional area. The RHS of (3.34) is nothing else than the thermal energy divergence of gas in the column. It can be easily checked by the following transformation:

$$\int_V dV\vec{\nabla}\cdot(\rho s_{\rm gas}\vec{v}) = \int_{\partial V} d\Sigma_i \rho s_{\rm gas} v^i = \Sigma v_{\rm r}\frac{ds_{\rm gas}}{dr}, \tag{3.35}$$

where V and ∂V are the three dimensional column and its boundary, $\rho s_{\rm gas}\vec{v}$ is the gas entropy current. In the last equal of (3.35), we used the mass conservation law (3.31). Therefore (3.34) indeed contain the effect of heat transport as the form of gas entropy. To parametrize how much viscous heat is converted to the thermal energy of gas, we introduce the parameter f as

$$Q^+_{\rm vis} - Q^-_{\rm rad} = fQ^+_{\rm vis} = f\frac{2\alpha\rho r^2 c_{\rm s}^3}{\Omega_{\rm K}^2}\left(\frac{d\Omega}{dr}\right)^2, \tag{3.36}$$

where we used the formula of viscous heat produced in the unit volume per unit time (3.11). Note that here we did not assume the Keplerian rotation. The parameter f takes value in $0 \le f \le 1$ and generally depends on radial coordinate r. However, for simplicity, we assume f is constant everywhere. This assumption is reasonable for ADAF whose cooling process is dominated by advection(energy transfer as the thermal energy of gas) and $f \sim 1$ is realized everywhere. If we assume an ideal gas, the RHS of (3.34) can be written in terms of $c_{\rm s}$ and the mass density ρ, by using formula

$$\frac{ds_{\rm gas}}{dr} = \frac{1}{\gamma-1}\frac{1}{T}\frac{dc_{\rm s^2}}{dr} - \frac{c_{\rm s}^2}{\rho T}\frac{d\rho}{dr}, \tag{3.37}$$

see Appendix A.3. Here $\gamma = c_{\rm P}/c_{\rm V}$ is the ratio of specific heat. Combining (3.34), (3.36) and (3.37) the energy equation of ADAF can be rewritten as

$$(3+3\epsilon)\frac{c_{\rm s}\rho v_{\rm r}}{\Omega_{\rm K}}\frac{dc_{\rm s}^2}{dr} - 2\frac{v_{\rm r}c_{\rm s}^3}{\Omega_{\rm K}}\frac{d\rho}{dr} = f\frac{2\alpha\rho r^2 c_{\rm s}^3}{\Omega_{\rm K}^2}\left(\frac{d\Omega}{dr}\right)^2, \tag{3.38}$$

where we defined ϵ by $\epsilon = (5/3-\gamma)/(\gamma-1)$. For monoatomic gas $\gamma = 5/3$, $\epsilon \to 0$.

Now let us move on to the derivation of self-similar solution of the equations (3.31),(3.32), (3.33), (3.38) with respect to four unknown variables $v_{\rm r}, \rho, \Omega, c_{\rm s}$. As one can easily show, these four equation has the following radial scale symmetry

$$r \to Ar,\ v_{\rm r} \to A^{-1/2}v_{\rm r},\ \rho \to A^{-3/2}\rho,\ c_{\rm s} \to A^{-1/2}c_{\rm s},\ \Omega \to A^{-3/2}\Omega, \tag{3.39}$$

with an arbitrary constant A. This symmetry implies that there is a solution in the form

$$v_{\rm r} = C_1 r^{-1/2},\ \rho = C_2 r^{-3/2},\ c_{\rm s} = C_3 r^{-1/2},\ \Omega = C_4 r^{-3/2}, \tag{3.40}$$

with constant C_1, C_2, C_3, C_4. Substituting the ansatz (3.40) for four basic equations we obtain the self-similar solution of ADAF as

$$v_{\rm r} = -(5+2\epsilon')\frac{g(\alpha,\epsilon')}{3\alpha}v_{\rm K}, \tag{3.41}$$

$$\Omega = \left(\frac{2\epsilon'(5+2\epsilon')g(\alpha,\epsilon')}{9\alpha^2}\right)^{1/2}\Omega_{\rm K}, \tag{3.42}$$

$$c_{\rm s} = \frac{\sqrt{2(5+2\epsilon')g(\alpha,\epsilon')}}{3\alpha}v_{\rm K}, \tag{3.43}$$

$$\text{with}\quad g(\alpha,\epsilon') := \left(1+\frac{18\alpha^2}{(5+2\epsilon')^2}\right)^{1/2} - 1, \tag{3.44}$$

where $\epsilon' := \epsilon/f$, $v_{\rm K} := \sqrt{GM/r}$ is the Keplerian velocity. The mass density can be obtained from the integrated form of (3.31) that is $-4\pi r H \rho v_{\rm r} = \dot{M} = \text{const.}$. Since $\alpha \ll 1$ usually holds, the above self-similar solutions reduce to

$$v_{\rm r} \sim -\frac{3\alpha}{5+2\epsilon'}v_{\rm K}, \tag{3.45}$$

$$\Omega \sim \left(\frac{2\epsilon'}{5+2\epsilon'}\right)^{1/2}\Omega_{\rm K}, \tag{3.46}$$

$$c_{\rm s} \sim \sqrt{\frac{2}{5+2\epsilon'}}v_{\rm K}. \tag{3.47}$$

Observe that for ADAF($f \sim 1$) of monoatomic gas($\epsilon \to 0$), the self similar solution becomes

$$v_{\rm r} \sim -\frac{3\alpha}{5}v_{\rm K}, \tag{3.48}$$

$$\Omega \sim \sqrt{\frac{2\epsilon}{5}}\Omega_{\rm K} \ll \Omega_{\rm K}, \tag{3.49}$$

$$c_{\rm s} \sim \sqrt{\frac{2}{5}}v_{\rm K}. \tag{3.50}$$

Since the relation (3.29) does not depend on the energy equation, it also holds for ADAF. Therefore, the self-similar solution (3.50) implies that ADAF is geometrically thick $H \sim r$ and hot comparable to Virial temperature $T \sim T_{\rm vir}$. The

temperature of the ADAF maximally becomes $10^{12}\mathrm{K} \sim 10^{8}\mathrm{eV}$. This implies that, unlike the standard disk, ADAF can radiate a sufficient amount of hard X-rays and gamma-rays as the thermal bremsstrahlung, etc..

The self-similar solution of the ADAF implies that ADAF has a tendency to emit an outflow. Let us qualitatively observe this property. Firstly, substituting the self-similar solution (3.40) for radial EoM (3.33), one can derive [6]

$$\frac{1}{2}v_{\mathrm{r}}^2 + r^2\left(\Omega^2 - \Omega_{\mathrm{K}}^2\right) + \frac{5}{2}c_{\mathrm{s}}^2 = 0. \tag{3.52}$$

Secondly, we define the normalized Bernoulli parameter as follows:

$$\frac{\mathrm{Be}}{v_{\mathrm{K}}^2} := \frac{1}{v_{\mathrm{K}}^2}\left\{\frac{1}{2}v_{\mathrm{r}}^2 + \frac{1}{2}(\Omega r)^2 - r^2\Omega_{\mathrm{K}}^2 + \frac{\gamma}{\gamma-1}c_{\mathrm{s}}^2\right\} \tag{3.53}$$

Be denotes the original Bernoulli parameter. The first and second terms of the Bernoulli parameter correspond to the kinetic energy of the fluid particle. The third term corresponds to Newtonian gravitational potential energy. The fourth term is the enthalpy w of the fluid particle defined by [7]

$$w := u + p\frac{1}{\rho}, \tag{3.54}$$

where u is the internal energy per unit mass, $1/\rho$ is the specific volume(volume occupied by unit mass). Substituting (A.19) and (A.21) for (3.54), one can rewrite the enthalpy as

$$w = \frac{\gamma}{\gamma-1}c_{\mathrm{s}}^2. \tag{3.55}$$

Now, substituting (3.52) for (3.53) and using the self-similar solution (3.45), (3.46),(3.47), one can rewrite the Bernoulli parameter as

$$\frac{\mathrm{Be}}{v_{\mathrm{K}}^2} = \frac{3\epsilon - \epsilon'}{5 + 2\epsilon'}. \tag{3.56}$$

[6] In this calculation, we replace the derivative with respect to r with $1/r$. For example, the derivative of radial speed $v_{\mathrm{r}} = C_1 r^{-1/2}$ becomes

$$\frac{dv_{\mathrm{r}}}{dr} = -\frac{1}{2}\frac{v_{\mathrm{r}}}{r}. \tag{3.51}$$

[7] Enthalpy(per unit mass) has the physical meaning of energy stored when a unit volume of a fluid particle is injected into a fluid with pressure p. A fluid particle of a given volume ΔV can be considered to have a potential energy of $p\Delta V$ due to the ambient pressure, just by existing in the fluid.

Observe that when $f > 1/3$ the Bernoulli parameter becomes positive. The Bernoulli parameter has a physical meaning of the total energy of a fluid particle plus potential due to ambient pressure, and is conserved along the streamline if the flow is adiabatic. Therefore its positivity implies that in ADAF if a particle moves away from the BH in some way, it can reach infinity with a positive energy. This strongly suggests that ADAF is related to jets and other outflows.

3.4 Geometry of Accretion Disks

In this section, we review the possible geometry of a real accretion disk. Firstly let us start with the SED of our galactic center SgrA*(see Fig.3.7). It is the supermassive black hole with mass $M = 4.14 \times 10^6 M_\odot$ [45]. The outstanding feature of the SgrA* spectrum is its extremely low luminosity. Its fraction to Eddington luminosity is only $10^{34}\mathrm{ergsec}^{-1}/L_{\mathrm{Edd}} \sim 10^{-11}$. In addition, there is no optical-UV excess(blue bump) as seen in the SED of typical quasar 3C273(Fig. 3.1). These two facts imply the absence of optically thick standard disks at small radii of the SgrA*. Instead of the optically thick disk, because of its low luminosity feature, it is natural to assume that a radiatively inefficient hot disk such as ADAF dominates small radii of SgrA*. In Fig.3.7, the thick line shows the ADAF model spectrum. It matches well with the observations.

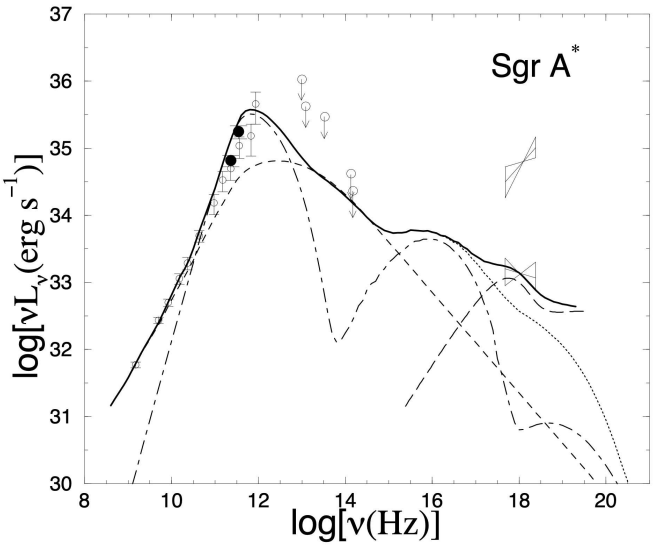

Figure 3.7: SED of SgrA* with ADAF model spectrum(thick solid line) from [46]. Two bowties represent X-ray data in the quiescent state(below) and flare(above).

There is another type of galactic center called the X-ray bright, optically nor-

mal galaxies(XBONGs). Their prominent features are no nuclear signature in the optical spectrum and brightness in the X-ray band. Some of them are considered to be obscured AGNs, but this scenario does not explain all of them. The other possible and simple scenario is the radiatively inefficient disk at small radii. Because the weak optical spectrum implies an absence of the optically thick standard disk at small radii, this scenario is natural. Yuan et al. show that the simple accretion disk geometry, inner ADAF plus outer optically thick standard disk explains the observed SED of two of the XBONGs(Source1 and P3) [47]. In their model, two distinct disks are connected at transition radius $r_{\rm tr}$. Fig.3.8 shows the spectral fit of the Source1 by their model with $r_{\rm tr} \sim 40, 60\, r_{\rm S}$.

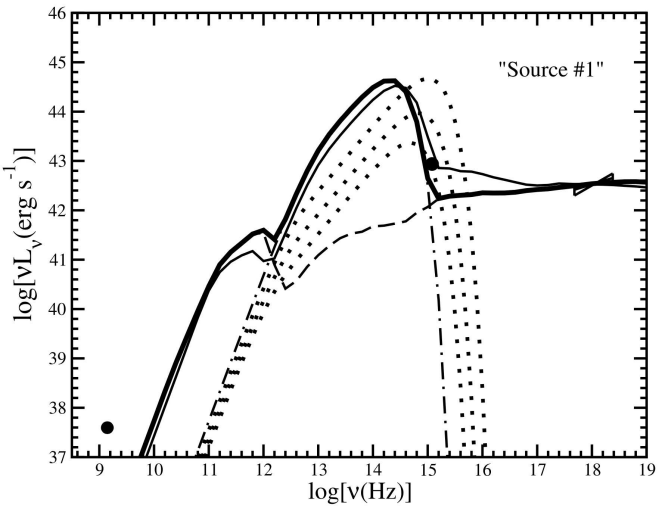

Figure 3.8: Spectral fit of the XBONGs Source 1 with the inner ADAF model from [47]. The thick solid line shows the combined spectrum from the standard disk for radii $r > 60r_{\rm S}$(dot-dashed line) and an ADAF for $r < 60r_{\rm S}$(dashed line), incorporating the mass loss. The thin solid line also shows the result of the inner ADAF model with the constant accretion rate and the transition radius $r_{\rm tr} = 40r_{\rm S}$. The three dotted lines show the spectrums from pure standard disks down to ISCO with $\dot{M}/\dot{M}_{\rm Edd} = 5 \times 10^{-5}, 2 \times 10^{-4}$, and 10^{-3} from bottom to top. These are excluded because they cannot reproduce the observed X-ray spectrum.
As a side note, Source1 is the XBONG with central black hole mass $\sim 3 \times 10^9 M_\odot$. Its X-ray luminosity is $L_{\text{2-10keV}} \sim 5.6 \times 10^{42}\text{ergsec}^{-1}$.

Finally, as we saw in section3.1, SED of 3C273(Fig. 3.1) shows the thermal signature of the optically thick standard disk so-called blue bump. Therefore a large part of a quasar's accretion disk might be dominated by the standard disk. The above observations naturally lead to the inner ADAF paradigm for various types of accretions(Fig.3.9). The simple geometry of accretion disk which explains

many types of galaxies such as LLAGN, XBONGs, and Quasars. The transition radius $r_{\rm tr}$ is controlled by the accretion rate $\dot{M}$.

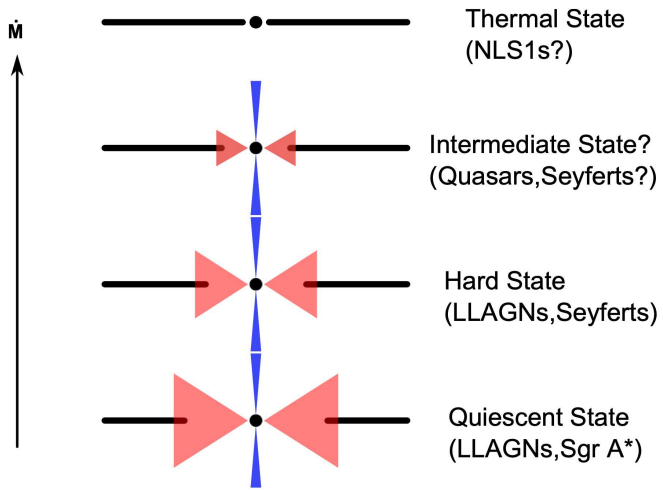

Figure 3.9: Schematic illustration of the Inner ADAF paradigm for various types of galaxies from [48].

Chapter 4

Photon Graviton Conversion

General relativity and Maxwell's electrodynamics are well supported by various experiments. Their combination, the electrodynamics in curved spacetime, predicts the mixing of photon and graviton in the presence of a background magnetic field. In other words, this implies that a photon generates a graviton in a background magnetic field. Since the resulting graviton has a same frequency as an incident photon, it is expected that the existence of the guaranteed sources of high-frequency GWs through the photon graviton conversion. In this chapter, following [27] and [49], we derive the probability of graviton production through the photon graviton conversion and the condition which makes conversion efficient. Using them, in chapter 5, we calculate GW luminosity from SMBH through the photon graviton conversion.

4.1 Einstein-Maxwell Action

We start with the following action describing gravity and electromagnetic field:

$$S_{\rm EM} = \frac{M_{\rm pl}^2}{16\pi}\int d^4x\sqrt{-g}R + \int d^4x\sqrt{-g}\left[-\frac{1}{4}F_{\mu\nu}F^{\mu\nu} + \frac{\alpha^2}{90m_{\rm e}^4}\left((F_{\rho\sigma}F^{\rho\sigma})^2 + \frac{7}{4}(F_{\rho\sigma}\tilde{F}^{\rho\sigma})^2\right)\right], \tag{4.1}$$

where $F_{\mu\nu} = \partial_\mu A_\nu - \partial_\nu A_\mu$ is field strength, and its dual is defined by $\tilde{F}^{\mu\nu} := \frac{1}{2}\epsilon^{\mu\nu\rho\sigma}F_{\rho\sigma}$. The electric field and the magnetic field are defined by $E^i := F^{0i}$ and $B^i := \tilde{F}^{0i}$ respectively. $m_{\rm e} = 0.5110$MeV is the electron rest mass. Here we emphasize that (4.1) is written in natural Lorentz-Heaviside units where $\hbar = c = 1$ and the QED fine structure constant is given by $\alpha = e^2/4\pi$. In this thesis, we consider the application of the photon graviton conversion to an astrophysical

environment. For this purpose, it is more convenient to use natural cgs-gauss units where $\hbar = c = 1$ and $\alpha = e^2$. In natural cgs-gauss units, the Einstein-Maxwell action becomes [1]

$$S_{\rm EM} = \frac{M_{\rm pl}^2}{16\pi}\int d^4x\sqrt{-g}R + \int d^4x\sqrt{-g}\left[-\frac{1}{16\pi}F_{\mu\nu}F^{\mu\nu} + \frac{1}{16\pi^2}\frac{\alpha^2}{90m_{\rm e}^4}\left((F_{\rho\sigma}F^{\rho\sigma})^2 + \frac{7}{4}(F_{\rho\sigma}\tilde{F}^{\rho\sigma})^2\right)\right]. \tag{4.2}$$

In the rest of this thesis, we use (4.2).

Now we make a brief remark about fourth derivative terms in (4.2). These terms are leading quantum correction due to electron one loop and are called the Euler-Heisenberg effective action. Since it is an effective theory at lower energy than the electron rest mass, there must be a limitation for some physical quantity. It can be seen as follows: In (4.2), QED corrections should always be smaller than Maxwell's action. This gives the upper bound for a field strength as

$$F \ll \frac{\sqrt{90\pi}m_{\rm e}^2}{\alpha} = 0.869\times 10^{16}{\rm G}. \tag{4.3}$$

Therefore, when we apply an effective action (4.2) to some system, this condition should be satisfied.

Let us move on to derivation of the equation of motion. We make a note of the following useful derivatives for convenience in checking our calculations:

$$\delta_g\left(F_{\mu\nu}F^{\mu\nu}\right) = 2F^{\alpha}{}_{\mu}F^{\mu\beta}\delta g_{\alpha\beta}, \tag{4.4}$$

$$\delta_g\left(F_{\mu\nu}\tilde{F}^{\mu\nu}\right) = -\frac{1}{2}F_{\mu\nu}\tilde{F}^{\mu\nu}g^{\alpha\beta}\delta g_{\alpha\beta}, \tag{4.5}$$

$$\delta_A\left(F_{\mu\nu}F^{\mu\nu}\right) = 4F^{\alpha\beta}\partial_\alpha\delta A_\beta, \tag{4.6}$$

$$\delta_A\left(F_{\mu\nu}\tilde{F}^{\mu\nu}\right) = 4\tilde{F}^{\alpha\beta}\partial_\alpha\delta A_\beta. \tag{4.7}$$

Substituting above derivatives for deviation of action (4.2), we obtain the Einstein

[1] By comparing Maxwell equations in both natural Lorentz-Heaviside units and natural cgs-gauss units, one obtains the following transformation rules:

$$E_{\rm G} = \sqrt{4\pi}E_{\text{L-H}},\ \ B_{\rm G} = \sqrt{4\pi}B_{\text{L-H}},\ \ e_{\rm G} = e_{\text{L-H}}/\sqrt{4\pi},$$

where subscript G and L-H represent Gauss units and Heaviside-Lorentz units respectively. For example, $E_{\rm G}$ is an electric field in cgs-gauss units, and $e_{\rm G}$ is an electric charge in cgs-gauss units.

equation and the Maxwell equation,

$$G_{\mu\nu} = \frac{2}{M_{\rm pl}^2}\left(F_{\mu\alpha}F_{\nu\beta}g^{\alpha\beta} - \frac{1}{4}g_{\mu\nu}F_{\alpha\beta}F^{\alpha\beta}\right) + \frac{1}{4\pi}\frac{2}{M_{\rm pl}^2}\frac{\alpha^2}{90m_e^4}\left[g_{\mu\nu}(F_{\alpha\beta}F^{\alpha\beta})^2 - 8(F_{\alpha\beta}F^{\alpha\beta})F_{\mu\rho}F_{\nu\sigma}g^{\rho\sigma} - \frac{7}{4}g_{\mu\nu}(F_{\alpha\beta}\tilde{F}^{\alpha\beta})^2\right], \tag{4.8}$$

$$\nabla_\mu F^{\mu\nu} = \frac{1}{4\pi}\frac{\alpha^2}{45m_e^4}\nabla_\mu\left(4F_{\alpha\beta}F^{\alpha\beta}F^{\mu\nu} + 7F_{\alpha\beta}\tilde{F}^{\alpha\beta}\tilde{F}^{\mu\nu}\right), \tag{4.9}$$

where the Einstein tensor is defined by $G_{\mu\nu} = R_{\mu\nu} - \frac{1}{2}g_{\mu\nu}R$.

4.2 Perturbative Expansion of EoM around Background Field

Now, as a first step in describing the photon graviton conversion, let us linearize the EoM obtained in the previous section around the background field. For the metric we choose the flat spacetime background, and for the gauge field, at this point, we choose an arbitrary background field $\bar{A}_\mu(x)$:

$$g_{\mu\nu} = \eta_{\mu\nu} + \kappa h_{\mu\nu}(x),$$
$$A_\mu = \bar{A}_\mu(x) + \mathcal{A}_\mu(x),$$

with $\kappa := \sqrt{16\pi}/M_{\rm pl}$. The field strength of $\bar{A}_\mu$ and $\mathcal{A}_\mu$ are denoted as $\bar{F}_{\mu\nu}$ and $f_{\mu\nu}$ respectively. Note that in our notation both $h_{\mu\nu}$ and $\mathcal{A}_\mu$ have mass dimension one.

Since gauge symmetry for perturbations are still alive, $\delta\mathcal{A}_\mu = \partial_\mu\theta$, $\delta h_{\mu\nu} = -\frac{1}{\kappa}(\partial_\mu\xi_\nu + \partial_\nu\xi_\mu)$, we can always choose the Lorentz gauge regardless of whether the matter source exists or not:

$$\partial_\mu\mathcal{A}^\mu = 0, \qquad \partial^\mu\left(h_{\mu\nu} - \frac{1}{2}\eta_{\mu\nu}h\right) = 0. \tag{4.10}$$

Then let us linearize the Einstein equation, noting that the condition (4.3) can be written as

$$\varrho F^2 \ll 1 \quad \text{with} \quad \varrho := \frac{\alpha^2}{90\pi m_{\rm e}^4}. \tag{4.11}$$

In the RHS of (4.8), the second term has suppression factor ϱF^2 in addition to the Planck suppression. Therefore we neglect it in the following discussion. And

for the LHS of (4.8), we use the linearized Einstein tensor

$$G^{(1)}_{\mu\nu} = -\frac{\kappa}{2}\Box\left(h_{\mu\nu} - \frac{1}{2}\eta_{\mu\nu}h\right) \qquad \text{in the Lorentz gauge,} \tag{4.12}$$

where $\Box := \eta^{\mu\nu}\partial_\mu\partial_\nu$. Then the Einstein equation (4.8) can be linearized as

$$\Box\left(h_{\mu\nu} - \frac{1}{2}\eta_{\mu\nu}h\right) = \frac{\kappa}{4\pi}\left(\bar{F}_\mu{}^\beta f_{\beta\nu} + \bar{F}_\nu{}^\beta f_{\beta\mu} + \frac{1}{2}\eta_{\mu\nu}\bar{F}^{\alpha\beta}f_{\alpha\beta}\right), \tag{4.13}$$

in the Lorentz gauge. Note that, in a calculation, we drop the terms proportional to $\bar{F}^2h/M_{\rm pl}^2$. These terms correspond to the effective mass term of the graviton due to a background electromagnetic field. However the corresponding effective mass $\bar{F}/M_{\rm pl} \sim 5.67 \times 10^{-29}{\rm eV}(\bar{F}/10{\rm G})$ is extremely smaller than the effective mass of the photon, so these are negligible.

Before we work on linearizing the Maxwell equation (4.9), let us rewrite it in the following form:

$$\nabla_\mu F^{\mu\nu} = \frac{\varrho}{2}\left(4\partial_\mu(F_{\alpha\beta}F^{\alpha\beta})F^{\mu\nu} + 7\partial_\mu(F_{\alpha\beta}\tilde{F}^{\alpha\beta})\tilde{F}^{\mu\nu}\right), \tag{4.14}$$

where we use the Bianchi identity $\nabla_\mu\tilde{F}^{\mu\nu} = 0$ [2]. Note that (4.14) is equivalent to (4.9) with the precision up to the first order of ϱF^2. Also, note that (4.14) is valid in curved spacetime.

In order to simplify the linearized Maxwell equation, we consider the situation where the wavelength of the perturbations(i.e. photon and graviton) is much smaller than the typical spatial scale of the background. This condition is usually satisfied in the ordinary astrophysical system. Let $D_{\rm bg}$ and λ denote the spatial scale of variation of a background electromagnetic field $\bar{F}$ and the wavelength of perturbations(i.e. h and $\mathcal{A}$) respectively. Then the condition can be written as $\lambda \ll D_{\rm bg}$. Under this condition, many terms in (4.14) become negligible. For example, in the linear order, LHS of (4.14) contains two terms $(\partial\bar{F})h$ and $\bar{F}\partial h$. The ratio of these terms becomes

$$\frac{(\partial\bar{F})h}{\bar{F}\partial h} \sim \frac{\lambda}{D_{\rm bg}} \ll 1, \tag{4.15}$$

so the terms proportional to $(\partial\bar{F})h$ is negligible compared to $\bar{F}\partial h$. A similar relation holds for terms in RHS, and the terms containing the derivative of a

[2]The Bianchi identity of the Riemann curvature $R_{\mu[\nu\rho\sigma]} = 0$ guarantees the Bianchi identity of the field strength as

$$\nabla_\mu\tilde{F}^{\mu\nu} = \frac{1}{2}\epsilon^{\nu\sigma\rho\mu}R_{\alpha\sigma\rho\mu}A^\alpha = \frac{1}{2}\epsilon^{\nu\sigma\rho\mu}R_{\alpha[\sigma\rho\mu]}A^\alpha = 0.$$

background electromagnetic field vanish. Then we obtain the linearized Maxwell equation as

$$\Box\mathcal{A}^{\nu} + \kappa\bar{F}^{\alpha\mu}\partial_{\mu}h_{\alpha}{}^{\nu} = 2\varrho\left(4\bar{F}^{\mu\nu}\bar{F}^{\alpha\beta}\partial_{\mu}\partial_{\alpha}\mathcal{A}_{\beta} + 7\tilde{\bar{F}}^{\mu\nu}\tilde{\bar{F}}^{\alpha\beta}\partial_{\mu}\partial_{\alpha}\mathcal{A}_{\beta}\right), \tag{4.16}$$

in the Lorentz gauge, under the condition $\lambda \ll D_{\rm bg}$. Here $\tilde{\bar{F}}^{\alpha\beta} := \frac{1}{2}\hat{\epsilon}^{\alpha\beta\gamma\delta}\bar{F}_{\gamma\delta}$.
It is important to emphasize that we drop the derivative of $\bar{F}$ because we assume the condition $\lambda \ll D_{\rm bg}$, not the uniform background electromagnetic field.

So far we obtain the linearized EoM (4.13) and (4.16). According to these EoM, photon and graviton are coupled with the coupling constant proportional to $\kappa\bar{F}$. This coupling causes the photon graviton conversion, and the larger the background electromagnetic field, the larger will be their mixing efficiency. Note that the coupling between photon and graviton comes from Maxwell's action in curved spacetime, not the QED correction. This is an obvious fact because the coupling constant does not depend on $\varrho = \alpha^2/90\pi m_{\rm e}^4$.

4.3 Plane Waves in a Transverse Magnetic Field

In this section, we derive the linearized EoM for plane waves in a background magnetic field. In the following discussion, we ignore an electric field. This assumption is plausible for astrophysical environments, where the plasma is ubiquitous and an electric fields are immediately shielded by them. In addition, it is known that at least a magnetic field exists around the photon sphere of the SMBHs. We deal with this system in Chapter 5.

In the previous section, we find that a strong magnetic field makes the conversion efficient. As a matter of fact, not only the strength of a background magnetic field but also its direction is important for the photon graviton conversion. Let us explain this point. Firstly consider an incident light ray with an arbitrary wave vector. Since its conversion into graviton implies the nonconservation of spin of the particle, the configuration of the background magnetic field must break the axial symmetry with respect to the given wave vector. Therefore, a magnetic field component perpendicular to the trajectory of a light ray plays a significant role to realize the conversion. If a background magnetic field is completely parallel to the wave vector of a light ray, the axial symmetry is preserved, spin is conserved, and then conversion does not occur.

Now let us consider a straight light ray with the wave vector $\vec{k} = |\vec{k}|\vec{n}$ and assign the coordinate z to direction of $\vec{n}$. The light ray propagates in a transverse background magnetic field $\vec{\bar{B}}(z)$. We assign unit vector $\vec{v}$ to the direction of $\vec{\bar{B}}(z)$, so it can be written as $\vec{\bar{B}}(z) = \bar{B}(z)\vec{v}$. Here note that, for generality, we assume the strength of a background magnetic field varies along the ray. Thanks to this

generalization, our setup includes the case of a bending light ray that propagates in a uniform magnetic field. In this case, the transverse component of a magnetic field depends on coordinate z.

Under the above setting, let us derive the EoM for plane waves in a transverse magnetic field. Firstly, we impose the transverse-traceless(TT) gauge and the radiation gauge: [3]

$$h_{0\mu} = h = 0, \quad \partial_i h_{ij} = 0 \tag{4.17}$$

$$\mathcal{A}_0 = 0, \quad \partial_i \mathcal{A}_i = 0 \tag{4.18}$$

To make this gauge condition explicit, we introduce unit vector $\vec{u}$, which is orthogonal to $\vec{n}$ and $\vec{v}$. Then three unit vectors $\vec{u}$, $\vec{v}$ and $\vec{n}$ consist an orthonormal basis(see Figure 4.1). Using this basis, we define two polarization basis for the

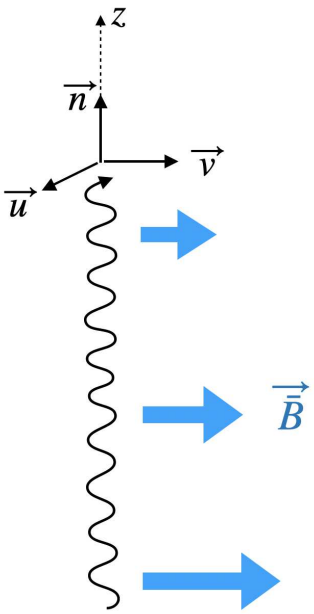

Figure 4.1: Definition of an orthonormal basis $\vec{u}$, $\vec{v}$ and $\vec{n}$

GWs by

$$e^{+}_{ij} = u_i u_j - v_i v_j, \quad e^{\times}_{ij} = u_i v_j + v_i u_j. \tag{4.19}$$

[3] As a matter of fact, the TT gauge cannot be taken exactly because of the existence of the energy momentum tensor due to the presence of a background magnetic field. Intuitively, however, it is hard to imagine that the presence of another four polarizations would significantly alter the results such as conversion probability. For this reason, we shall take the TT gauge despite the background is not a vacuum.

Since these basis are transverse and traceless, one can expand GWs as

$$h_{ij} = h^{+}(t,z)e^{+}_{ij} + h^{\times}(t,z)e^{\times}_{ij}. \tag{4.20}$$

Similarly, to make the radiation gauge explicit, we expand the photon in terms of the polarization vectors as

$$\mathcal{A}_i = i\left(\mathcal{A}^{+}(t,z)u_i + \mathcal{A}^{\times}(t,z)v_i\right). \tag{4.21}$$

Then, substituting (4.20) and (4.21) for the linear EoM (4.13) and (4.16), and projecting these into each polarization, we obtain the following EoM for plane waves:

$$\Box h^{+} = -2i\frac{\bar{B}(z)}{M_{\rm pl}}\partial_z\frac{\mathcal{A}^{+}}{\sqrt{4\pi}}, \tag{4.22}$$

$$\Box\frac{\mathcal{A}^{+}}{\sqrt{4\pi}} - 8\varrho\bar{B}^2(z)\partial_z^2\frac{\mathcal{A}^{+}}{\sqrt{4\pi}} = -2i\frac{\bar{B}(z)}{M_{\rm pl}}\partial_z h^{+}, \tag{4.23}$$

$$\Box h^{\times} = -2i\frac{\bar{B}(z)}{M_{\rm pl}}\partial_z\frac{\mathcal{A}^{\times}}{\sqrt{4\pi}}, \tag{4.24}$$

$$\Box\frac{\mathcal{A}^{\times}}{\sqrt{4\pi}} - 14\varrho\bar{B}^2(z)\partial_t^2\frac{\mathcal{A}^{\times}}{\sqrt{4\pi}} = -2i\frac{\bar{B}(z)}{M_{\rm pl}}\partial_z h^{\times}. \tag{4.25}$$

Observe that + and × polarizations are decoupled. Also, note that the above equations are only valid when the wavelength of perturbations λ are much shorter than the typical scale of variation of a background magnetic field $D_{\rm bg}$.

For the application to astrophysical systems, we have to take into account not only a magnetic field but also a plasma medium with the electron number density $n_{\rm e}$. The plasma effect can be effected by means of implementing replacement $\Box \to \Box - \omega_{\rm pl}^2$ in the EoM for photon, where

$$\omega_{\rm pl} := \sqrt{\frac{4\pi\alpha n_{\rm e}}{m_{\rm e}}} = 3.71\times10^{-11}{\rm eV}\left(\frac{n_{\rm e}}{1{\rm cm}^{-3}}\right)^{1/2} \tag{4.26}$$

is the plasma frequency in natural cgs-gauss units.

4.4 Eikonal Approximation

So far, in our calculation, we assume that the wavelength of the fluctuations is much smaller than the typical scale of variation of a background magnetic field(and a background gravitational field). This assumption holds for the photon graviton conversion in the vicinity of the photon sphere of SMBHs discussed in chapter5. As

we discuss later, hard X-rays are relevant to conversion and its wavelength are overwhelmingly smaller than the typical scale of the SMBHs(i.e. their Schwarzschild radius). Now, to make this situation more explicit, let us factorize fluctuations as

$$h^+(t,z) = \hat{h}^+(z)e^{-i(\omega(k)t-kz)}, \qquad \mathcal{A}^+(t,z) = \hat{\mathcal{A}}^+(z)e^{-i(\omega(k)t-kz)}, \tag{4.27}$$

where $\hat{h}^+(z)$ and $\hat{\mathcal{A}}^+(z)$ are the slowly varying amplitudes, and the exponential factor is a rapidly varying phase. In other words, amplitudes satisfy

$$\frac{d\hat{h}^+(z)}{dz} \ll k\hat{h}^+(z), \qquad \frac{d\hat{\mathcal{A}}^+(z)}{dz} \ll k\hat{\mathcal{A}}^+(z). \tag{4.28}$$

This is a so-called eikonal approximation. A similar decomposition is also available for $\times$ polarization.

Under the eikonal approximation (4.27) and (4.28), one can evaluate $\Box\mathcal{A}^+(t,z)$ as

$$\begin{aligned}\Box\mathcal{A}^+(t,z) &= \left(2ik\frac{d\hat{\mathcal{A}}^+}{dz} + (\omega^2(k)-k^2)\hat{\mathcal{A}}^+ + \frac{d^2\hat{\mathcal{A}}^+}{dz^2}\right)e^{-i(\omega t-kz)} \\ &\sim 2ik\frac{d\hat{\mathcal{A}}^+}{dz}e^{-i(\omega t-kz)},\end{aligned} \tag{4.29}$$

where, in the second line, we drop the term which is proportional to $(\omega^2(k) - k^2)$. This is because we consider the relativistic dispersion relation $\omega(k) \sim k$. Performing a similar calculation, (4.22) - (4.25) become

$$i\frac{d}{dz}\begin{pmatrix}\hat{h}(z)\\ \hat{\mathcal{A}}(z)/\sqrt{4\pi}\end{pmatrix}^{(\Lambda)} = \begin{pmatrix}0 & \Delta_{g\gamma}(z)\\ \Delta_{g\gamma}(z) & \Delta_\gamma^{(\Lambda)}(z)\end{pmatrix}\begin{pmatrix}\hat{h}(z)\\ \hat{\mathcal{A}}(z)/\sqrt{4\pi}\end{pmatrix}^{(\Lambda)}, \tag{4.30}$$

with the effective mass of photon

$$\Delta_\gamma^{(\Lambda)} := \frac{\omega_{\rm pl}^2}{2\omega} - c^{(\Lambda)}\varrho\omega\bar{B}^2, \tag{4.31}$$

and the photon graviton coupling

$$\Delta_{g\gamma} := \frac{\bar{B}(z)}{M_{\rm pl}}, \tag{4.32}$$

where subscript $\Lambda = +, \times$ represents polarization. [4] The constant $c^{(\Lambda)}$ becomes 4 for + mode and 7 for $\times$ mode. Here we incorporate plasma effect by the replacement $\Box \to \Box - \omega_{\rm pl}^2$ in the LHS of (4.23) and (4.25).

[4]The coefficient $1/\sqrt{4\pi}$ of $\hat{\mathcal{A}}(z)$ comes from the fact that we adopt cgs-gauss units for electromagnetism.

4.5 Conversion in a Uniform Background

In the previous section, we see that, under the eikonal approximation, linear EoM reduces to first-order ordinary differential equation (4.30) for slowly varying amplitudes. Now let us solve the EoM and describe the conversion quantitatively.

Here, we consider the simplest case where photons propagate in a uniform magnetic field and in a uniform plasma density, so $B(z) = B$, $n_{\rm e}(z) = n_{\rm e}$. The result obtained from this simplest case is relevant to photon propagation along an azimuthal direction in spherically symmetric astrophysical systems. In the case of a uniform background, a matrix in RHS of (4.30) becomes constant. Then by performing diagonalization, (4.30) reduces to decoupled first-order ordinary differential equation as follows:

$$i\frac{d}{dz}\begin{pmatrix} \hat{h}'(z) \\ \hat{\mathcal{A}}'(z)/\sqrt{4\pi} \end{pmatrix} = \begin{pmatrix} \lambda_+ & 0 \\ 0 & \lambda_- \end{pmatrix}\begin{pmatrix} \hat{h}'(z) \\ \hat{\mathcal{A}}'(z)/\sqrt{4\pi} \end{pmatrix}, \tag{4.33}$$

with

$$\lambda_\pm := \frac{\Delta_\gamma \pm \Delta_{\rm osc}}{2}, \qquad \Delta_{\rm osc} := \sqrt{\Delta_\gamma^2 + 4\Delta_{g\gamma}^2}, \tag{4.34}$$

where we have abbreviated the subscript for polarization. Readers should take care that the above calculation is performed for one of the polarization and that Δ_γ depends on the polarization. In (4.33), $\hat{h}'(z)$ and $\hat{\mathcal{A}}'(z)$ are defined by

$$\begin{pmatrix} \hat{h}'(z) \\ \hat{\mathcal{A}}'(z)/\sqrt{4\pi} \end{pmatrix} = \begin{pmatrix} \cos\vartheta & -\sin\vartheta \\ \sin\vartheta & \cos\vartheta \end{pmatrix}\begin{pmatrix} \hat{h}(z) \\ \hat{\mathcal{A}}(z)/\sqrt{4\pi} \end{pmatrix}, \tag{4.35}$$

$$\sin\vartheta\,\cos\vartheta = -\frac{\Delta_{g\gamma}}{\Delta_{\rm osc}}, \qquad \sin^2\vartheta = \frac{\lambda_+}{\Delta_{\rm osc}}, \qquad \cos^2\vartheta = -\frac{\lambda_-}{\Delta_{\rm osc}}. \tag{4.36}$$

By solving (4.33), we obtain the exact solution as

$$\begin{aligned} \hat{h}(z) = &\left(\cos^2\vartheta\,\hat{h}(0) - \sin\vartheta\cos\vartheta\,\hat{\mathcal{A}}(0)/\sqrt{4\pi}\right)e^{-i\lambda_+ z} \\ &+ \left(\sin^2\vartheta\,\hat{h}(0) + \sin\vartheta\cos\vartheta\,\hat{\mathcal{A}}(0)/\sqrt{4\pi}\right)e^{-i\lambda_- z}, \end{aligned} \tag{4.37}$$

$$\begin{aligned} \hat{\mathcal{A}}(z)/\sqrt{4\pi} = &\left(-\sin\vartheta\cos\vartheta\hat{h}(0) + \sin^2\vartheta\hat{\mathcal{A}}(0)/\sqrt{4\pi}\right)e^{-i\lambda_+ z} \\ &+ \left(\sin\vartheta\cos\vartheta\hat{h}(0) + \cos^2\vartheta\hat{\mathcal{A}}(0)/\sqrt{4\pi}\right)e^{-i\lambda_- z}, \end{aligned} \tag{4.38}$$

with the arbitrary initial condition at $z = 0$.

To discuss the conversion from photon to graviton, we consider the following situation: Initially, at $z = 0$, there are pure photon state with $\hat{h}(0) = 0$, $\hat{\mathcal{A}}(0) \neq 0$,

and while it propagates to $+z$ direction, mixing between photon and graviton occurs as one can observe from (4.37) and (4.38). Then, at a point z, the ratio of energy transfer from photon to graviton is [5]

$$P_{\gamma g}(z) := \frac{|\hat{h}(z)|^2}{|\hat{\mathcal{A}}(0)/\sqrt{4\pi}|^2} = \frac{4\Delta_{g\gamma}^2}{\Delta_{\rm osc}^2}\sin^2\left(\frac{\Delta_{\rm osc}}{2}z\right) \leq 1. \tag{4.39}$$

This is the probability of conversion into graviton. Observe that when $\Delta_\gamma \sim 0$, the conversion becomes efficient. In this case, the conversion probability becomes a more simpler form as

$$P_{\gamma g}(z) = \sin^2\left(\frac{\bar{B}}{M_{\rm pl}}z\right), \tag{4.40}$$

and complete conversion($P \sim 1$) is possible after propagating the distance $\frac{\pi}{2}\frac{M_{\rm pl}}{\bar{B}}$. The condition for resonance $\Delta_\gamma \sim 0$ is possible when the incident photon has a special frequency called a resonance frequency given by

$$\omega_{\rm r}^{(\Lambda)} \sim \frac{1}{\sqrt{2c^{(\Lambda)}}}\frac{\omega_{\rm plasma}}{\sqrt{\varrho\bar{B}^2}} = \sqrt{\frac{180\pi^2}{c^{(\Lambda)}\alpha}\frac{m_{\rm e}^3 n_{\rm e}}{\bar{B}^2}}, \tag{4.41}$$

if the incident photon has polarization Λ.

Here, we shall comment on how far from the resonance frequency we can obtain a conversion probability of the same order as (4.40). To see this, assume the incident photon with the frequency $\omega = \omega_r + \Delta\omega_{\rm r}$. Then let us find small deviation $\Delta\omega_{\rm r}$ such that coefficient of conversion probability $\frac{4\Delta_{g\gamma}^2}{\Delta_{\rm osc}^2}$ becomes order of unity [6]. As a result, we obtain

$$|\Delta\omega_{\rm r}^{(\Lambda)}| = \frac{\Delta_{g\gamma}}{c^{(\Lambda)}\varrho\bar{B}^2} = 1.18\times 10^{16}{\rm Hz}\left(\frac{10{\rm G}}{\bar{B}}\right), \tag{4.42}$$

where in the last equal, we replace $c^{(\Lambda)}$ with its mean value 5.5.

---

[5] Note that, in cgs-gauss units, the energy of the electromagnetic wave is given by $2\times\frac{(\partial_t\mathcal{A})^2}{8\pi} \propto \omega^2\left(\frac{\mathcal{A}}{\sqrt{4\pi}}\right)^2$.

[6] Here we consider $\frac{4\Delta_{g\gamma}^2}{\Delta_{\rm osc}^2} \sim \frac{1}{2}$

Chapter 5

High-frequency GWs from the Photon Sphere of SMBHs

This is the main chapter of this thesis. The results are based on our work [30]. In chapter 4, we confirmed that photons propagating in a magnetic field are converted to gravitons with the same frequency. In this chapter, we consider the application of the photon graviton conversion to the system of the SMBH and its accretion disk. There are following three reasons to focus on the photon sphere of the SMBH.

- The existence of the strong magnetic field inside $r \lesssim 5M$ of order 10G. Here r is the radial component of the Schwarzschild coordinates, M is the mass of a BH.
- The existence of the photon sphere(at $r = 3M$ for the Schwarzschild BH) that temporally traps photons in the strong magnetic field.
- The existence of the accretion disk surrounding a BH, which shines brightly in a wide frequency band.

The first and second point makes the conversion probability(4.40) large. We will confirm that the sufficient mean free path of a photon is ensured around the photon sphere in section 5.1. The third point implies that sufficient photons flow into the vicinity of the photon sphere. The larger the number of photons, the larger will be the number of produced gravitons through the conversion.

According to the above three points, the following scenario seems to be realized: Firstly, some of the photons emitted from the accretion disk flow into the vicinity of the photon sphere, and while they propagate around the photon sphere under the influence of the magnetic field, some are converted into the GW and radiated(see also Fig.1.2). In the following section, we will quantitatively discuss the GW emission from this scenario.

5.1 Estimation of the Resonance Frequency

In section 4.5, we see that the photon graviton conversion becomes efficient when the incident photon has a specific frequency so-called the resonance frequency. The resonance frequency is determined by the strength of a background magnetic field and background plasma density as $\omega_{\rm r}(n_{\rm e}, \bar{B})$. For simplicity, in the following discussion, let us consider the background configuration near the photon sphere as spherically symmetric. Then the resonance frequency can be written as $\omega_{\rm r}(r)$.

Since the conversion probability is proportional to z^2, where z is the propagation length in a background magnetic field, graviton production is more efficient in the photon sphere than in the radially escaping orbit [1]. From this observation, it is expected that the dominant contribution to the GW through the conversion comes from the photon sphere, and the spectrum of the GW has a peak at the resonance frequency $\omega_{\rm r}(3M)$.

To estimate $\omega_{\rm r}(3M)$ equivalently the typical frequency of the GW through the conversion, we have to specify the structure of the accretion disk. From the observation of the galactic center's spectrum, it is speculated that there are two distinct accretion flows, a cool standard disk and hot accretion flows such as ADAF. The existence of a hot accretion flow is required to explain observed hard X-ray emission. Following the discussion in Section3.4, we adopt the inner hot disk and outer standard disk geometry as Fig. 5.1. The two distinct disks are connected at the transition radius $r_{\rm tr}(\geq 3r_{\rm S})$.

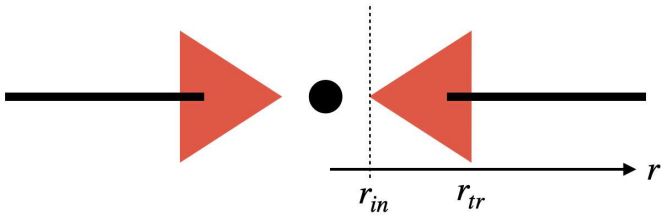

Figure 5.1: Black circle represents a central SMBH. Red region represents an optically thin, geometrically thick, hot accretion disk. Black thin line represents an optically thick, geometrically thin, cold accretion disk.

Now let us rewrite the formula of resonance frequency(4.41) to the suitable

[1]Note that the absorption of photons by plasma is negligible around the photon sphere(see the end of this section for this fact).

form for the above setting. It becomes

$$\omega_{\rm r} = \sqrt{\frac{180\pi^2}{5.5\alpha}\frac{m_{\rm e}^3 n_{\rm e}}{\bar{B}^2}} = 0.867\times 10^5 {\rm eV}\left(\frac{\beta}{0.01}\right)^{1/2}\left(\frac{v_{\rm K}(3M)}{c_{\rm s}}\right), \tag{5.1}$$

$$\text{with}\quad \beta := \frac{P_{\rm gas}}{P_{\rm mag}} = \frac{\rho c_{\rm s}^2}{\bar{B}^2/8\pi}, \tag{5.2}$$

where for simplicity we ignore the effect of polarization $c^{(\Lambda)}$ and replace it with mean value 5.5. We assume the gas as pure ionized Hydrogen with mean molecular weight $\mu = 1/2$. The constant β is the ratio of gas pressure to magnetic field pressure so-called *plasma* β. To evaluate the resonance frequency, we have to specify two quantities: The plasma β near the photon sphere and the sound speed near the photon sphere.

The plasma β is determined by the coevolution of the magnetic field and the accretion disk. However, this is a difficult problem of the magnetohydrodynamics(MHD) and cannot be approached analytically. Here motivated by the result of 3D-GRMHD simulation of non radiative disk $\beta \sim 0.01$-1 [50, 51](see also [48]), let us normalize β near photon sphere by 0.01. This should be considered an assumption for making progress, but a slight change in the order of magnitude of β does not dramatically change the resonance frequency because it is proportional to $\beta^{1/2}$.

The sound speed $c_{\rm s}$ near the photon sphere is determined by the accretion dynamics. Since we naturally adopt the hot accretion flow for the inner region, we can assume the sound speed of the inner disk is comparable to Keplerian velocity as we saw in the self-similar solution of ADAF (3.50). Then the resonance frequency can be estimated as $\omega_{\rm r} = 0.867\times 10^5$eV, equivalently $f_{\rm r} = 2.10\times 10^{19}$Hz at the photon sphere.

Now let us comment on the background profile of SMBHs and confirm that the sufficient mean free path is ensured around the photon sphere. The equipartition relation (5.2) connects the strength of the background magnetic field and plasma density by

$$\bar{B} = 11.2{\rm G}\left(\frac{\beta}{0.01}\right)^{-1/2}\left(\frac{c_{\rm s}}{v_{\rm K}(3M)}\right)\left(\frac{n_{\rm e}}{10^2{\rm cm}^{-3}}\right)^{1/2}, \tag{5.3}$$

where we again assumed the pure ionized hydrogen gas with $\mu = 1/2$. To make progress, let us use the observational value of the magnetic field near the photon sphere. According to the EHT experiment for SgrA* and M87*, the mean magnetic field strength within $r \sim 5M$ are estimated as $\bar{B} \sim 29$G [31] and 10G respectively. Based on these results, we fix the magnetic field to 10G in the following discussion. Then the corresponding electron density is $n_{\rm e} \sim 10^2{\rm cm}^{-3}$. From this, we can

estimate the mean free path of photons near the photon sphere as

$$l_{\rm T} = \frac{1}{n_{\rm e}\sigma_T} = 1.503 \times 10^{22}{\rm cm}\left(\frac{n_{\rm e}}{10^2{\rm cm}^{-3}}\right)^{-1}, \tag{5.4}$$

where $\sigma_{\rm T} = 0.6652 \times 10^{-24}{\rm cm}^2$ is the Thomson scattering cross section. The ratio of $l_{\rm T}$ to Schwarzschild radius is

$$\frac{l_{\rm T}}{r_{\rm S}} = 0.509 \times 10^8 \left(\frac{n_{\rm e}}{10^2{\rm cm}^{-3}}\right)^{-1} \left(\frac{M}{10^9 M_\odot}\right)^{-1}. \tag{5.5}$$

Therefore photons can sufficiently propagate around the photon sphere without being absorbed by the gas.

5.2 Xray Flux into the Photon Sphere

In the previous section, we find that the relevant frequency to the photon graviton conversion is hard X-rays. Such hard X-rays are supplied by the inner hot accretion flow due to its high temperature. On the other hand, as we saw in Section3.2, the temperature of the outer standard disk is too low to emit sufficient X-rays. Based on this observation, in the rest of this section, let us calculate the photon flux from the inner region(i.e. $r_{\rm in} \leq r \leq r_{\rm tr}$) into the vicinity of the photon sphere.

Now for simplicity, we neglect the geometrical thickness of the hot accretion flow in the computation of photon flux into the vicinity of the photon sphere. We consider the arbitrary emission point on the inner disk surface and denote it by $p_{\rm e}$, where subscript "e" emphasizes this is the emission point. The light rays emitted from an infinitesimal $dA_{\rm e}$ area centered at $p_{\rm e}$ are parametrized by a polar coordinates $\theta_{\rm e}$ and $\phi_{\rm e}$ as in Fig. 5.2. Note that this is the local polar coordinates at an emission point $p_{\rm e}$, and different from the Schwarzschild coordinate (r, θ, ϕ) whose origin is placed at the center of a BH. Then, the number of photons with proper frequency $\omega_{\rm e}$ emitted from $dA_{\rm e}$ into solid angle $d\Omega_{\rm e}$, in infinitesimal proper time $d\tau_{\rm e}$, in infinitesimal proper frequency band $d\omega_{\rm e}$ is given by [2]

$$d^6N = I^{(\rm N)}_{\omega_{\rm e}}(r)\cos\theta_{\rm e} dA_{\rm e} d\tau_{\rm e} d\Omega_{\rm e} d\omega_{\rm e}, \tag{5.6}$$

where $I^{(\rm N)}_{\omega_{\rm e}}(r)$ is the specific photon "number" intensity. Since the accretion dynamics is axisymmetric, it is reasonable to assume $I^{(\rm N)}_{\omega_{\rm e}}$ only depends on the radial coordinate r. The proper area element, proper time, and proper frequency can be written in terms of the Schwarzschild coordinates as

$$dA_{\rm e} = \frac{r}{\sqrt{f(r)}} dr d\phi, \quad d\tau_{\rm e} = \sqrt{f(r)}dt, \quad d\omega_{\rm e} = \frac{1}{\sqrt{f(r)}} d\omega. \tag{5.7}$$

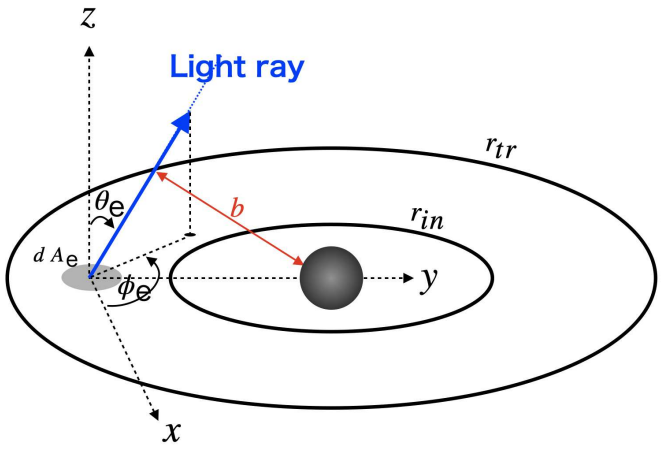

Figure 5.2: Photon emission from the inner hot region. Blue line shows light rays. Black sphere shows a central BH.

In the next section, in order to estimate the graviton luminosity through the photon graviton conversion, we parametrize light rays with their impact parameter. Now let us rewrite the photon number flux into the photon sphere as a function of the impact parameter. To do so, it is convenient to retake the local polar coordinates at the emission point p_e as shown in Fig.5.3. In this coordinates, the zenith angle is measured from the line connecting a BH and the emission point. Two polar coordinates (θ_e, ϕ_e) and (Θ_e, Φ_e) at the emission point p_e are related by

$$\begin{cases} X = z \\ Y = x \\ Z = y \end{cases} \rightarrow \begin{cases} \sin\Theta_e \cos\Phi_e = \cos\theta_e \\ \sin\Theta_e \sin\Phi_e = \sin\theta_e \cos\phi_e \\ \cos\Theta_e = \sin\theta_e \sin\phi_e \end{cases}, \tag{5.8}$$

where the three equations on the left are obvious from Fig.5.3. On the other hand, the right side is the cartesian coordinates written in terms of corresponding polar coordinates.

Now, let us rewrite (5.6) in terms of new local polar coordinates (Θ_e, Φ_e). Since the solid angle is an invariant area element, we can rewrite $\cos\theta_e d\Omega_e$ as follows:

$$\begin{aligned} \cos\theta_e d\Omega_e &= \cos\theta_e(\sin\theta_e d\phi_e d\theta_e) \\ &= \sin\Theta_e|\cos\Phi_e|(\sin\Theta_e d\Phi_e d\Theta_e) \\ &= \sin^2\Theta_e|\cos\Phi_e| d\Phi_e d\Theta_e, \end{aligned} \tag{5.9}$$

where in the second line we use the first equation of (5.8). Then (5.6) becomes

$$d^6N = I^{(N)}_{\omega_e}(r) dA_e d\tau_e d\omega_e \sin^2\Theta_e|\cos\Phi_e| d\Phi_e d\Theta_e. \tag{5.10}$$

[2]The number of derivatives in the LHS counts how many infinitesimal values are contained in the RHS.

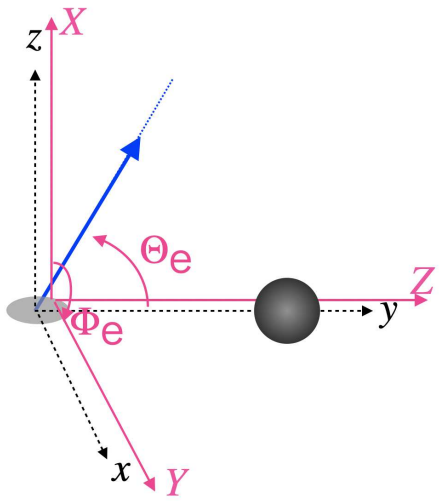

Figure 5.3: The relation between two local polar coordinates at the emission point $p_{\rm e}$. Black sphere shows a central BH.

Substituting the explicit form of the proper quantities (5.7) for this, we obtain

$$d^6N = \frac{r}{\sqrt{3f(r)}} I^{(\mathrm{N})}_{\omega_{\rm e}}(r) dr d\phi dt d\omega_{\rm c} \sin^2\Theta_{\rm e} |\cos\Phi_{\rm e}| d\Phi_{\rm e} d\Theta_{\rm e}, \tag{5.11}$$

where $\omega_{\rm c} = \sqrt{3}\omega$ is the proper frequency at the photon sphere.

The impact parameter can be written in terms of the zenith angle $\Theta_{\rm e}$ as

$$b = \frac{r}{\sqrt{f(r)}} \sin\Theta_{\rm e}, \tag{5.12}$$

see appendix A.5 for derivation. Then replacing $\Theta_{\rm e}$ with the impact parameter, (5.11) becomes

$$d^6N = \frac{1}{2} \times \frac{1}{\sqrt{3}} \frac{\sqrt{f(r)}}{r} \frac{b^2 db}{\sqrt{r^2/f(r) - b^2}} I^{(\mathrm{N})}_{\omega_{\rm e}}(r) dr d\phi dt d\omega_{\rm c} |\cos\Phi_{\rm e}| d\Phi_{\rm e}. \tag{5.13}$$

Here note that an additional $1/2$ is inserted at the front of this equation by hand. This is because a given impact parameter corresponds to two light rays toward $\Theta_{\rm e}$ and $\pi - \Theta_{\rm e}$ direction, of which only the photons emitted in $0 < \Theta_{\rm e} < \pi/2$ are directed towards a BH.

Now that we have parametrized the specific intensity in terms of the impact parameter, let us sum up (5.13) with respect to all emission points(i.e. r and ϕ) and $\Phi_{\rm e}$. Integrating $\Phi_{\rm e}$ and ϕ, we obtain

$$d^4N = \frac{4\pi}{\sqrt{3}} \frac{\sqrt{f(r)}}{r} \frac{b^2 db}{\sqrt{r^2/f(r) - b^2}} I^{(\mathrm{N})}_{\omega_{\rm e}}(r) dr dt d\omega_{\rm c} \tag{5.14}$$

In the following section, we consider the photon flux into the vicinity of the photon sphere. Since such rays have approximately critical impact parameter $b \sim b_{\rm crit} = 3\sqrt{3}M$, one can replace b with critical value in (5.14), and it becomes

$$\frac{d^4N}{dtd\omega_{\rm c}dbdr} = \frac{4\pi}{\sqrt{3}}\frac{\sqrt{f(r)}}{r}\frac{27M^2}{\sqrt{r^2/f(r) - 27M^2}}I^{(\rm N)}_{\omega_{\rm e}}(r). \tag{5.15}$$

Here observe that to make the denominator of the RHS real, the radial coordinate of the emission point must satisfy $r/\sqrt{f(r)} > 3\sqrt{3}M \sim 5.196M$. If we take $r_{\rm in} = 4M$ this condition is satisfied because in this case $r/\sqrt{f(r)} \sim 5.657M$.

Finally, let us integrate the radial coordinate r. Here we assume the specific intensity is constant as a trial. Then, we obtain the photon number emitted into $b \sim b_{\rm crit}$, per unit impact parameter, unit time, unit proper frequency at the photon sphere as

$$\frac{d^3N}{dtd\omega_{\rm c}db} = MI^{(\rm N)}_{\omega}\xi(r_{\rm in}, r_{\rm tr}), \tag{5.16}$$

$$\xi(r_{\rm in}, r_{\rm tr}) = \frac{4\pi}{\sqrt{3}}\int_{\tilde{r}_{\rm in}}^{\tilde{r}_{\rm tr}} d\tilde{r}\frac{\sqrt{f(\tilde{r})}}{\tilde{r}}\frac{27}{\sqrt{\tilde{r}^2/f(\tilde{r}) - 27}}, \tag{5.17}$$

where $\tilde{r} := r/M$. The Fig.5.4 shows the typical value of the dimensionless coefficient $\xi(r_{\rm in}, r_{\rm tr})$.

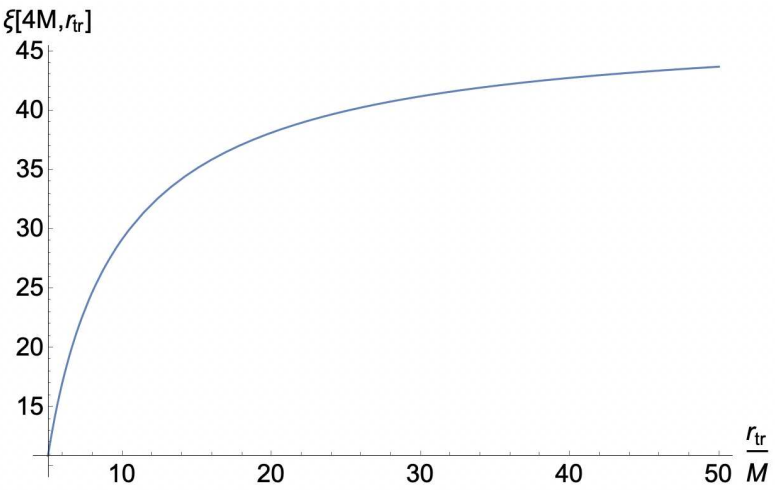

Figure 5.4: The typical value of $\xi(r_{\rm in}, r_{\rm tr})$. We choose $r_{\rm in} = 4M$ as a reference.

5.3 Luminosity of the GWs from the Photon Sphere

Now let us estimate the GW luminosity from the photon sphere of a BH through the conversion. For a given impact parameter b, the orbiting time around the photon sphere is given by (2.37) in the Schwarzschild time. [3] Then, the propagation length around the photon sphere is given by the proper time interval $T(b)/\sqrt{3}$ at the photon sphere. Using the propagation length, the conversion probability for the light ray with a given impact parameter b can be written as $P_{\gamma g}(T(b)/\sqrt{3})$(see section 4.5 for its explicit form). Since the transport of photons from the accretion disk into the photon sphere is stationary, the number of gravitons produced in a given impact parameter b, per unit time, unit impact parameter, and unit frequency is given by

$$P_{\gamma g}\left(\frac{T(b)}{\sqrt{3}}\right)\frac{d^3N_{\rm crit}}{dtdbd\omega_{\rm c}}, \tag{5.18}$$

where $\omega_{\rm c}$ is the proper frequency at the photon sphere(i.e. at $r = 3M$).

In order to estimate the total GW luminosity, it is sufficient to consider the light rays around the resonance frequency $\omega_{\rm r} = 0.867 \times 10^5$eV. Multiplying the energy per single graviton $\omega_{\rm r}$ to (5.18), and integrating the impact parameter and frequency around the resonance, we obtain the total GW luminosity as

$$\frac{dE_{\rm GW}}{dt} = \int_{b_{\rm crit}}^{b_{\rm crit}+2\sqrt{3}M} db\Delta\omega_{\rm r}P_{\gamma g}\left(\frac{T(b)}{\sqrt{3}}\right)\frac{d^3N_{\rm crit}}{dtdbd\omega_{\rm c}}\omega_{\rm r}, \tag{5.19}$$

where we take the upper limit of integration for b as the impact parameter which gives zero orbiting time. Substituting (5.16) into (5.19) and performing integration with respect to the impact parameter b the GW luminosity becomes

$$\frac{dE_{\rm GW}}{dt} = \sqrt{3}\xi(r_{\rm in}, r_{\rm tr})M^2\frac{9\left(r_{\rm S}\frac{\bar{B}}{M_{\rm pl}}\right)^2}{1+9\left(r_{\rm S}\frac{\bar{B}}{M_{\rm pl}}\right)^2}I^{(\rm N)}_{\omega_{\rm r}}\omega_{\rm r}\Delta\omega_{\rm r}, \tag{5.20}$$

where we used an analytic formula $\int_0^1 \sin^2(a\log|y|)\,dy = \frac{1}{2}\frac{(2a)^2}{1+(2a)^2}$. Here observe that the dimension less parameter $r_{\rm S}\frac{\bar{B}}{M_{\rm pl}}$ is always small for SMBHs,

$$r_{\rm S}\Delta_{g\gamma} = r_{\rm S}\frac{\bar{B}}{M_{\rm pl}} = 0.849\times10^{-9}\left(\frac{M}{10^9M_\odot}\right)\left(\frac{\bar{B}}{10{\rm G}}\right). \tag{5.21}$$

[3] We have defined orbiting time as the time until the radial deviation from the photon sphere becomes unity, in the unit of the mass of BH.

Because of this fact, (5.20) becomes

$$\frac{dE_{\rm GW}}{dt} = \frac{0.211\xi(r_{\rm in}, r_{\rm tr})M^2}{A(r_{\rm in}, r_{\rm tr})}\left(\frac{\bar{B}}{10{\rm G}}\right) \times 10^{-21}\left(L_{\omega_{\rm r}} 10^{20}{\rm Hz}\right)\left(\frac{M}{10^9 M_\odot}\right)^2, \quad (5.22)$$

where we used the formula of the resonance band (4.42). Here, we defined specific luminosity at the resonance frequency by [4]

$$L_{\omega_{\rm r}} = 2 \times \pi I^{(\rm N)}_{\omega_{\rm r}} \omega_{\rm r} A(r_{\rm in}, r_{\rm tr}), \quad (5.23)$$

where $A(r_{\rm in}, r_{\rm tr})$ denotes the emission area of hard X-rays, and factor 2 counts top and bottom surface of a disk.

In our work, we consider the SMBHs with the Eddington luminosity in the X-ray band, that is so-called quasars. The Eddington luminosity is given by

$$L_{\rm Edd} := \frac{4\pi G M m_{\rm p}}{\sigma_{\rm T}} = 1.26 \times 10^{47}{\rm erg\,sec^{-1}}\left(\frac{M}{10^9 M_\odot}\right). \quad (5.24)$$

Then the GW luminosity can be written as the function of the mass of the black hole and magnetic field as

$$\frac{dE_{\rm GW}}{dt} = \frac{0.266\xi(r_{\rm in}, r_{\rm tr})M^2}{A(r_{\rm in}, r_{\rm tr})}\left(\frac{\bar{B}}{10{\rm G}}\right) \times 10^{26}{\rm erg\,sec^{-1}}\left(\frac{M}{10^9 M_\odot}\right)^3. \quad (5.25)$$

This is a significantly weak signal but the first prediction of $10^{19\text{-}20}$Hz gravitational waves from a known astrophysical object. Note that since the emission region $A(r_{\rm in}, r_{\rm tr})$ is proportional to $r_{\rm S}^2 \propto M^2$, the prefactor $M^2/A(r_{\rm in}, r_{\rm tr})$ in (5.25) is independent of the mass of BH. Thus the luminosity $dE_{\rm GW}/dt$ is proportional to M^3.

5.4 Observation as the Stochastic GWs Background

As we discussed in section 5.1, the typical frequency of GW from the photon sphere is the resonance frequency (5.1). It is determined by the dimensionless plasma β and the sound velocity of the hot accretion flow at the photon sphere. Therefore it is reasonable to assume that the resonance frequency is not sensitive to the mass of a central BH. If so, GWs from different SMBHs can not be resolved, and what we observe is the superposition of GWs from the photon sphere of all SMBHs in

[4]The specific particle number flux from a unit area on the disk per unit time is $\pi I^{(\rm N)}_{\omega}$

our universe. Here, we give an optimistic estimation of the energy density of this stochastic GWs background.

Firstly, we define the number density of SMBHs. It is supposed to be spatially flat and power law for mass, and then is given by

$$n(\vec{x}, M) = C(p)\frac{N_{\rm Galaxy}}{\frac{4\pi}{3}(cH_0^{-1})^3}M^{-p}, \tag{5.26}$$

where $\vec{x}$ is spatial coordinate, $p \geq 0$ is power exponent, $N_{\rm Galaxy}$ is total number of galaxies. The coefficient $C(p)$ is determined by the normalization condition

$$\int_{10^6 M_\odot}^{10^{11} M_\odot} dM \int_{|\vec{x}| \leq cH_0^{-1}} d^3\vec{x} n(\vec{x}, M) = N_{\rm Galaxy} \tag{5.27}$$

as

$$C(p) = \left(\int_1^{10^5} dy\ y^{-p} \right)^{-1} (10^6 M_\odot)^{p-1}. \tag{5.28}$$

Now let us take our position at origin $\vec{x} = \vec{0}$. Then, at the origin, GW energy density from SMBHs in $\vec{x} \sim \vec{x} + d\vec{x}$ with mass band $M \sim M + dM$ can be obtained as

$$\begin{aligned} &\frac{dE_{\rm GW}}{dt} n(\vec{x}, M) d^3\vec{x} dM = 4\pi |\vec{x}|^2 c\ \rho_{\rm GW}(\vec{x}, M) d^3\vec{x} dM \\ &\rightarrow \rho_{\rm GW}(\vec{x}, M) = \frac{1}{4\pi c |\vec{x}|^2}\ n(\vec{x}, M) \frac{dE_{\rm GW}}{dt}. \end{aligned} \tag{5.29}$$

Here $\rho_{\rm GW}(\vec{x}, M)$ denotes the energy density of GW at the origin. Its arguments are the position and the mass of a given SMBHs.

Summing up all spatial coordinates in the observable universe and the mass band of SMBHs, the energy density parameter of the stochastic GWs is given by

$$\begin{aligned} \Omega_{\rm GW} &= \frac{1}{\rho_{c0}} \int_{10^6 M_\odot}^{10^{11} M_\odot} dM \int_{|\vec{x}| \leq cH_0^{-1}} d^3\vec{x} \rho_{\rm GW}(\vec{x}, M) \\ &= \frac{3N_{\rm Galaxy}}{4\pi c \rho_{c0} (cH_0^{-1})^2} C(p) (10^6 M_\odot)^{1-p}\, 10^{17} {\rm erg\,sec^{-1}} \\ &\quad \times \int_{10^6 M_\odot}^{10^{11} M_\odot} d\left(\frac{M}{10^6 M_\odot}\right) \frac{0.266 \xi(r_{\rm in}, r_{\rm tr}) M^2}{A(r_{\rm in}, r_{\rm tr})} \left(\frac{\bar{B}}{10{\rm G}}\right) \left(\frac{M}{10^6 M_\odot}\right)^{3-p}. \end{aligned} \tag{5.30}$$

Here note that the factor $M^2/A(r_{\rm in}, r_{\rm tr})$ is independent of M. In addition to this, we assume that the magnetic field near the photon sphere does not depend on the mass of a central BH. We assume these values are constant in the integration with respect to M. Then the density parameter becomes

$$\Omega_{\rm GW} = 2.93 \left(\frac{\xi(r_{\rm in}, r_{\rm tr})}{20}\right) \left(\frac{\bar{B}}{10{\rm G}}\right) \left(\frac{M^2}{A(r_{\rm in}, r_{\rm tr})}\right) \left(\frac{N_{\rm Galaxy}}{10^{12}}\right) 10^{-30} D(p), \quad (5.31)$$

$$D(p) := \frac{\int_1^{10^5} dy'\ y'^{3-p}}{\int_1^{10^5} dy\ y^{-p}}. \quad (5.32)$$

Here, $N_{\rm Galaxy}$ is normalized by the total number of galaxies in the universe up to $z = 8$ [52]. Therefore the density parameter highly depends on the power exponent of the number density of SMBHs. The value of factor $D(p)$ is shown in Fig.5.5. We conclude that the maximal energy density parameter roughly is $\Omega_{\rm GW} \sim 10^{-15}$.

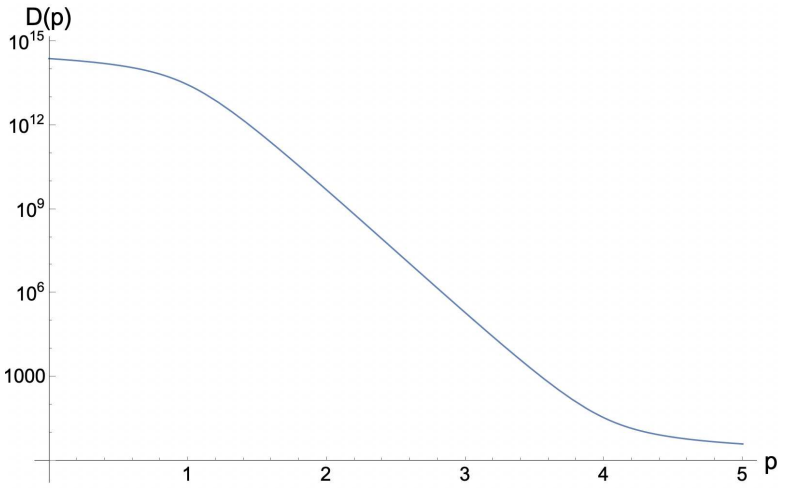

Figure 5.5: The value of $D(p)$.

Since the relation between the energy density parameter and the GW strain is given by

$$h \sim 0.893\, h_0 10^{-20} \left(\frac{100Hz}{f_{GW}}\right) \sqrt{\Omega_{GW}}, \quad (5.33)$$

the upper bound for the GW strain is $h \lesssim 10^{-45}$.

Note that the final results (5.31) strongly depends on the mean transition radius of quasars. As can be seen from Fig.5.4, the order of magnitude of $\xi(r_{\rm in}, r_{\rm tr})$ does not greatly vary with the transition radius, but the emission area of hard X-rays

does. Therefore, in order to give a more precise prediction, we have to wait for the elucidation of the hard X-ray emission mechanism in quasars.

Chapter 6

Application to Axion Search

In this chapter, we would like to discuss an interesting application of graviton production around the photon sphere that we have been working on.

As mentioned in the introduction, the photon-graviton coupling has the same form as the photon-axion coupling. Therefore, if the axion exists in our universe, photons propagating in a magnetic field are also converted into axions. Especially, just as the graviton production around the photon sphere that we have considered so far, the axion is also produced by the photon axion conversion in the photon sphere. This implies that the photon sphere dims by the amount of photons converted into axions. In our paper [53], we show that the photon sphere of M87* is dimmed by up to 10% in the X-ray band due to the photon axion conversion in the presence of axions with photon axion coupling $g_{\phi\gamma} \sim 10^{-11}\mathrm{GeV}^{-1}$ and the mass $m_\phi \lesssim 10^{-8}\mathrm{eV}$. This fact may provide a novel way to search for axions in this parameter region. In the rest of this chapter, we will briefly summarize this idea.

Firstly, the conversion probability from photon to axion is given by(see appendix A.6 for derivation)

$$P_{\gamma\phi}(z) = \frac{4\Delta_{\phi\gamma}^2}{\Delta_{\mathrm{osc}}^2} \sin^2\left(\frac{\Delta_{\mathrm{osc}}}{2} z\right) \tag{6.1}$$

with

$$\Delta_{\mathrm{osc}} = \sqrt{(\Delta_{\mathrm{pl}} - \Delta_{\mathrm{vac}}^{\parallel} - \Delta_\phi)^2 + 4\Delta_{\phi\gamma}^2}. \tag{6.2}$$

Here $\Delta_{\phi\gamma}, \Delta_\phi, \Delta_{\rm pl}, \Delta^{\parallel}_{\rm vac}$ are defined as follows:

$$\Delta_{\phi\gamma} = \frac{1}{2} g_{\phi\gamma} \frac{\bar{B}}{\sqrt{4\pi}} = 0.977 \times 10^{-21}{\rm eV} \left(\frac{g_{\phi\gamma}}{10^{-11}{\rm GeV}^{-1}}\right) \left(\frac{\bar{B}}{10{\rm G}}\right), \tag{6.3}$$

$$\Delta_\phi = \frac{m_\phi^2}{2\omega} = 0.500 \times 10^{-18}{\rm eV} \left(\frac{m_\phi}{{\rm neV}}\right)^2 \left(\frac{1{\rm eV}}{\omega}\right), \tag{6.4}$$

$$\Delta_{\rm pl} = \frac{\omega_{\rm pl}^2}{2\omega} = 0.688 \times 10^{-17}{\rm eV} \left(\frac{n_{\rm e}}{10^4{\rm cm}^{-3}}\right) \left(\frac{1{\rm eV}}{\omega}\right), \tag{6.5}$$

$$\Delta^{\parallel}_{\rm vac} = 7\varrho\omega\bar{B}^2 = 0.928 \times 10^{-29}{\rm eV} \left(\frac{\bar{B}}{10{\rm G}}\right)^2 \left(\frac{\omega}{1{\rm eV}}\right). \tag{6.6}$$

The condition for efficient conversion is $\Delta_\phi, \Delta_{\rm pl}, \Delta^{\parallel}_{\rm vac} \ll \Delta_{\phi\gamma}$. [1] This condition can also be written as

$$0.512 \times 10^3 \left(\frac{m_\phi}{{\rm neV}}\right)^2 \ll \left(\frac{g_{\phi\gamma}}{10^{-11}{\rm GeV}^{-1}}\right) \left(\frac{\bar{B}}{10{\rm G}}\right) \left(\frac{\omega}{1{\rm eV}}\right) \tag{6.7}$$

$$0.704 \times 10^4 \left(\frac{n_{\rm e}}{10^4{\rm cm}^{-3}}\right) \ll \left(\frac{g_{\phi\gamma}}{10^{-11}{\rm GeV}^{-1}}\right) \left(\frac{\bar{B}}{10{\rm G}}\right) \left(\frac{\omega}{1{\rm eV}}\right) \tag{6.8}$$

$$\left(\frac{\omega}{1{\rm eV}}\right) \ll 1.05 \times 10^8 \left(\frac{g_{\phi\gamma}}{10^{-11}{\rm GeV}^{-1}}\right) \left(\frac{10{\rm G}}{\bar{B}}\right). \tag{6.9}$$

If we fix the photon axion coupling, the mass of the axion, the magnetic field near the photon sphere, and the plasma density near the photon sphere, the first or second equation gives the lower bound for the frequency band that makes the conversion efficient. On the other hand, the last equation gives the upper bound. Let us fix these parameters as follows: For axion, we take $g_{\phi\gamma} \sim 10^{-11}{\rm GeV}^{-1}$ and $m_\phi \lesssim 10^{-8}$eV. In this mass range, recent studies of axion production in the pulsar poplar caps [54] and magnetic white dwarf polarization [55] have imposed an upper limit approaching about $g_{\phi\gamma} \sim 10^{-12}{\rm GeV}^{-1}$. However, since the tension between TeV gamma-ray observations and the cosmic infrared background observations remains at present [56], we conservatively take $g_{\phi\gamma} \sim 10^{-11}{\rm GeV}^{-1}$. For a SMBH, we admit the magnetic field and plasma density profile of M87* reported by EHT collaboration, that is $\bar{B} \sim 30$G, $n_{\rm e} \sim 10^4{\rm cm}^{-3}$ within $r = 5M$ [32]. Then we find that photons with $\omega \gtrsim 10^4$eV realize the efficient conversion.

Now, let us estimate the conversion rate in the photon sphere. We consider the photons emitted from the accretion flow surrounding the photon sphere. Part of these photons flows into the vicinity of the photon sphere $3M < r < 4M$ and are converted to axions. The number of photons emitted from the whole of accretion

[1] In this chapter, we ignore the resonance phenomena for simplicity.

flow into impact parameter range $b \sim b + db$ per unit Schwarzschild time, unit proper frequency, unit impact parameter is denoted by

$$\frac{d^3N}{dtd\omega_c db}, \tag{6.10}$$

where ω_c is the proper frequency at the photon sphere. It is related to the proper frequency for the observer at infinity ω as $\omega = \omega_c/\sqrt{3}$. Since the conversion occurs in the photon sphere, we used the proper frequency at the photon sphere in the above equation. Then the total number of axions produced in $3M < r < 4M$ per unit time, unit proper frequency is obtained as

$$\frac{dN_{\gamma\to\phi}}{dtd\omega_c} = \chi \int_{b_{\rm crit}}^{b_{\rm crit}+2\sqrt{3}M} db \frac{d^3N}{dtd\omega_c db} P_{\gamma\phi}\left(\frac{T(b)}{\sqrt{3}}\right). \tag{6.11}$$

where the factor $0 < \chi < 1$ is the fraction of photons polarized to the direction of a magnetic field. This is required because only the polarization component parallel to a magnetic field is relevant to the conversion. $T(b)$ is the time in which a light ray with the impact parameter b is trapped within $3M < r < 4M$(see (2.37) for its explicit form). $P_{\gamma\phi}(T(b)/\sqrt{3})$ is the conversion probability for the light ray with impact parameter b. The explicit form of $P_{\gamma\phi}(T(b)/\sqrt{3})$ is

$$P_{\gamma\phi}\left(\frac{T(b)}{\sqrt{3}}\right) = \frac{4\Delta_{\phi\gamma}^2}{\Delta_{\rm osc}^2}\sin^2\left(\frac{3M\Delta_{\rm osc}}{2}\log\left|\frac{b-b_{\rm crit}}{2\sqrt{3}M}\right|\right). \tag{6.12}$$

To evaluate the integral (6.11), let us observe the behavior of function $P_{\gamma\phi}(T(b)/\sqrt{3})$. When the efficient conversion is realized(i.e. $\Delta_{\rm osc} \sim 2\Delta_{\phi\gamma}$), it becomes

$$P_{\gamma\phi}\left(\frac{T(b)}{\sqrt{3}}\right) \to \sin^2\left(\frac{6M\Delta_{\phi\gamma}}{2}\log\left|\frac{b-b_{\rm crit}}{2\sqrt{3}M}\right|\right). \tag{6.13}$$

Here the dimensionless factor $6M\Delta_{\phi\gamma}$ can be estimated as

$$6M\Delta_{\phi\gamma} = 4.39\times10^{-3}\left(\frac{M}{10^9 M_\odot}\right)\left(\frac{g_{\phi\gamma}}{10^{-11}{\rm GeV}^{-1}}\right)\left(\frac{\bar{B}}{1{\rm G}}\right). \tag{6.14}$$

Inserting this into (6.13), we can numerically calculate the conversion probability as a function of b, see Fig.6.1. Here we assumed the mass and magnetic field profile of M87* given by $M \sim 6.5\times10^9 M_\odot$ and $\bar{B} \sim 30$G near photon sphere. The figure shows that the conversion probability intensely oscillates for small impact parameter deviation $\delta b/M < 0.1$.

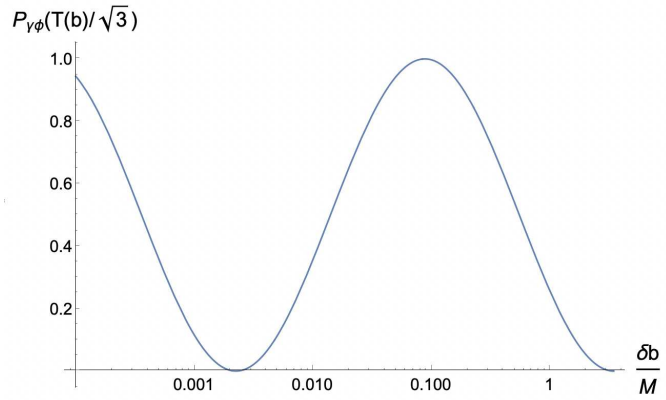

Figure 6.1: The conversion probability in the vicinity of photon sphere $3M < r < 4M$ as a function of $\delta b = b - b_{\rm crit}$. Here we assumed photon axion coupling $g_{\gamma\phi} = 10^{-11}{\rm GeV}^{-1}$. For a BH, we admit the M87* profile, $M \sim 6.5 \times 10^9 M_\odot$, $\bar{B} \sim 30{\rm G}$.

In (6.11), $d^3N/dtd\omega_{\rm c}db$ does not so rapidly oscillate with respect to impact parameter compared to the conversion probability. Therefore we can replace $d^3N/dtd\omega_{\rm c}db$ as its value at critical impact parameter and obtain

$$\begin{aligned}\frac{dN_{\gamma\to\phi}}{dtd\omega_{\rm c}} &= \chi \left.\frac{d^3N}{dtd\omega_{\rm c}db}\right|_{b=b_{\rm crit}} \int_{b_{\rm crit}}^{b_{\rm crit}+2\sqrt{3}M} db P_{\gamma\phi}\left(\frac{T(b)}{\sqrt{3}}\right) \\ &= \chi \left.\frac{d^3N}{dtd\omega_{\rm c}db}\right|_{b=b_{\rm crit}} \frac{4\Delta_{\phi\gamma}^2}{\Delta_{\rm osc}^2}\sqrt{3}M\frac{(3M\Delta_{\rm osc})^2}{1+(3M\Delta_{\rm osc})^2}, \end{aligned} \tag{6.15}$$

where we used an analytic formula $\int_0^1 \sin^2(a\log|y|)\,dy = \frac{1}{2}\frac{(2a)^2}{1+(2a)^2}$. If we approximate photon number flowing into $3M < r < 4M$ per unit time and unit proper frequency as

$$\left.\frac{d^2N}{dtd\omega_{\rm c}}\right|_{3M<r<4M} \sim 2\sqrt{3}M \times \left.\frac{d^3N}{dtd\omega_{\rm c}db}\right|_{b=b_{\rm crit}}, \tag{6.16}$$

the ratio of axion produced in $3M < r < 4M$ to photon number flowing into $3M < r < 4M$ is roughly given by

$$\frac{d^2N_{\gamma\to\phi}}{dtd\omega_{\rm c}} \Big/ \left.\frac{d^2N}{dtd\omega_{\rm c}}\right|_{3M<r<4M} \sim \frac{\chi}{2}\frac{4\Delta_{\phi\gamma}^2}{\Delta_{\rm osc}^2}\frac{(3M\Delta_{\rm osc})^2}{1+(3M\Delta_{\rm osc})^2}. \tag{6.17}$$

Now, let us estimate the fraction of axion produced by conversion near the photon sphere of the M87*. We consider the photons with frequency $\omega_{\rm c} \gtrsim 10^4{\rm eV}$(i.e.X-rays) from the accretion flow. As we discussed, this frequency range realizes efficient conversion in the presence of the axion with $g_{\phi\gamma} \sim 10^{-11}{\rm eV}$ and $m_\phi \lesssim 10^{-8}{\rm eV}$.

In this case,the dimensionless factor (6.14) becomes $6M\Delta_{\phi\gamma} = 0.856$. Therefore, the conversion rate (6.17) becomes

$$\frac{d^2N_{\gamma\to\phi}}{dtd\omega_{\rm c}}\Big/\left.\frac{d^2N}{dtd\omega_{\rm c}}\right|_{3M<r<4M} \sim 0.211\chi. \tag{6.18}$$

If the polarization of the photons emitted from the accretion flow is random, we can set $\chi = 1/2$. Therefore, we conclude that there is 10% dimming of the photon sphere of M87 in the X-ray band.

Chapter 7

Conclusion

In this thesis, we proposed a new high-frequency GW with the following profile:

- **Source**:
  Around the photon sphere of quasars.

- **Emission mechanism**:
  In the presence of a background magnetic field, photon and graviton are mixed, and an incident photon is converted into a graviton with a certain probability. Especially, there is a strong magnetic field produced by the hot accretion flow around the photon sphere of a quasar, and part of the photons that enter the photon sphere are converted into gravitons and emitted to infinity. As a side note, the source of photons flowing into the photon sphere is the plasma composing the hot accretion flow.

- **Frequency of the GW** :
  We assume the strength of a magnetic field near the photon sphere as $\bar{B} \sim 10\mathrm{G}$. Then, we find that the frequency of the GW is around $10^{19}\mathrm{Hz}$. Here, the magnetic field strength of 10G refers to the result from the EHT experiment of SgrA* and M87*, which are much less luminous than quasars. The most significant reason for this treatment is the lack of observations of the magnetic field around the photons sphere of quasars. However, since the hot accretion flow of the same nature is expected to exist in the inner disk region whether it is a quasar or low-luminosity AGN, assuming the same magnetic field would give reasonable results as a trial.

- **GW luminosity from a single quasar** :
  The luminosity of the GW from a single quasar is roughly estimated as

$$\frac{dE_{\mathrm{GW}}}{dt} \sim 0.532 \times \left(\frac{\bar{B}}{10\mathrm{G}}\right) \times 10^{27}\mathrm{erg\,sec}^{-1} \left(\frac{M}{10^9 M_\odot}\right)^3 .$$

where M is the mass of the quasar.

- **Energy density as the stochastic GWs background** :
  Since the frequency of the GW is not sensitive to the mass of a BH, we observe it as the stochastic GWs background. We estimated its energy density parameter. The result is maximally $\Omega_{\rm GW} \sim 10^{-15}$. This is equivalent to $h \sim 10^{-45}$ in terms of the GW strain. Note that in this estimation, the mass band of quasars is assumed to be $10^6 \sim 10^{11} M_\odot$, and the magnetic field is assumed to be independent of the mass of a BH. In reality, there may be some mass dependence, but the observed magnetic field of SgrA* and M87* suggest that the magnetic field around the photon sphere is roughly independent of the mass of a central BH.

GWs above 10^{14}Hz is a region where co-growth with axion experiments is possible and it is significant that we were able to propose the first guaranteed source there. In addition, since photons can also be converted into axions under a magnetic field, we discussed in chapter 6 that this GW generation mechanism can be applied to axion search. We showed that the conversion is efficient for the photon sphere of the M87* and that the spectrum of the photon sphere is dimmed up to 10% in the X-ray band in the presence of the axion with photon axion coupling $g_{\phi\gamma} \sim 10^{-11}{\rm GeV}^{-1}$ and the mass $m_\phi \lesssim 10^{-8}$eV. This fact may provide a novel way to search axion in this parameter region.

Finally, we would like to mention future direction. Unfortunately, the amplitude of the GW we proposed is so small that it cannot be reached even if the axion detector is improved in the future. We must continue our efforts to propose a guaranteed source above 10^{14}Hz. To do that, obviously, we should consider a different mechanism from the GW radiation of binary systems. We should reconsider not only the photon graviton conversion but also the GW from microscopic physics such as the collision in the thermal plasma.

Acknowledgments

I owe my gratitude to Prof. Jiro Soda for guiding my research. I thank my collaborators Associate Prof. Hirotaka Yoshino and Kimihiro Nomura for working together. I thank Prof. Hisaya Kurashige for giving me valuable comments on this thesis. I am also very grateful to all the members of the theoretical physics group, in particular, Associate Prof. Toshifumi Noumi, Emi Masaki, and Yuki Nagatani. Finally, I am grateful to my family for supporting me throughout my Ph.D. studies.

This work was supported by JST SPRING, Grant Number JPMJSP 2148.

Appendices

Appendix A

Apeendices

A.1 Perturbative Expansion Around a Curved Background

In this appendix, we write down the perturbative expansion of geometric quantities around an arbitrary background space-time. Since generally, the background space-time is dynamical, it is nontrivial to identify the true perturbation part of the metric. However, in this appendix, we only mention the algebraic formulae and put aside the physical issue.
We decompose the metric by

$$g_{\mu\nu}(x) = \bar{g}_{\mu\nu}(x) + h_{\mu\nu}(x), \tag{A.1}$$

where $\bar{g}$ and h are the background and perturbation respectively.
In the following calculations, we will implement the perturbative expansion with respect to h with the accuracy of $\mathcal{O}(h^2)$. The inverse metric is given by

$$g^{\mu\nu} = \bar{g}^{\mu\nu} - h^{\mu\nu} + h^{\mu}{}_{\alpha}h^{\alpha\nu} + \mathcal{O}(h^3), \tag{A.2}$$

where the index of perturbation is raised and downed by $\bar{g}_{\mu\nu}$ and $g^{\mu\nu}$ satisfy $g^{\mu\nu}g_{\nu\rho} = \delta^{\mu}_{\rho} + \mathcal{O}(h^3)$. By using this formula, one can expand the Christoffel symbols as

$$\Gamma^{\rho}_{\mu\nu} = \bar{\Gamma}^{\rho}_{\mu\nu} + \bar{g}^{\rho\alpha}\gamma_{\alpha\mu\nu} - h^{\rho\alpha}\gamma_{\alpha\mu\nu} + \mathcal{O}(h^3) \tag{A.3}$$

with

$$\bar{\Gamma}^{\rho}_{\mu\nu} := \frac{1}{2}\bar{g}^{\rho\alpha}\left(\partial_{\mu}\bar{g}_{\alpha\nu} + \partial_{\nu}\bar{g}_{\alpha\mu} - \partial_{\alpha}\bar{g}_{\mu\nu}\right), \tag{A.4}$$

$$\gamma_{\alpha\mu\nu} := \frac{1}{2}\left(\bar{D}_\mu h_{\alpha\nu} + \bar{D}_\nu h_{\alpha\mu} - \bar{D}_\alpha h_{\mu\nu}\right), \tag{A.5}$$

where $\bar{D}_\mu$ is covariant derivative regarding background metric $\bar{g}_{\mu\nu}$ (i.e. $\bar{\Gamma}^\rho_{\mu\nu}$). Similarly, one can expand the Riemann tensor as

$$R^\mu{}_{\nu\rho\sigma} = \bar{R}^\mu{}_{\nu\rho\sigma} + R^{(1)\mu}{}_{\nu\rho\sigma} + R^{(2)\mu}{}_{\nu\rho\sigma} + \mathcal{O}(h^3) \tag{A.6}$$

with

$$R^{(1)\mu}{}_{\nu\rho\sigma} = \bar{g}^{\mu\alpha}\bar{D}_\rho\gamma_{\alpha\nu\sigma} - \bar{g}^{\mu\alpha}\bar{D}_\sigma\gamma_{\alpha\nu\rho}, \tag{A.7}$$

$$R^{(2)\mu}{}_{\nu\rho\sigma} = \bar{D}_\sigma\left(h^{\mu\alpha}\gamma_{\alpha\nu\rho}\right) - \bar{D}_\rho\left(h^{\mu\alpha}\gamma_{\alpha\nu\sigma}\right) + \bar{g}^{\mu\beta}\bar{g}^{\alpha\gamma}\left(\gamma_{\beta\alpha\rho}\gamma_{\gamma\nu\sigma} - \gamma_{\beta\alpha\sigma}\gamma_{\gamma\nu\rho}\right). \tag{A.8}$$

Here, $\bar{R}^\mu{}_{\nu\rho\sigma}$ denotes the Riemann tensor of the background metric.
Then the perturbative expansion of the Ricci tensor is given by

$$R_{\mu\nu} = R^\alpha{}_{\mu\alpha\nu} = \bar{R}_{\mu\nu} + R^{(1)}{}_{\mu\nu} + R^{(2)}{}_{\mu\nu} + \mathcal{O}(h^3) \tag{A.9}$$

with

$$R^{(1)}{}_{\mu\nu} = \frac{1}{2}\left(\bar{D}^\alpha\bar{D}_\mu h_{\nu\alpha} + \bar{D}^\alpha\bar{D}_\nu h_{\mu\alpha} - \bar{D}^\alpha\bar{D}_\alpha h_{\mu\nu} - \bar{D}_\nu\bar{D}_\mu h\right), \tag{A.10}$$

$$\begin{aligned} R^{(2)}{}_{\mu\nu} = \frac{1}{2}\Bigg[& \frac{1}{2}(\bar{D}_\mu h_{\alpha\beta})(\bar{D}_\nu h^{\alpha\beta}) + (\bar{D}^\rho h_\nu{}^\alpha)(\bar{D}_\rho h_{\mu\alpha} - \bar{D}_\alpha h_{\mu\rho}) \\ & + h^{\alpha\beta}\left(\bar{D}_\nu\bar{D}_\mu h_{\alpha\beta} + \bar{D}_\alpha\bar{D}_\beta h_{\mu\nu} - \bar{D}_\alpha\bar{D}_\mu h_{\beta\nu} - \bar{D}_\alpha\bar{D}_\nu h_{\beta\mu}\right) \\ & + \left(\frac{1}{2}\bar{D}^\alpha h - \bar{D}_\rho h^{\rho\alpha}\right)\left(\bar{D}_\mu h_{\nu\alpha} + \bar{D}_\nu h_{\mu\alpha} - \bar{D}_\alpha h_{\mu\nu}\right) \Bigg], \end{aligned} \tag{A.11}$$

where $h := \bar{g}^{\alpha\beta}h_{\alpha\beta}$.

A.2 Stress Tensor of a Viscous Fluid

In this appendix, we revisit the nonrelativistic hydrodynamics as a fundamental tool for describing accretion disks, especially the stress tensor of a viscous fluid. This appendix is based on the text book [57].

Let us start with the definition of viscosity. Firstly, the equation of continuity for momentum density is given by

$$\frac{\partial\rho v^i}{\partial t} = -\frac{\partial\Pi^{ij}}{\partial x^j}, \tag{A.12}$$

$$\Pi^{ij} := p\delta^{ij} - \sigma'^{ij} + \rho v^i v^j, \tag{A.13}$$

where ρ is mass density of a fluid and v^i represents velocity of the fluid element. The viscous stress tensor σ'^{ij} in the momentum flux density represents the effect of viscosity. Its most general form is given by

$$\sigma'^{ij} = \eta\left(\frac{\partial v^j}{\partial x^i} + \frac{\partial v^i}{\partial x^j} - \frac{2}{3}\delta^{ij}\partial\cdot v\right) + \zeta\left(\partial\cdot v\right)\delta^{ij}, \tag{A.14}$$

where η and ζ are viscosity coeficients. The above parametrization of viscous effect((A.13) and (A.14)) gives positive η and ζ. [1]

Usually, we regard fluid as incompressible(i.e. $\rho = \text{constant} \to \partial\cdot v = 0$). Then viscous stress tensor becomes simpler form

$$\sigma'^{ij} = \eta\left(\frac{\partial v^j}{\partial x^i} + \frac{\partial v^i}{\partial x^j}\right). \tag{A.15}$$

Therefore, the incompressible fluid is characterized by only one viscous coefficient η. We often introduce kinematic viscosity ν as $\eta = \nu\rho$. The kinematic viscosity has the dimension of velocity $\times$ length. Observe that (A.15) only holds in cartesian coordinate. Since σ'^{ij} depends not on the derivative of velocity components but on the derivative of velocity including basis vector, for a general coordinate system, σ'^{ij} becomes

$$\sigma' = \eta\left(\nabla\vec{v} + (\nabla\vec{v})^T\right). \tag{A.16}$$

We enumerate components of σ' in the cylindrical coordinates as follows:

(**Cylindrical coordinates**)

$$\begin{aligned} dl^2 &= dr^2 + r^2 d\phi^2 + dz^2 \\ \vec{v} &= v^r\vec{e}_r + v^\phi\vec{e}_\phi + v^z\vec{e}_z \\ \nabla &= \vec{e}_r\partial_r + \vec{e}_\phi\frac{1}{r}\partial_\phi + \vec{e}_z\partial_z \end{aligned}$$

$$\begin{aligned} &\sigma'^{rr} = 2\eta\partial_r v^r, \qquad \sigma'^{r\phi} = \eta\left(\frac{1}{r}\partial_\phi v^r + \partial_r v^\phi - \frac{v^\phi}{r}\right), \\ &\sigma'^{rz} = \eta\left(\partial_r v^z + \partial_z v^r\right), \qquad \sigma'^{\phi\phi} = 2\eta\left(\frac{1}{r}\partial_\phi v^\phi + \frac{v^r}{r}\right), \\ &\sigma'^{\phi z} = \eta\left(\frac{1}{r}\partial_\phi v^z + \partial_z v^\phi\right), \qquad \sigma'^{zz} = 2\eta\partial_z v^z. \end{aligned} \tag{A.17}$$

[1] The positivity of viscosity coefficients followed from the requirement that energy dispersion of fluid is negative.

A.3 Thermodynamics

Here, we provide a summary of the thermodynamics necessary to discuss ADAF. The purpose of this appendix is to give the formula for the entropy of an ideal gas. In addition to this aim, we will clarify our notations for thermodynamic quantities. In the main chapter, we often discuss thermodynamics with quantities per unit mass. Then the first law of thermodynamics is given by

$$du = Tds - pd\frac{1}{\rho}, \tag{A.18}$$

where u is the internal energy per unit mass, s is the entropy per unit mass, ρ is the mass density. The internal energy of an ideal gas is given by

$$u = c_{\rm V}T, \tag{A.19}$$

where $c_{\rm V} = \left(\frac{\partial u}{\partial T}\right)_{V,N}$ is the specific heat at constant volume. Together with specific heat at constant pressure $c_{\rm P}$, this satisfies Mayer's relation [2]

$$c_{\rm P} - c_{\rm V} = \frac{k_{\rm B}}{m_{\rm p}\mu}. \tag{A.20}$$

Often we introduce the ratio of specific heat $\gamma := c_{\rm P}/c_{\rm V}$. For monoatomic and diatomic gas γ becomes $5/3, 7/5$ respectively. Using this ratio, the specific heat at constant volume can be written as

$$c_{\rm V} = \frac{1}{\gamma - 1}\frac{k_{\rm B}}{\mu m_{\rm p}} = \frac{1}{\gamma - 1}\frac{c_{\rm s}^2}{T}, \tag{A.21}$$

where we used the definition of sound speed for an ideal gas. Now let us derive the entropy of an ideal gas. Substituting the equation of state and internal energy (A.19) for the first law of thermodynamics (A.18), we obtain

$$ds_{\rm gas} = c_{\rm V}\, d\log\frac{T}{\rho^{\gamma-1}}. \tag{A.22}$$

Integrating this equation, one obtains the entropy of an ideal gas as

$$s_{\rm gas} = c_{\rm V}\log\frac{T}{\rho^{\gamma-1}} + \text{const.} = c_{\rm V}\log\frac{c_{\rm s}^2}{\rho^{\gamma-1}} + \text{const.}. \tag{A.23}$$

[2]Note that for the heat capacity $C_{\rm V} = \left(\frac{\partial U}{\partial T}\right)_{V,N}$, Mayer's equation become $C_{\rm P} - C_{\rm V} = nR$, where $R = N_{\rm A}k_{\rm B}$, n is number of moles of a given system.

A.4 Collective Effects in a Plasma

This appendix is based on the text book [58]. Here we mainly focus on the derivation of the plasma frequency used in Chapter4.

A.4.1 Debye Shielding

In a plasma, electrons and protons can move freely, and thereby a positively(negatively) charged test particle attracts electrons(protons) around it. This is called the Debye shielding effect. Due to this effect, the original Coulomb potential of the test charge is exponentially suppressed.

Let's quantify the above observation. We consider the plasma with the mean electron number density $\bar{n}$ and the temperature T. Here the number density of the proton is also given by $\bar{n}$ due to charge neutrality. The mean number density $\bar{n}$ obeys Maxwell distribution, so $\bar{n} \propto e^{-E/T}$, where E is the energy of electron. Now, examine the situation when we put the test particle with charge Q in this plasma. We introduce the cartesian coordinates $\vec{r}$ whose origin is at the test particle. The test charge modifies the number density of electrons and protons from its original value $\bar{n}$, because of the aforementioned shielding effect. The modified number density of electrons and protons are denoted by $n_{\mathrm{e}}(\vec{r})$ and $n_{\mathrm{p}}(\vec{r})$. Then the electrostatic potential generated by the net charge distribution is given by the Poisson equation

$$\Delta\Phi(\vec{r}) = -4\pi \left(e n_{\mathrm{p}}(\vec{r}) - e n_{\mathrm{e}}(\vec{r})\right) - 4\pi Q\delta(\vec{r}), \tag{A.24}$$

in the cgs-Gauss units, where $e(>0)$ is the elementary charge.
Here the modified number density $n_{\mathrm{e}}(\vec{r})$ and $n_{\mathrm{p}}(\vec{r})$ can be estimated from the statistical mechanics. Consider the point $\vec{r}$ outside the test charge, at this point, electrons(protons) feel the electrostatic potential $-e\Phi(\vec{r})(+e\Phi(\vec{r}))$. Therefore the original Maxwell distribution is shifted as

$$n_{\mathrm{e}}(\vec{r}) = \bar{n} e^{e\Phi(\vec{r})/T} \sim \bar{n}\left(1 + \frac{e\Phi(\vec{r})}{T}\right), \tag{A.25}$$

$$n_{\mathrm{p}}(\vec{r}) = \bar{n} e^{-e\Phi(\vec{r})/T} \sim \bar{n}\left(1 - \frac{e\Phi(\vec{r})}{T}\right), \tag{A.26}$$

where we assume $|e\Phi(\vec{r})| \ll T$. Substituting this for the Poisson equation, we obtain

$$\left(\Delta - \frac{8\pi\alpha\bar{n}}{T}\right)\Phi(\vec{r}) = -4\pi Q\delta(\vec{r}), \tag{A.27}$$

where $\alpha = e^2$ is the fine structure constant. This problem can be solved by using the fundamental solution of the Helmholtz equation defined by

$$\left(\Delta_{\vec{x}} + m^2\right) G(\vec{x} - \vec{x}') = -\delta(\vec{x} - \vec{x}'). \tag{A.28}$$

The explicit form of the fundamental solution $G(\vec{x} - \vec{x}')$ is given by

$$G(\vec{x} - \vec{x}') = \frac{1}{4\pi|\vec{x} - \vec{x}'|} e^{im|\vec{x}-\vec{x}'|}. \tag{A.29}$$

Then we obtain the solution of (A.27) as

$$\Phi(\vec{r}) = \frac{Q}{r} e^{-\sqrt{2}r/\lambda_{\mathrm{D}}}, \tag{A.30}$$

with the Debye length defined by

$$\lambda_{\mathrm{D}} := \sqrt{\frac{T}{4\pi\alpha\bar{n}}} = 6.90\mathrm{cm} \left(\frac{T}{1\mathrm{K}}\right)^{1/2} \left(\frac{\bar{n}}{1\mathrm{cm}^{-3}}\right)^{-1/2}. \tag{A.31}$$

As we expected, the Coulomb potential of the test charge is exponentially suppressed due to the Debye shielding, and for $r \gtrsim \lambda_{\mathrm{D}}$ charged particles cannot feel the potential of the test charge. Therefore the Debye length λ_{D} can be roughly interpreted as the thickness of the shielding cloud.

A.4.2 Derivation of the Plasma Frequency

The Debye length can be interpreted as the electrostatic correlation length in a plasma. Now, let's estimate the electrostatic correlation time, the time until the shielding cloud around the test charge is formed. Because the electron is much lighter than the proton, we can assume only electrons can move to shield the original Coulomb potential of the test charge. These electrons have the thermal velocity defined by $\langle v_{\mathrm{e}} \rangle := \sqrt{T/m_{\mathrm{e}}}$. Then the electrostatic correlation time is given by

$$t_{\mathrm{D}} = \lambda_{\mathrm{D}} / \langle v_{\mathrm{e}} \rangle = \sqrt{\frac{m_{\mathrm{e}}}{4\pi\alpha\bar{n}}}. \tag{A.32}$$

Here observe that the correlation time does not depend on the temperature of a plasma. This correlation time can be interpreted as the time required for plasma to erase the external electromagnetic field. So electromagnetic waves which have a smaller oscillation period of time than t_{D} can path through a plasma medium without shielding by it. In other words, electromagnetic fields oscillating faster than the frequency

$$\omega_{\mathrm{pl}} := 1/t_{\mathrm{D}} = \sqrt{\frac{4\pi\alpha\bar{n}}{m_{\mathrm{e}}}} = 3.71 \times 10^{-11}\mathrm{eV} \left(\frac{\bar{n}}{1\mathrm{cm}^{-3}}\right)^{1/2} \tag{A.33}$$

can propagate without shielding by plasma. This ω_{pl} is called the plasma frequency.

A.5 Derivation of (5.12)

In this appendix, we derive the formula (5.12) which connects the impact parameter and the local emission angle $\Theta_{\rm e}$ in Fig. 5.3.

Let us consider the light ray emitted from an arbitrary emission point $p_{\rm e}$. Let k denotes the four-wave vector of the light ray. We retake the zenith angle of the Schwarzschild coordinates so that the spatial component of k lies in the $\theta = \pi/2$ plane. Then the light trajectory remains in the $\theta = \pi/2$ plane after time passes due to the angular momentum conservation. Then the emission angle Θ_e is given by(see Fig. A.1)

$$\begin{aligned}\tan\Theta_{\rm e} &= \frac{g(k, e_{\hat{\phi}})}{g(k, e_{\hat{r}})} \\ &= \frac{g\left(k, \frac{1}{r}\partial_\phi\right)}{g(k, \sqrt{f(r)}\partial_r)} \\ &= \frac{1}{r\sqrt{f(r)}}\frac{k^\phi g_{\phi\phi}}{k^r g_{rr}} \\ &= r\sqrt{f(r)}\frac{d\phi/d\lambda}{dr/d\lambda} = r\sqrt{f(r)}\frac{d\phi/dt}{dr/dt}.\end{aligned} \tag{A.34}$$

Using the geodesic equation of massless particle (2.24) and (2.25), this becomes

$$\tan^2\Theta_{\rm e} = \frac{b^2 f(r)/r^2}{1 - b^2 f(r)/r^2}. \tag{A.35}$$

From this relation, we find the formula connecting the impact parameter and the local emission angle as

$$b = \frac{r}{\sqrt{f(r)}}\sin\Theta_{\rm e}. \tag{A.36}$$

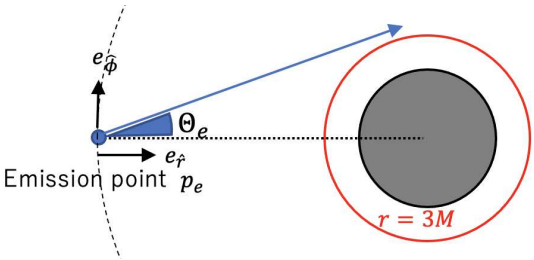

Figure A.1: A sketch of the local emission angle and tetrad in the $\theta = \pi/2$ plane.

A.6 Axion Photon Conversion

The ultra-light particle called the axion is predicted as a solution to the strong CP problem. To prove the axion, it is most promising to use coupling to the photon and resulting phenomenon. In this context, here we will review the photon axion conversion phenomenon. This is an analog of photon graviton conversion, which is reviewed in Chapter4. Since calculations are almost the same, we will skip the detailed calculation and discussion on the validity of approximation. This appendix based on [27, 59].

Axion Electrodynamics

We will consider the system of axion and photon with electron one loop correction in the flat spacetime.

$$S = \int d^4x \left[-\frac{1}{16\pi} F_{\mu\nu}F^{\mu\nu} + \frac{1}{16\pi^2}\frac{\alpha^2}{90m_{\rm e}^4}\left((F_{\rho\sigma}F^{\rho\sigma})^2 + \frac{7}{4}(F_{\rho\sigma}\tilde{F}^{\rho\sigma})^2 \right) \right.$$
$$\left. -\frac{1}{2}\left((\partial_\mu\phi)^2 + m_\phi^2\phi^2 \right) - \frac{1}{16\pi} g_{\phi\gamma}\phi F_{\mu\nu}\tilde{F}^{\mu\nu} \right], \qquad \text{(A.37)}$$

where ϕ and m_ϕ are the axion field and it's mass respectively. $g_{\phi\gamma}$ is the photon axion coupling. Note that this action is written in natural cgs-gauss units.

From the action (A.37), EoM for axion and photon are given by

$$\left(\Box - m_\phi^2\right)\phi = \frac{1}{16\pi} g_{\phi\gamma} F_{\mu\nu}\tilde{F}^{\mu\nu} \qquad \text{(A.38)}$$

$$\Box A^\nu = \frac{\varrho}{2}\left(4\partial_\mu(F_{\alpha\beta}F^{\alpha\beta})F^{\mu\nu} + 7\partial_\mu(F_{\alpha\beta}\tilde{F}^{\alpha\beta})\tilde{F}^{\mu\nu} \right) - g_{\phi\gamma}(\partial_\mu\phi)\tilde{F}^{\mu\nu}, \qquad \text{(A.39)}$$

where we used Bianchi identity $\partial_\mu\tilde{F}^{\mu\nu} = 0$ and imposed Lorentz gauge $\partial_\mu A^\mu = 0$, we defined ϱ as $\varrho := \alpha^2/(90\pi m_{\rm e}^4)$. Also note that when we derive (A.39), we neglect the subleading terms $(\varrho F^2)^2$ and $\varrho F^2 g_{\phi\gamma}$.

Perturbative Expansion of EoM

In this section, we derive the linear EoM of the photon axion system. Firstly, let us decompose the fields as follows:

$$\phi = \bar{\phi}(x) + \frac{\delta\phi(x)}{\sqrt{4\pi}},$$
$$A_\mu = \bar{A}_\mu(x) + \mathcal{A}_\mu(x).$$

At this moment, the background configurations $\bar{\phi}(x)$ and $\bar{A}_\mu(x)$ are arbitrary. The field strength of $\bar{A}_\mu$ and $\mathcal{A}_\mu$ are denoted by $\bar{F}_{\mu\nu}$ and $f_{\mu\nu}$ respectively.

Assume that the scale of variation of background configurations $D_{\rm bg}$ is sufficiently bigger than the wavelength of perturbations λ. Then we can neglect the derivative of the background configurations compared to that of perturbations, and linear EoM is approximately obtained as

$$\left(\Box - m_\phi^2\right)\delta\phi = \frac{1}{\sqrt{4\pi}} g_{\phi\gamma} \tilde{\bar{F}}^{\mu\nu}\partial_\mu \mathcal{A}_\nu, \tag{A.40}$$

$$\Box \mathcal{A}^\nu = 2\varrho\left(4\bar{F}^{\mu\nu}\bar{F}^{\alpha\beta}\partial_\mu\partial_\alpha\mathcal{A}_\beta + 7\tilde{\bar{F}}^{\mu\nu}\tilde{\bar{F}}^{\alpha\beta}\partial_\mu\partial_\alpha\mathcal{A}_\beta\right) - \frac{1}{\sqrt{4\pi}} g_{\phi\gamma}(\partial_\mu\delta\phi)\tilde{\bar{F}}^{\mu\nu}. \tag{A.41}$$

Here we give an important remark: Ignoring the derivative of the background does not mean that we have restricted our discussion to uniform backgrounds. As long as the background variation is not so drastic as to violate the condition $\lambda \ll D_{\rm bg}$, we can use this linear EoM for the analysis of conversion in an inhomogeneous background.

Plane Wave in a Uniform Magnetic Field and the Eikonal Approximation

Now let us consider the plane wave propagating in a transverse magnetic field. We assign coordinate z to the direction of the wave vector $\vec{k} = |\vec{k}|\vec{n}$. Then the transverse magnetic field is defined by $\vec{B} = \bar{B}(z)\vec{e}_\parallel$, where $\vec{e}_\parallel$ is unit vector perpendicular to $\vec{n}$. By introducing unit vector $\vec{e}_\perp$ which is perpendicular both $\vec{n}$ and $\vec{e}_\parallel$, three vectors $\vec{n}, \vec{e}_\parallel, \vec{e}_\perp$ constitute an orthonormal basis.

For simplicity let us impose the radiation gauge, then one can expand the vector potential as

$$\vec{\mathcal{A}} = i(\mathcal{A}_\parallel(t,z)\vec{e}_\parallel + \mathcal{A}_\perp(t,z)\vec{e}_\perp). \tag{A.42}$$

Under the above setup, the linear EoM (A.40) and (A.41) becomes

$$\left(\Box - m_\phi^2\right)\phi(t,z) = i\frac{g_{\phi\gamma}\bar{B}(z)}{\sqrt{4\pi}}\partial_t\mathcal{A}_\parallel, \tag{A.43}$$

$$\Box\mathcal{A}_\parallel(t,z) = 14\varrho\bar{B}^2(z)\partial_t^2\mathcal{A}_\parallel + i\frac{g_{\phi\gamma}\bar{B}(z)}{\sqrt{4\pi}}\partial_t\phi, \tag{A.44}$$

$$\Box\mathcal{A}_\perp(t,z) = 8\varrho\bar{B}^2(z)\partial_z^2\mathcal{A}_\perp. \tag{A.45}$$

Here $\delta\phi$ is rewritten as ϕ(as it will be in the following).

Further simplification is possible by assuming the eikonal approximation

$$\begin{aligned}\phi(t,z) &= \hat{\phi}(z)e^{-i(\omega(k)t-kz)},\\ \mathcal{A}_\parallel(t,z) &= \hat{\mathcal{A}}_\parallel(z)e^{-i(\omega(k)t-kz)},\\ \mathcal{A}_\perp(t,z) &= \hat{\mathcal{A}}_\perp(z)e^{-i(\omega(k)t-kz)},\end{aligned} \tag{A.46}$$

where $\hat{\phi}, \hat{\mathcal{A}}_\parallel, \hat{\mathcal{A}}_\perp$ are the slowly varying amplitudes, $\omega(k)$ satisfy relativistic dispersion relation $\omega(k)^2 = k^2 + m_\phi^2 \sim k^2$. The deformation of linear EoM into the Schrodinger-type equation under the eikonal approximation is the same as that of the photon graviton conversion case. Then, focusing on the polarization parallel to a background magnetic field which is relevant to conversion, the resulting Schrodinger-type form of linear EoM is

$$i\frac{d}{dz}\begin{pmatrix}\hat{\phi}\\ \hat{\mathcal{A}}_\parallel\end{pmatrix} = \begin{pmatrix}\Delta_\phi & \Delta_{\phi\gamma}(z)\\ \Delta_{\phi\gamma}(z) & \Delta_{\rm plasma}(z) - \Delta^\parallel_{\rm vac}(z)\end{pmatrix}\begin{pmatrix}\hat{\phi}\\ \hat{\mathcal{A}}_\parallel\end{pmatrix}, \tag{A.47}$$

$$\Delta_\phi := \frac{m_\phi^2}{2\omega}, \tag{A.48}$$

$$\Delta_{\phi\gamma}(z) := \frac{1}{2}g_{\phi\gamma}\frac{\bar{B}(z)}{\sqrt{4\pi}}, \tag{A.49}$$

$$\Delta_{\rm plasma} := \frac{\omega^2_{\rm plasma}}{2\omega}, \tag{A.50}$$

$$\Delta^\parallel_{\rm vac} := 7\varrho\omega\bar{B}^2(z), \tag{A.51}$$

where we introduced photon effective mass by plasma.

Photon Axion Conversion in a Uniform Background

Here we consider photon axion conversion in a uniform background, where $\bar{B}(z) =$ const and $n_{\rm e}(z) =$ const. The calculations are the same as the photon graviton conversion. By solving the linear EoM (A.47) with the initial condition $\hat{\phi}(0) = 0$, $\hat{\mathcal{A}}_\parallel(0) = 1$, the conversion probability is given by

$$P_{\gamma\phi} := |\hat{\phi}(z)|^2 = \frac{4\Delta^2_{\phi\gamma}}{\Delta^2_{\rm osc}}\sin^2\left(\frac{\Delta_{\rm osc}}{2}z\right) \tag{A.52}$$

with

$$\Delta_{\rm osc} = \sqrt{(\Delta_{\rm plasma} - \Delta^\parallel_{\rm vac} - \Delta_\phi)^2 + 4\Delta^2_{\phi\gamma}}. \tag{A.53}$$

A.7 Dictionary of Physical Constants

A.7.1 Particle Physics

The Thomson scattering cross section(cross section for scattering of low energy photon by an electron):

$$\sigma_{\mathrm{T}} = \frac{8\pi}{3}\left(\frac{e^2}{m_{\mathrm{e}}c^2}\right)^2 = 0.6652 \times 10^{-24}\mathrm{cm}^2 \tag{A.54}$$

A.7.2 Cosmology

- **Hubble constant**:

$$H_0 = 3.241 \times 10^{-18} h_0 \mathrm{sec}^{-1}, \tag{A.55}$$

  where h_0 is dimensionless Hubble constant.

- **Hubble horizon**:

$$cH_0^{-1} = 0.9250 \times 10^{28} h_0^{-1}\mathrm{cm}. \tag{A.56}$$

- **Critical energy density**:

$$\rho_{\mathrm{c0}} = \frac{3c^2H_0^2}{8\pi G} = 1.054 h_0^2 \times 10^4\,\mathrm{eVcm}^{-3}. \tag{A.57}$$

A.7.3 Astrophysics

Schwarzschild radius:

$$r_{\mathrm{S}} := \frac{2GM}{c^2} = 2.953\mathrm{km}\frac{M}{M_\odot} \tag{A.58}$$

A.7.4 Conversion from natural unit

$$\hbar c = 1.973 \times 10^{-5}\mathrm{eV}\cdot\mathrm{cm} \tag{A.59}$$

$$1\mathrm{Hz} = 6.582 \times 10^{-16}\mathrm{eV}/\hbar \tag{A.60}$$

$$1\mathrm{G} = \mathrm{dyn}^{1/2}\mathrm{cm}^{-1} = 6.925 \times 10^{-2}\mathrm{eV}^2 \tag{A.61}$$

$$1K = 0.8617 \times 10^{-4}\mathrm{eV}/k_{\mathrm{B}} \tag{A.62}$$

Bibliography

[1] B. P. Abbott *et al.*, "Observation of Gravitational Waves from a Binary Black Hole Merger," *Phys. Rev. Lett.*, vol. 116, no. 6, p. 061102, 2016.

[2] M. G. Haehnelt, "Low frequency gravitational waves from supermassive black holes," *Mon. Not. Roy. Astron. Soc.*, vol. 269, p. 199, 1994.

[3] A. H. Jaffe and D. C. Backer, "Gravitational waves probe the coalescence rate of massive black hole binaries," *Astrophys. J.*, vol. 583, pp. 616–631, 2003.

[4] J. S. B. Wyithe and A. Loeb, "Low - frequency gravitational waves from massive black hole binaries: Predictions for LISA and pulsar timing arrays," *Astrophys. J.*, vol. 590, pp. 691–706, 2003.

[5] A. Sesana, F. Haardt, P. Madau, and M. Volonteri, "Low - frequency gravitational radiation from coalescing massive black hole binaries in hierarchical cosmologies," *Astrophys. J.*, vol. 611, pp. 623–632, 2004.

[6] Sesana, A. and Haardt, F. and Madau, P. and Volonteri, M., "The gravitational wave signal from massive black hole binaries and its contribution to the LISA data stream," *Astrophys. J.*, vol. 623, pp. 23–30, 2005.

[7] R. D. Peccei and H. R. Quinn, "CP Conservation in the Presence of Instantons," *Phys. Rev. Lett.*, vol. 38, pp. 1440–1443, 1977.

[8] Peccei, R. D. and Quinn, Helen R., "Constraints Imposed by CP Conservation in the Presence of Instantons," *Phys. Rev. D*, vol. 16, pp. 1791–1797, 1977.

[9] F. Wilczek, "Problem of Strong P and T Invariance in the Presence of Instantons," *Phys. Rev. Lett.*, vol. 40, pp. 279–282, 1978.

[10] S. Weinberg, "A New Light Boson?" *Phys. Rev. Lett.*, vol. 40, pp. 223–226, 1978.

[11] M. Dine, W. Fischler, and M. Srednicki, "A simple solution to the strong cp problem with a harmless axion," *Physics Letters B*, vol. 104, no. 3, pp. 199–202, 1981.

[12] P. Svrcek and E. Witten, "Axions In String Theory," *JHEP*, vol. 06, p. 051, 2006.

[13] A. Arvanitaki, S. Dimopoulos, S. Dubovsky, N. Kaloper, and J. March-Russell, "String Axiverse," *Phys. Rev. D*, vol. 81, p. 123530, 2010.

[14] A. Arvanitaki and S. Dubovsky, "Exploring the String Axiverse with Precision Black Hole Physics," *Phys. Rev. D*, vol. 83, p. 044026, 2011.

[15] H. Yoshino and H. Kodama, "Gravitational radiation from an axion cloud around a black hole: Superradiant phase," *PTEP*, vol. 2014, p. 043E02, 2014.

[16] J. Ghiglieri and M. Laine, "Gravitational wave background from Standard Model physics: Qualitative features," *JCAP*, vol. 07, p. 022, 2015.

[17] J. Ghiglieri, G. Jackson, M. Laine, and Y. Zhu, "Gravitational wave background from Standard Model physics: Complete leading order," *JHEP*, vol. 07, p. 092, 2020.

[18] A. Ringwald, J. Schütte-Engel, and C. Tamarit, "Gravitational Waves as a Big Bang Thermometer," *JCAP*, vol. 03, p. 054, 2021.

[19] J. Ghiglieri, J. Schütte-Engel, and E. Speranza, "Freezing-In Gravitational Waves," 11 2022.

[20] A. D. Dolgov, P. D. Naselsky, and I. D. Novikov, "Gravitational waves, baryogenesis, and dark matter from primordial black holes," 9 2000.

[21] R. Anantua, R. Easther, and J. T. Giblin, "GUT-Scale Primordial Black Holes: Consequences and Constraints," *Phys. Rev. Lett.*, vol. 103, p. 111303, 2009.

[22] A. D. Dolgov and D. Ejlli, "Relic gravitational waves from light primordial black holes," *Phys. Rev. D*, vol. 84, p. 024028, 2011.

[23] N. Aggarwal *et al.*, "Challenges and opportunities of gravitational-wave searches at MHz to GHz frequencies," *Living Rev. Rel.*, vol. 24, no. 1, p. 4, 2021.

[24] V. Anastassopoulos *et al.*, "New CAST Limit on the Axion-Photon Interaction," *Nature Phys.*, vol. 13, pp. 584–590, 2017.

[25] M.E.Gertsenshtein, "Wave resonance of light and gravitational waves," *Sov.Phys.JETP*, vol. 14, no. 84, 1962.

[26] Ya.B.Zeldvich, "Electromagnetic and gravitational waves in a stationary magnetic field," *Zh. Eksp. Teor.Fiz*, vol. 65, no. 1311, 1973.

[27] G. Raffelt and L. Stodolsky, "Mixing of the Photon with Low Mass Particles," *Phys. Rev. D*, vol. 37, p. 1237, 1988.

[28] A. Ejlli, D. Ejlli, A. M. Cruise, G. Pisano, and H. Grote, "Upper limits on the amplitude of ultra-high-frequency gravitational waves from graviton to photon conversion," *Eur. Phys. J. C*, vol. 79, no. 12, p. 1032, 2019.

[29] S. Weinberg, *Gravitation and Cosmology: Principles and Applications of the General Theory of Relativity.* New York: John Wiley and Sons, 1972.

[30] K. Saito, J. Soda, and H. Yoshino, "Universal 1020 Hz stochastic gravitational waves from photon spheres of black holes," *Phys. Rev. D*, vol. 104, no. 6, p. 063040, 2021.

[31] K. Akiyama *et al.*, "First Sagittarius A* Event Horizon Telescope Results. V. Testing Astrophysical Models of the Galactic Center Black Hole," *Astrophys. J. Lett.*, vol. 930, no. 2, p. L16, 2022.

[32] Akiyama, Kazunori and others, "First M87 Event Horizon Telescope Results. VIII. Magnetic Field Structure near The Event Horizon," *Astrophys. J. Lett.*, vol. 910, no. 1, p. L13, 2021.

[33] N. I. Shakura and R. A. Sunyaev, "Black holes in binary systems. Observational appearance," *Astron. Astrophys.*, vol. 24, pp. 337–355, 1973.

[34] I. D. Novikov and K. S. Thorne, "Astrophysics of black holes." in *Black Holes (Les Astres Occlus)*, Jan. 1973, pp. 343–450.

[35] D. Lynden-Bell and J. E. Pringle, "The Evolution of viscous discs and the origin of the nebular variables." *Mon. Not. Roy. Astron. Soc.*, vol. 168, pp. 603–637, 1974.

[36] S. Ichimaru, "Bimodal behavior of accretion disks - Theory and application to Cygnus X-1 transitions," *Astrophys. J.*, vol. 214, pp. 840–855, 1977.

[37] R. Narayan and R. Popham, "Hard x-rays from accretion disk boundary layers," *Nature*, vol. 362, p. 820, 1993.

[38] R. Narayan and I.-s. Yi, "Advection dominated accretion: A Selfsimilar solution," *Astrophys. J. Lett.*, vol. 428, p. L13, 1994.

[39] S. L. Shapiro and S. A. Teukolsky, *Black holes, white dwarfs, and neutron stars: The physics of compact objects*, 1983.

[40] R. M. Wald, *General Relativity*. Chicago, USA: Chicago Univ. Pr., 1984.

[41] H. Yoshino, K. Takahashi, and K.-i. Nakao, "How does a collapsing star look?" *Phys. Rev. D*, vol. 100, no. 8, p. 084062, 2019.

[42] M. Schmidt, "3C 273 : A Star-Like Object with Large Red-Shift," *Nature*, vol. 197, no. 4872, p. 1040, 1963.

[43] S. Paltani and M. Turler, "The Mass of the black hole in 3C 273," *Astron. Astrophys.*, vol. 435, p. 811, 2005.

[44] S. Soldi *et al.*, "The multiwavelength variability of 3C 273," *Astron. Astrophys.*, vol. 486, p. 411, 2008.

[45] T. Do *et al.*, "Relativistic redshift of the star S0-2 orbiting the Galactic center supermassive black hole," *Science*, vol. 365, no. 6454, pp. 664–668, 2019.

[46] F. Yuan, E. Quataert, and R. Narayan, "Nonthermal electrons in radiatively inefficient accretion flow models of Sagittarius A*," *Astrophys. J.*, vol. 598, pp. 301–312, 2003.

[47] F. Yuan and R. Narayan, "On the nature of x-ray bright optically normal galaxies," *Astrophys. J.*, vol. 612, pp. 724–728, 2004.

[48] Yuan, Feng and Narayan, Ramesh, "Hot Accretion Flows Around Black Holes," *Ann. Rev. Astron. Astrophys.*, vol. 52, pp. 529–588, 2014.

[49] E. Masaki and J. Soda, "Conversion of Gravitons into Dark Photons in Cosmological Dark Magnetic Fields," *Phys. Rev. D*, vol. 98, no. 2, p. 023540, 2018.

[50] J.-P. De Villiers, J. F. Hawley, and J. H. Krolik, "Magnetically driven accretion flows in the kerr metric I: models and overall structure," *Astrophys. J.*, vol. 599, p. 1238, 2003.

[51] J. C. McKinney, "General relativistic magnetohydrodynamic simulations of jet formation and large-scale propagation from black hole accretion systems," *Mon. Not. Roy. Astron. Soc.*, vol. 368, pp. 1561–1582, 2006.

[52] C. J. Conselice, A. Wilkinson, K. Duncan, and A. Mortlock, "The evolution of galaxy number density at $z < 8$ and its implications," *The Astrophysical Journal*, vol. 830, no. 2, p. 83, 2016.

[53] K. Nomura, K. Saito, and J. Soda, "Observing axions through photon ring dimming of black holes," 12 2022.

[54] D. Noordhuis, A. Prabhu, S. J. Witte, A. Y. Chen, F. Cruz, and C. Weniger, "Novel Constraints on Axions Produced in Pulsar Polar Cap Cascades," 9 2022.

[55] C. Dessert, D. Dunsky, and B. R. Safdi, "Upper limit on the axion-photon coupling from magnetic white dwarf polarization," *Phys. Rev. D*, vol. 105, no. 10, p. 103034, 2022.

[56] K. Kohri and H. Kodama, "Axion-Like Particles and Recent Observations of the Cosmic Infrared Background Radiation," *Phys. Rev. D*, vol. 96, no. 5, p. 051701, 2017.

[57] L.D.Landau and E.M.Lifshitz., *Fluid Mechanics*. New York: Pergamon, 1959.

[58] K. S. Thorne and R. D. Blandford, *Modern Classical Physics*. Princeton, New Jersey: Princeton university press, 2017.

[59] E. Masaki, A. Aoki, and J. Soda, "Photon-Axion Conversion, Magnetic Field Configuration, and Polarization of Photons," *Phys. Rev. D*, vol. 96, no. 4, p. 043519, 2017.